1995

Laser machining and its thermal effects on silicon nitride and steel

Aloke K. Ray
Iowa State University

Laser machining and its thermal effects on silicon nitride and steel

by

Aloke K. Ray

A Dissertation Submitted to the

Graduate Faculty in Partial Fulfillment of the

Requirements for the Degree of

DOCTOR OF PHILOSOPHY

Department: Mechanical Engineering
Major: Mechanical Engineering

Approved:

Signature was redacted for privacy.

Signature was redacted for privacy.

In Charge of Major Work

Signature was redacted for privacy.

For the Major Department

Signature was redacted for privacy.

For the Graduate College

Iowa State University
Ames, Iowa
1995

TABLE OF CONTENTS

LIST OF FIGURES

LIST OF TABLES

ACKNOWLEDGMENTS

I would first of all like to express my sincere gratitude to my major professors, Dr. P. A. Molian and Dr. J. L. Hall, for their continuous guidance and encouragement. I am grateful to the members of my examining committee for their insightful suggestions and encouragement. I would like to thank Dr. R. J. Scrutton, Dr. R. M. Nelson and Dr. J. M. Prusa for their valuable guidance and suggestions specially for mathematical modeling considered in my dissertation work. I would also thank to Mr. Hap Steed and Ms. Rosalie Enfield, for their help throughout the years.

I would also like to acknowledge the departmental support in the form of teaching assistantship that made it possible for me to pursue my doctorate degree.

I want to express my sincere appreciation to my father-in-law Mr. C. R. Chowdhury for his encouragement and guidance. I would like to thank Dr. Chin Kooi (Jerry) Lim for his unlimited help and guidance and Mr. Ray Welterlin, Engineering Manager of Buehler Products Inc., Cary, NC. and Dr. Subroto Bhattacharya of IBM Corporation of Raleigh, NC. for their support and encouragement for completion of this work. I am fortunate to have my wife, Indrani, and two little daughter Amrita and Tiara, here with me at Ames for the last two years. No words can describe the sacrifices my wife made to make this great success. This dissertation is dedicated to her.

1. GENERAL INTRODUCTION

The laser is a unique tool which has been applied in many engineering applications. Over the past decade, the laser has become the tool of choice for many manufacturers. From prototype to production, the role of laser continues to expand in the industry, and the options available with lasers continue to grow. With the introduction of updated and user-friendly software and more reliable resonators, the laser technique can be viewed as a modern way to shape different materials.

The application of lasers to materials processing has increased dramatically over the past decade. Laser processing is mainly governed by thermal action. This is based on the rapid temperature rise in the small area of the material surface due to the irradiation by the focused laser beam. The laser beam is highly intense, coherent and highly directional. Figure 1.1 shows the comparison between laser light and ordinary light. Most of the laser beams used for machining process usually exhibit a spatial energy distribution that is Gaussian and is called as TEM_{00} (Transverse Electro Magnetic) mode (Figure 1.2) [1-3].

Using a focused beam of high energy density, laser processing exhibits many features:

1. The processing speed is very high and the heat affected zone is very small compared with other machining methods.

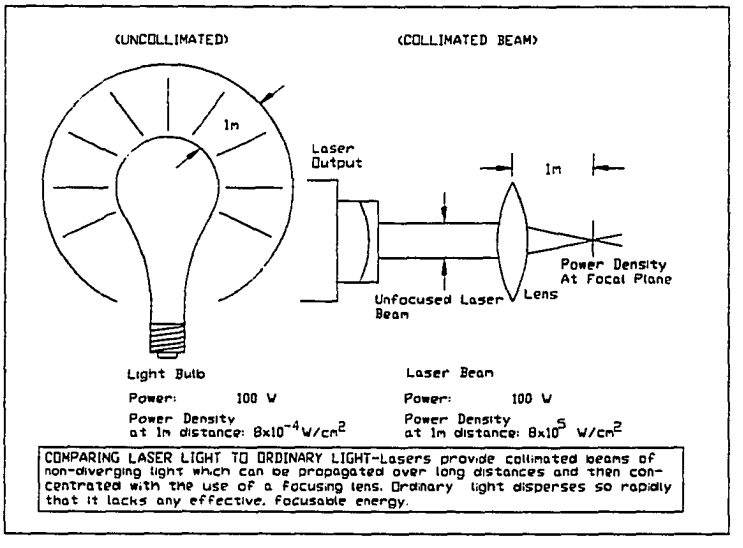

Figure 1.1: Comparison of Laser Light with Ordinary Light [2] [8]

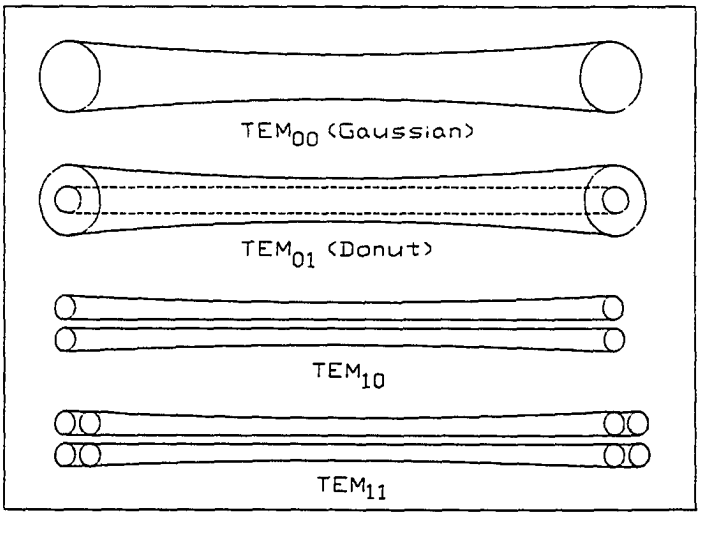

Figure 1.2: TEM Modes for Laser Beam [2]

2. Workpieces need not be clamped tightly because there is no force involved when the laser beam contacts with the workpiece.

3. The processing can be performed under ordinary atmospheric conditions.

4. The processing does not generate harmful X-rays.

5. The beam can be transmitted to long distances with minimum attenuation.

6. The beam can be applied in various kinds of material processing by controlling the power density and irradiation time (see Figure 1.3)

The distinct and diverse material properties of the lasing medium lead to numerous characteristics of the beam output, such as wave length, power density, coherence and divergence. These mainly determine the type of applications for which a particular laser can be employed. The three most important types of lasers are

1. Solid-state lasers

2. Gaseous lasers and

3. Semi conductor lasers

Each type involves a different generic approach to gain "population inversion" i.e. a state in which the power radiated by stimulated emission exceeds the power absorbed by the atoms and positive feed back.

Of all the lasers available today only two are routinely used for nearly all material processing applications. These are the Nd-YAG (neodymium doped yttrium-alumina garnet) and CO_2 (carbon dioxide) lasers. Almost ninety percent of laser material processing applications employ either or both of them.

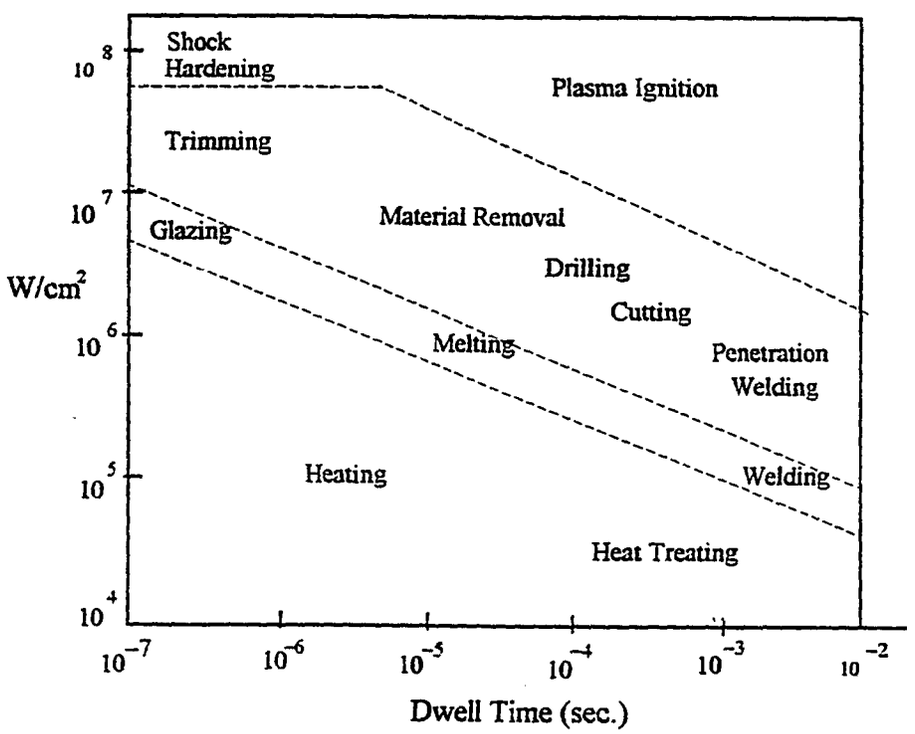

Figure 1.3: Regions of Laser Irradiation and Interaction Time suitable for Material Processing Applications for CO_2 and Nd:YAG Laser [4]

Laser machining is a material removal process and includes cutting,drilling, milling, scribing, micro-machining and cleaning. Laser machining is applied to a variety of materials such as metals, plastics, composites, ceramics, clothes etc. The different thermal and physical mechanisms associated with laser machining are summarized as [2-3]:

1. Melt and blow: Here the laser beam initially makes a drilled hole or cut on the substrate and subsequently the molten material is blown away by the assist gas jet.

2. Vaporization: Here the surface of the material is heated to boiling temperature, and a groove or keyhole is generated, which absorbs energy. Material from the groove or keyhole is vaporized.

3. Reactive fusion machining: If an assist gas such as oxygen is introduced in the process, an exothermic reaction takes place causing an oxide layer formation which adheres to the base metal. High assist gas pressure can easily remove the oxide layer, when machining metals.

4. Controlled fracture: For very brittle materials (ceramics), the laser beam initiates thermal stresses which ultimately produce cracks and fracturing in the material.

5. Scribing: In this process, low energy, high power density pulses are used to produce a groove , which weakens the structure so that mechanical snapping is possible.

6. Cold machining: Here a high power excimer laser working in the ultraviolet range is used. Due to the high photon energy, the bonding of the material is broken and physical ablation occurs.

In this investigation, the laser milling of silicon nitride and the laser cutting of steels were conducted and thoroughly studied to understand the effect of laser-material interactions on the process capabilities such as dimensional accuracy, surface finish, recast layer formation, and thermal degradation. The CO_2 lasers were employed for this purpose. In addition to the experimental work, heat flow models and finite element models were developed to verify the experimental data.

1.1 Dissertation Organization

This dissertation is presented as three papers that have been or will be submitted for publication. The papers are preceded by literature review and followed by conclusions. References cited in the General Introduction and Literature Review (Sections 1 and 2), are listed following the general conclusions.

2. LITERATURE REVIEW

2.1 Laser Machining

Laser machining is a very broad term, which includes hole drilling, grooving, cutting, scribing and milling. Laser machining techniques have become very popular, because no special tool or (tool change) is required to perform the various operations. Hence production rate is high compared to those obtained in conventional machining techniques.

Laser machining depends on various parameters such as [3]:

1. Beam Parameters: These include the wavelength, polarization spot size, TEM mode, the power and type of laser beam (pulsed or continuous wave).

2. Transport Parameters: These include the laser cutting speed and focal position.

3. Gas Flow Parameters: These include the nozzle size, nozzle shape, jet velocity, and gas composition.

4. Material Properties: The relevant properties here are optical and thermal.

2.2 Different Laser Machining Techniques

2.2.1 Drilling (One-Dimensional Laser Machining)

Laser drilling is a one-dimensional laser machining technique in which the laser beam and the workpiece remain stationery. Due to the high laser power density, material is melted or vaporized from the workpiece. Laser drilling is governed by an energy balance (Figure 2.1) between the irradiating energy from the laser beam and the conduction heat into the workpiece. Some of the energy is lost to the environment and the rest of the energy is required for phase change in the workpiece. Laser drilling techniques are applied where very small diameter holes with high production rate are required.

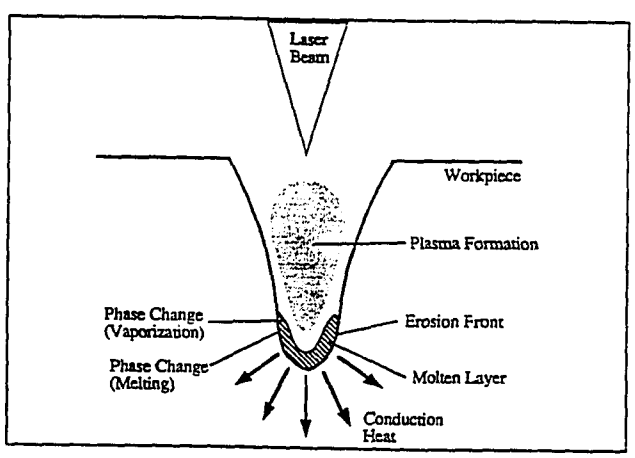

Figure 2.1: Laser Drilling [2]

It has many advantages compared to conventional hole drilling techniques [2]:

1. A laser beam can be aimed optically, hence precise and accurate holes can be produced.
2. The material removal process is by vaporization. Conventional processes produces chips and burrs.
3. No direct contact occurs with the material.
4. The process can produce a hole sharply angled to a surface (up to 80^0 from the vertical axis).
5. Soft, hard as well as brittle materials can be machined.
6. A narrow heat affected zone (HAZ) is produced.
7. Small diameter holes (as small as 0.013 mm) can be drilled.
8. Production rate is very high compared to conventional drilling, where frequent tool changes are required.

The principle disadvantages of laser hole drilling are (Figure 2.2) [12].

1. A laser beam cannot drill a hole in many thick-sectioned workpieces due to limited depth of focus, high thermal conductivity of the material and high reflectivity of the surface.
2. The temperature gradient is so high that thermal stresses induce microcracks on the surface. This effect is very common when machining ceramics.

3. Any molten material which is not completely expelled or vaporized, condenses inside and around the hole, forming a recast layer. The presence of an excessive recast layer may often obstruct drilling of the hole, and result in a poor quality product.

4. Erosion caused by the expulsion of molten and vaporized material results in taper and barreling.

5. Re-condensed and vaporized material around the entrance of the hole creates debris.

High power densities, short pulse widths and low repetition rates can reduce recast layer formation and minimize micro-cracking around the surface of the drilled hole. Hole taper can be reduced to a great extent by using a low pulse energy, a large number of pulses, a short pulse width, and an improved beam quality.

2.2.2 Cutting (Two-Dimensional Laser Machining)

The principle of laser cutting is similar to that of laser hole drilling. In this case, due to the relative beam/workpiece movement, an erosion front is created in front of the laser beam, which travels along the workpiece in the direction of beam movement. The temperature inside the workpiece depends only on the distance from the erosion front and is completely independent of time. When the material removal mechanism is melting, the molten material near the erosion front can be blown away through the bottom of the kerf by using a coaxial gas jet (Figure 2.3) [2]. Laser cutting has several unique advantages compared to conventional cutting. These are listed below [2]:

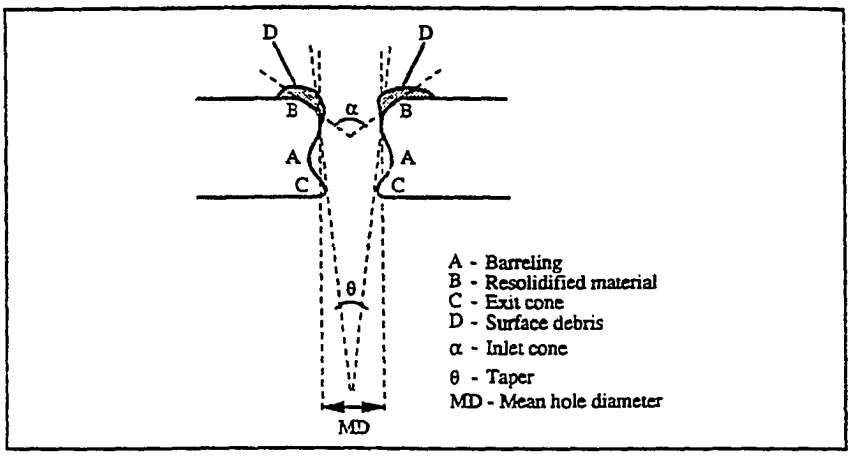

Figure 2.2: Features of Laser-Drilled Holes [7]

1. Laser cutting can remove material much more quickly than conventional cutting.

2. The kerf width produced by laser cutting is much narrower than that produced by mechanical cutting, hence less material is wasted during the process.

3. When cutting fibrous material, such as wood, paper or composite material, the laser beam vaporizes the material along the cutting edge, leading to a smooth and clean cut.

4. Any curved shape can be machined when the motion of the laser source is subjected to a multi-axis position control system.

There are however three disadvantages. These are [2],

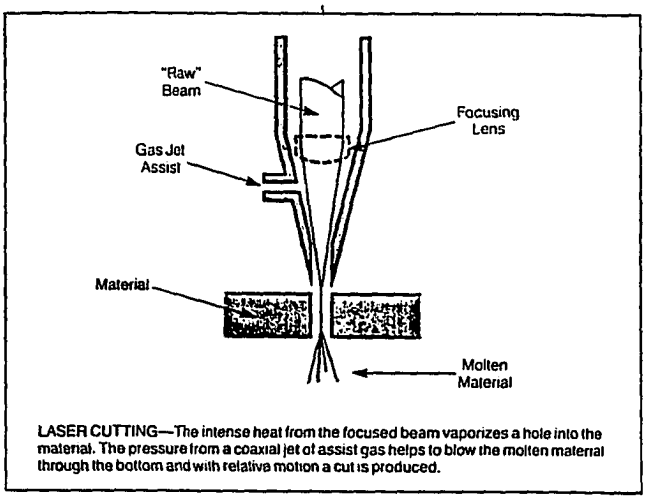

Figure 2.3: Laser Through-Cutting [8]

1. The effectiveness (penetration of laser beam) or depth of cut gradually reduces as the thickness of the workpiece increases or vice versa. As the thickness increases the surface quality of the cut edge detoriates.

2. A laser beam produces a tapered kerf shape during the cutting process, whereas a conventional cutting process produces a straight kerf shape. The nature of the taper shape is caused by the divergence of the laser beam, which gradually increases as the thickness of the workpiece increases. This taper can be reduced by focusing the laser beam to the interior of the workpiece.

3. Due to the high reflectivity, metals like, Cu, Ag, Mo are difficult to cut by a laser beam.

2.2.3 Grooving, Turning/Milling

The laser grooving technique is similar to the laser cutting process, but in this case no through hole or cut is made, i.e. the laser beam does not penetrate through the entire thickness of the workpiece. Three-dimensional laser machining is possible by using a laser beam such that the material removal technique is either by multiple grooving, (where scanning pitch is smaller than the spot size of the laser beam) or by laser turning/milling, where two laser beams are positioned at an oblique angle on the workpiece (Figure 2.4-2.5) [2] [10].

Three dimensional laser machining has the following advantages compared to the conventional machining process [2],

1. On hard and brittle materials, three dimensional laser machining can perform

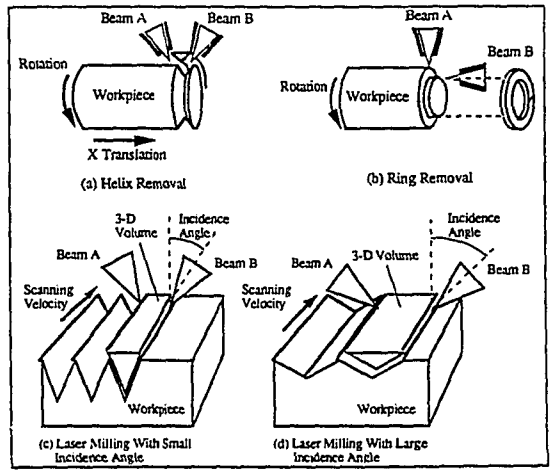

Figure 2.4: Three Dimensional Laser Machining [2]

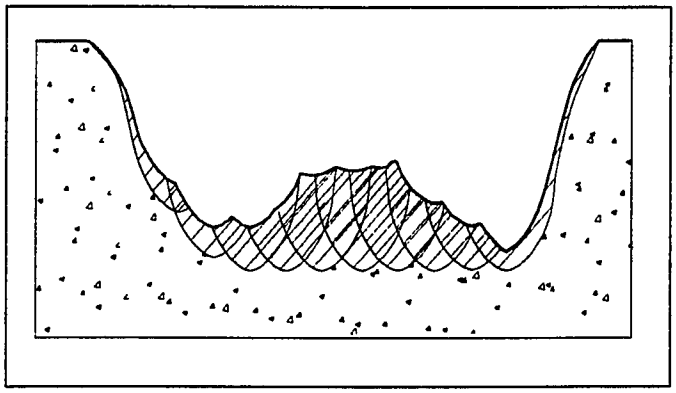

Figure 2.5: Schematic Representation of Multiple Laser Grooving [10]

turning, threading as well as milling operations, which are not cost effective with conventional machining.

2. The method is ideal for micro-machining, because the laser beams can be focussed to a small spot. The technique has been used for repairing integrated circuit components.

However three-dimensional laser machining has the following disadvantages [2] [10]:

1. During machining, molten material accumulates at the erosion front. When this occurs the assist gas pressure is not sufficient to blow away most of the molten material from the work piece. Hence a rougher surface is obtained.

2. During the multiple grooving process, the preheating temperature is very high. A higher depth of cut is obtained with more recast layer, which initiates cracks.

This is a very common problem during milling of ceramics.

2.2.4 Scribing (Three-Dimensional Machining)

The laser scribing process which is a special case of three-dimensional machining and is similar to the laser grooving process, creates a blind groove on the workpiece, but the ratio of the groove depth to groove width is close to unity and also groove depths are very small. Laser scribing produces a permanent indentation on the workpiece, and also does not result in tool wear which is characteristic of the conventional scribing process. The method is very cost effective for brittle and hard materials, specially for ceramics. The laser scribing process is used for creating permanent identification patterns on metallic and ceramic parts in industry [2].

2.3 Laser Cutting

Laser cutting is a thermal process. It is therefore necessary to understand the thermal characteristics of the material as well as the laser-material interaction during the cutting process. The laser beam produces thermal energy which is absorbed by the material, and which raises the energy level of the electrons in the conduction bands of the metal. Heat is then transfered through the material according to classical heat conduction theory. Due to rapid heating, material can melt and if the temperature is high enough, evaporation from the workpiece can occur. Thermal diffusivity plays a very important role in determining the rate of dissipation of energy from the workpiece. If the material diffusivity is low, the diffusion of energy from the workpiece is also low, hence a larger depth of cut can easily be obtained [5].

Laser cutting is a very complex process , which is influenced by the following

parameters [6]:

1. The laser beam: The parameters affecting the laser beam are the laser power, wavelength, types of polarization, wave length, types of mode and spot size.

2. Laser-material interaction: This interaction depends on the thermal, electrical, optical and chemical properties of the material.

3. Gas dynamics of the assist gas: This factor includes chemical composition, flow rate, pressure and nozzle characteristics; type, and design as well as position of the nozzle above the top of the workpiece.

4. Type of workpiece : The workpiece material can be divided into four, namely composites, ceramics, polymers or metals.

5. Fluid dynamics: The viscosity of the molten material or slag.

The quality of the laser cut is described by (Figure 2.6):

1. Kerf width: This is the width of the laser cut. Since spot size depends on the wave length of the laser beam; the smaller the spot size the narrower the kerf width obtained.

2. Heat affected zone (HAZ): This is the region adjacent to the kerf, which is affected thermally during the laser cutting process. The lower the laser cutting speed, the larger the HAZ obtained, and the larger the region containing thermal residual stresses.

3. Edge Striations: The height and spacing of the ridge-like striations determines the smoothness of the edges of the cut. The height of the striations is denoted by

the roughness number, R_a. The edge of the cut is much smoother when cutting thinner sheet metal, hence a lower roughness number, R_a may be expected.

4. Dross attachment: When cutting metal, the molten material that is not blown away by the assist gas, or dross adheres to the cutting edge. Dross attachment is very undesirable and releases the energy back to the workpiece leading to a larger HAZ.

5. Thermal deformation: During the laser cutting process, the cut edge may expand due to martensitic phase transformation and then shrink during cooling, causing thermal stresses and permanent deformation along the cut edge [11].

Powell [9] conducted laser cutting experiments on steel, using a continuous wave CO_2 laser. For oxygen assist laser cutting, he observed that pure oxygen resulted in

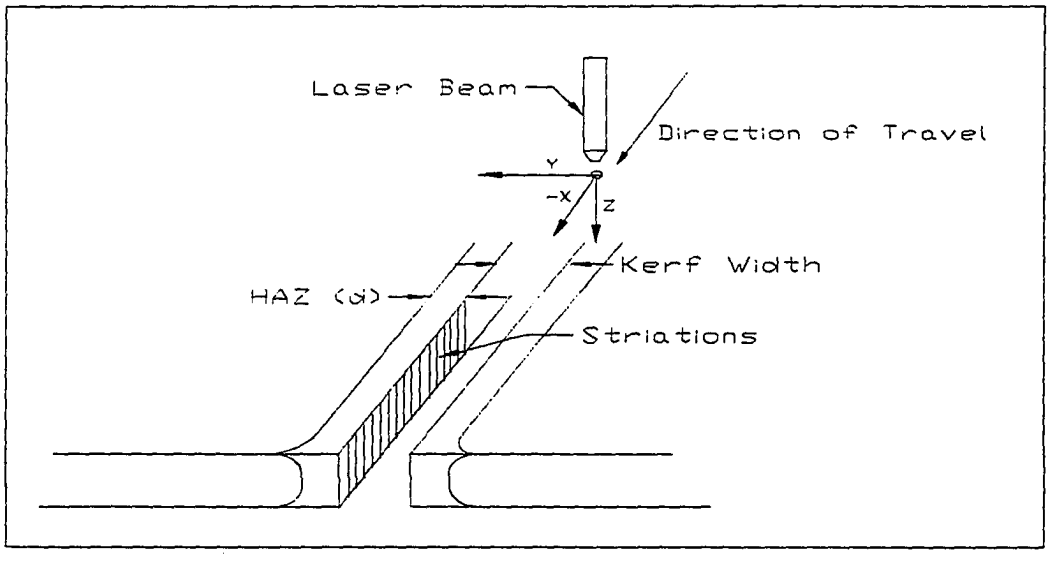

Figure 2.6: Schematic of a typical Laser-cut Sample

exothermic reactions with the metal, thereby producing much heat, which accelerated the laser cutting process. He estimated that this oxygen provides half of the thermal energy and at the same time produces a low-viscosity oxidized melt, which does not adhere to the workpiece. Therefore a clean-cut surface is expected. Also if the purity of oxygen increases, the thermal energy across the cutting edge increases, leading to a deeper cut. The percentage of purity of oxygen plays very important role in improving cutting productivity and cut quality [13-14]. It is concluded that the purity of oxygen directly influences the cutting speed and dramatically reduces weight percent of oxidized iron from the cutting edge.

In order to cut material equally well in all directions a circularly polarized laser beam should be used. Care should be taken so that the cutting nozzle is not contaminated during the cutting process [9]. It is observed that as the thickness of mild steel is increased, a larger diameter nozzle with a lower oxygen pressure performs better and that no burnt edge is observed. At speeds lower than 8.47 mm/sec, CO_2 lasers do not cut mild steel particularly well due to high conductive thermal losses. In these circumstances a burnt zone is created at the cut edge, resulting in a rough surface [9]. A superior cut quality can be achieved by pulsing the laser output in the frequency range 200 to 1000 Hz, depending on the application. The burnt effect can also be avoided by spraying water mist onto the cut edge [9].

Nozzle design is very important when cutting thick steel plate. In this case, oxidation is observed on the cut walls due to the entrainment of oxygen from the surrounding atmosphere. This problem can be minimized by using a wider nozzle, where the possibility of entrainment is low, but on the other hand gas consumption in these circumstances can be very high. Neill et al. [15] designed a nozzle (Figure

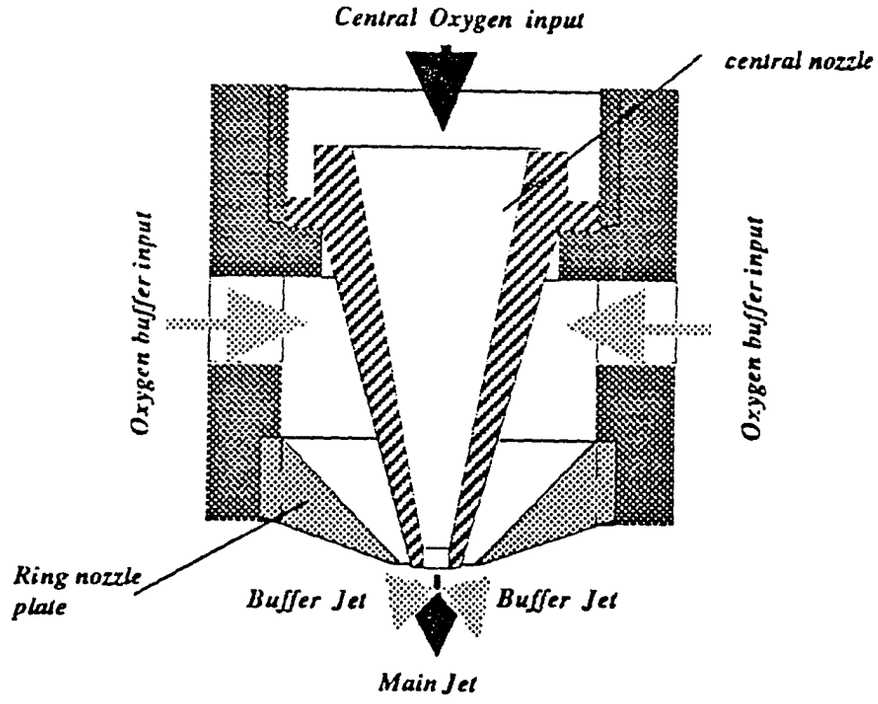

Figure 2.7: Buffer Nozzle [15]

2.7), which consists of a buffer oxygen jet. This nozzle allows a turbulent jet mixing zone across the cut edge, thus preventing oxidation reaction. In their experiment, by using a buffer nozzle, a much deeper cut was observed.

Stainless steel contains 10-20% of chromium and tends to obstruct the oxidation reaction process. During the cutting process chromium oxide is formed which partially prevents the oxidation reaction with stainless steel. Hence the cutting speed must be reduced and also due to partial oxidation, the melt is not completely ejected. As a result residual melt or dross can be expected on the lower edge of the cut [9]. For nonferrous metals such as aluminum alloys, which are highly reflective with respect to a CO_2 laser beam and whose thermal conductivity is also high, most of the heat

is lost during the cutting process and also aluminum forms an oxide layer, which prevents oxygen from flowing freely across the cut edge. Hence higher power and slower cutting speed are recommended.

2.4 Laser Milling of Ceramics

Three dimensional laser machining or laser milling is a very new field in ceramics application. Very little research has been carried out in this area. The laser milling process is similar to laser grooving, but in this case multiple grooving is carried out with an overlapping distance, which is usually smaller than the laser spot size. For ceramics, thermal conductivities as well as coefficients of thermal expansion have low values. Hence when high thermal energy is applied, the material cannot expand but nevertheless absorbs most of the energy, creating thermal shocks in the material, which ultimately leads to microcracks. For reaction bonded silicon nitride (RBSN), with 18% porosity, microcrack formation is low [10] compared to hot isostatically pressed silicon nitride(HIPSN). During the machining of RBSN, some of the thermal shocks are likely to be absorbed due to the presence of porosity. Hence limited cracking may be expected. For sintered ceramics, the crystal lattice along the grain boundaries restricts displacements, during the machining process. This constraint also intensifies thermal shocks. Therefore more microcracks may be expected.

Laser machining of silicon nitride takes place at a temperature of 2150 K, where silicon nitride decomposes into silicon and nitrogen. If oxygen is used as an assist gas, this reacts with silicon to produce silicon dioxide as a molten slag, which is blown away by the assist gas. During the multiple laser grooving process, the first pass is similar to a single pass grooving process. As the number of grooving passes

increases with a very small overlapping scan, the temperature from the previous pass (preheating temperature) contributes to the next grooving process and hence a deeper second groove is formed. This process is continued until a steady state preheating temperature is reached along the cut edge, after which the depth of cut remains fairly constant. Also, due to multiple reflections of the laser beam from the cut surface (which bounces back and forth on the two side walls), a shallow taper cut is created near the initial cut edge. The same phenomenon was observed by Wallace et al. [16]. As more groove is cut, the reflections from the wall become weaker and weaker, until no more taper groove can be expected. During this process, due to the set-up assist gas pressure, most of the molten slag is blown away. It is to be noted that the viscosity of the molten slag is much lower than the viscosity of the cut edge. Also due to the high temperature a wetting phenomenon can be expected. If the assist gas pressure is high enough, most of the molten silicon cannot adhere along the side walls. As the width of the groove increases, the pressure across the groove decreases. In this case the assist gas cannot drive away most of the molten silicon from the cut surface. The molten silicon even with low viscosity adheres on the wall where the wetting takes place. It is also observed that during the driving mechanism, the molten silicon loses its energy, hence its viscosity gradually increases hence it gets deposited on the top of the previously formed groove surface. This process continues, which leads to gradual build-up of a recast layer on the cut edge. During this process, the temperature on the cut edge is very high and the grain boundaries (of HIPSN) prevent any more thermal expansion of the material, leading to microcracks on the cut edge. When using a pulsed laser, the thermal load can be minimized to a great

extent. Therefore the microcracks can be minimized by preheating the cutting zone and then slowly cooling at atmospheric pressure.

3. CARBON-DIOXIDE LASER MILLING OF REACTION BONDED SILICON NITRIDE

A paper submitted to the International Journal of High Technology Ceramics, Leeds, U. K.

Aloke Ray*, P. A. Molian*, R. F. Scrutton†, and A. K. Mitra‡

3.1 Abstract

Laser milling of ceramics is a thermal process governed by vaporization or chemical decomposition or thermal fracture of the material. This paper presents the experimental methods and thermal modeling of milling of reaction bonded silicon nitride (RBSN) using a continuous wave CO_2 laser. The work is focused on an understanding of the influence of laser parameters on depth of cut, surface roughness, microcrack and recast layer formation and preheating temperature(due to overlapping laser scans) and its effects. The experiments involved scanning a 1 kW continuous wave,TEM_{00} CO_2 laser beam on RBSN test samples using a computer numerical controlled(CNC)

*Department of Mechanical Engineering, Iowa State University

†Department of Industrial & Manufacturing System Engineering, Iowa State University

‡Department of Aerospace Engineering and Engineering Mechanics, Iowa State University

X-Y table.

Experimental results showed that the material removal mechanism was chemical decomposition where the depth of cut ranged from 0.01 mm to 2 mm (depending on the beam scan rate) when oxygen was used as the assist gas. Deeper cuts ($\geq$ 0.5 mm) were accompanied by a high density of cracks, rough surfaces and the production of a significant recast layer. A comparison between grooving and milling showed that milling produced deeper cuts due to the preheating temperature and multiple beam reflections associated with multiple, overlapping laser scans. However milling generated a recast layer that built-up in thickness with the increasing number of overlapping scans. The type of assist gas played a major role in affecting the depth of cut and recast layer formation in laser machining. Oxygen produced deeper cuts than nitrogen in grooving while the opposite effect was true in milling. Analytical models used to predict the depth of cut were in excellent agreement with experimental data in grooving but were only fair in milling.

Deeper cuts generated rough surfaces ($R_a > 30$ μm) due to the presence of a recast layer. A double- milling procedure that involved defocused beams was capable of improving the surface roughness to R_a 2.8 μm in deeper cuts by selectively reducing the recast layer. Deeper cuts and fewer cracks were observed in laser milling of RBSN compared to hot-pressed Si_3N_4 due to the presence of large amount of porosity that enabled better absorption of laser energy and reduction of thermal stresses.

3.2 Nomenclature

T	Temperature, K
t	Time, sec

k	Thermal diffusivity, m^2/sec
K	Thermal conductivity, W/m K
P'	Power per unit length in the cutting direction, W/m
r	$\sqrt{(x^2+y^2)}$
$K_0(vr/2k)$	Modified Bessel function of the second kind and zero order
v	Scan rate, m/sec
t_p	Dwell time, sec
T_v	Decomposition temperature, K
T_0	Initial temperature of the material, K
T_i	Preheating temperature at a specific speed
I	Laser intensity, $Watt/m^2$
P	Laser power, Watt
ϵ	Absorptivity
w	Spot size (radius), m
C	Specific heat, W/kg K
ρ	Density, kg/m^3
L_v	Latent heat of vaporization, J/kg
f	Scanning pitch, m
λ	Wave length of laser beam, nm

3.3 Introduction

Laser machining of ceramics is a technology that is progressing at a rapid rate. Laser drilling, grooving and cutting of silicon nitride, alumina and zirconia have been successfully accomplished under controlled conditions [1-2]. Laser milling has not yet been developed to a high degree of success especially for metals and alloys for two reasons: first; the intensity required to evaporate a thin layer of metal is very high; second; significant melting accompanies thermal evaporation resulting in a recast layer that is detrimental to surface finish and mechanical properties. Laser milling may conceived to be a promising technique for ceramics because the laser-ceramic interactions are quite different from those of laser-metal interactions.

Advanced structural ceramics such as silicon nitride(Si_3N_4) are currently used in several engineering applications due to their excellent physical and chemical properties such as high hardness, high thermal resistance, chemical inertness and low electrical and thermal conductivity [3]. However these excellent properties make Si_3N_4 extremely difficult to machine using conventional machining techniques. The commercially available machining technique for Si_3N_4 is diamond grinding which unfortunately does not allow machining of small pockets, cavities and unusual shapes. During diamond grinding, process flaws and tensile residual stresses are introduced into the surface with a resulting loss in fatigue strength. It is also found that as the diamond wheel feed rate is increased, increased power is required to obtain the same depth of cut, while at the same time wheel wear is also increased resulting in rougher surfaces. During diamond grinding, the high porosity in ceramics, contributes to poor surface finish. Since ceramics are very brittle and hard, higher grinding forces and power are required which in turn shortens wheel life [3].

Laser-silicon nitride interactions are significantly dependent upon the laser wavelength and the type of assist gas used. When CO_2 laser (λ=10,600 nm) is used as the source of heating the silicon nitride, the following decomposition occurs at a temperature of 2150 K.

$$Si_3N_4 \rightarrow 3Si(l) + 2N_2(g)$$

Silicon liquid resolidifies on the workpiece resulting in the formation of a recast layer. In the presence of oxygen gas, the reaction is as follows:

$$Si_3N_4 + 3\ O_2 \rightarrow 3SiO_2(s) + 2N_2(g)$$

When a Nd:YAG laser beam(λ=1064 nm) interacts with silicon nitride, the following reaction is expected due to higher photon energy and improved absorption of laser energy by the material.

$$Si_3N_4 \rightarrow 3Si(g) + 2N_2(g)$$

Silicon is removed from the surface as a gas or condenses on the walls of the hole resulting in the formation of a recast layer. In general, less recast layer is expected when Nd:YAG laser is used as compared with a CO_2 laser.

Excimer lasers(λ=193-351 nm) offer very high photon energies and result in a stronger interaction with silicon nitride because the absorption coefficient is higher. Most of the energy is deposited on the surface layers and generates the following reaction.

$$Si_3N_4 \rightarrow 3Si(g) + 4N(g)$$

The gas evolution is very pronounced in this case and hence the recast layer can be expected to be insignificant.

Morita [4] conducted laser machining of Si_3N_4, using a pulsed YAG laser. He found that, due to sub-surface layer damage(which included the heat affected layer

and the residual stress layer) compressive strength was reduced to 80-90% compared with that of diamond ground specimens. X-ray analysis of laser machined surfaces revealed that the recast layer consisted of only Si. He believed that the recast layer was due to the decomposition of Si_3N_4 in which silicon vapor was saturated in the hole and was condensed into liquid form. The study also indicated that the propagation of cracks depended directly on peak power and pulse duration. It was observed that a repetition frequency higher than 10 kHz propagated cracks and thickened the recast layer. It was concluded that crack development is a result of thermal shock and thermal expansion mismatch between the recast layer and the original workpiece material. In his experiment this author found that residual stresses were present in larger amounts on the diamond ground specimen than on laser milled surfaces.

Solomah [5] conducted laser cutting experiments using continuous wave and pulsed CO_2 lasers. He found that laser power is the key factor in controlling surface finish. A high power caused thermal shock due to the lower heat conductivity of ceramics. High levels of differential thermal strains were also generated between the top and bottom surfaces of the workpiece. The cutting mechanism essentially consisted of oxidation of Si_3N_4 to SiO_2. The recast layer was silica for a thickness 150 to 350 μm. He also observed that the pore density and pore size decreased with increasing cutting depth. Scanning electron microscopy(SEM) analysis revealed that the top layer underwent significant oxidation. He noticed that, under an inert atmosphere, fracture occurred at all laser power levels and also that the cutting mechanism was mainly by decomposition/evaporation processes. But for a pulsed mode, using the same power level, a significant reduction in fracture was observed due to diminished thermal shock compared to that caused by the continuous mode

operation. SEM also revealed that the porosity was more uniformly distributed in the pulsed cutting mode when compared with continuous mode operation.

Yamamoto et al. [6] investigated laser machining of silicon nitride using TEM_{00} CO_2 laser. Fracture occurred on thicker plates(6-8 mm) as a result of thermal shock, when higher power($\geq$ 600 W) was employed. It was therefore necessary to reduce the power level in order to reduce thermal shock. These workers also observed formation of SiO_2 at the surface when oxygen was used as an assist gas and that the flexural strength was reduced to one third of that of the original sintered Si_3N_4. About 80% of the flexural strength was recovered by post-annealing of laser machined Si_3N_4 in a nitrogen atmosphere at 1773 K. In their experiment the oxygen assist gas pressure was found not to affect the depth of cut.

Kitagawa et al. [7] conducted experiments to determine optimum CO_2 laser processing conditions for Si_3N_4 and SiC ceramics. Si_3N_4 chemically decomposes or dissociates as per the following reactions:

$$\text{(Decomposition)} \quad : \quad Si_3N_4(s) \rightarrow 3Si\ (s) + 2N_2(g)$$

$$\text{(Dissociation)} \quad : \quad Si_3N_4(s) \rightarrow 3Si(g) + 4N(g)$$

The energy required for decomposition is less than the energy required for dissociation. From the standard heat of atomization, it is estimated that the energy for dissociation of Si_3N_4 is 0.03 J/gm. Kitagawa et al. [7] observed that in laser machining of Si_3N_4 the energy required was 0.01-0.017 J/gm which indicates that the material removal in Si_3N_4 should have occurred through decomposition rather than by dissociation. It is to be noted that the decomposition temperature of silicon nitride(2150 K) is lower than the evaporation temperature of metal silicon(2608 K). By contrast, laser machining of SiC is a dissociation process, because the energy

required for dissociation is 0.031 J/gm , which is close to that observed in laser machining(0.032 J/gm). The silicon carbide dissociation temperature(3259 K) is higher than the evaporation temperature of metal silicon(2608 K) while the graphite sublimation temperature(3643 K) is higher than the dissociation temperature.

Ramanathan et al. [8] conducted experiments to measure beam energy absorptance in hot pressed silicon nitride. It was found that the absorptance changes sharply with temperature when using a CO_2 laser due to high temperature effects such as oxidation or decomposition. For a laser power of 540 W, absorptance reached a steady-state value of 0.63.

Wallace and Copley [9] performed laser shaping of Si_3N_4(involving overlapping of multiple laser grooves), using a continuous wave (CW) CO_2 laser beam scanning on a rotating workpiece. The material removal rate and surface roughness were correlated with the laser process parameters. The significant results of this study were that the material removal rate in laser shaping was higher than in diamond profile pantograph grinding but that deep grooving produced a large number of cracks. The number of cracks produced was reduced by using a lower laser power and orienting the electric field vector of the light wave perpendicular to the walls. Morita et al. [10] studied the Nd:YAG laser machining of hot-pressed Si_3N_4, using both normal pulsed (msec) and Q-switched (nsec) lasers. The results indicated that cracking was reduced by reducing the pulse length from msec to nsec or decreasing the pulse repetition rate from 50 kHz to 0.1 kHz. The recast layer thickness was also reduced. Short pulses and low repetition rates assisted in reducing the thermal stresses and the number of thermal shocks as well as in preventing formation of a recast layer. However the peak power for a given pulse length increased both cracking and the thickness of the

recast layer. X-ray analysis of the recast layer revealed the presence of Si rather than SiO_2 or Si_3N_4. It was concluded that the recast layer is formed by condensation of vaporized silicon generated by the decomposition of Si_3N_4. Morita et al. [10] further observed that the bending strength of laser machined specimens is about 15% lower than that of those produced by diamond ground specimens because of the absence of compressive residual stresses in the laser machined specimens. Wehner and Burstrom [11] investigated the excimer laser finishing of diamond-ground Si_3N_4 in an attempt to eliminate the surface defects including cracks. The excimer laser beam was able to ablate a micron-thick layer per pulse due to the high intensity and thereby heal the surface defects. Tests indicated that the bending strength exceeded 600 MPa after excimer laser removal of the surface layer by about 30 to 40μm.

Hsu and Copley [12] conducted a laser milling study on graphite using a pulsed CO_2 laser. Material removal occurred while scanning the focused beam across the workpiece in parallel, overlapping grooves. By tilting the beam or workpiece, steps and cylindrical contours were generated. Chryssolouris et al. [13] performed laser grooving of carbon/teflon and glass/polyester composites and reported a linear relationship between groove depth and energy density of the laser beam. However the dimensional accuracy and surface finish could not be correlated with the energy density alone. These authors developed models to predict the groove depth, but such models overestimated the experimental values when using a CW beam and underestimated the experimental values for a pulsed laser beam. They subsequently added the corrections for heat losses and chemical interactions to improve the model and thereby obtained better agreement with the experimental data.

It is clear from the above discussion that a systematic investigation of laser

milling is essential to fill the gaps created by other researchers. Hence the objective of the present study was to better understand the laser milling process so as to obtain increased material removal rate, improved surface finish and tolerance and the production of crack-free surfaces.

3.4 Experimental Details

3.4.1 Material

Reaction-bonded silicon nitride (RBSN) is a ceramic material that is difficult to machine due to its brittleness and quasi-isotropic nature. It is obtained by heating silicon powder at temperatures in the range 1400-1700 K in a nitrogen atmosphere to form silicon nitride. The reaction occurs by either a gas/solid or a gas/vapor interaction, depending on temperature, to form very small crystals of silicon nitride, which tend to fill the porosity in the original compact, with a minimum change in dimensions. Since penetration of nitrogen gas to the center of the shape is difficult to achieve, density rarely exceeds 85% of the theoretical 3.19 Mg/m^3 [14].

The microstructure of RBSN consists of two phases of crystals (alpha- and beta-Si_3N_4), with a considerable amount of porosity. Open porosity is generally an undesirable feature, since it offers a large internal surface area for absorption of dirt and attack of corrosive liquids, but in the case of laser processing, this high volume porosity allows the laser beam energy to be effectively absorbed. Open porosity is also desirable for optimizing thermal shock resistance for filter media, for catalyst supports and for friable or crushable material. Microstructure is also important in determining thermal conductivity, because the types of phase and their distribution within a material can also be varied. The presence of porosity and minor phases at

grain boundaries influence thermal conductivity by the scattering effect of phonon and radiation. The decomposition temperature for silicon nitride can be assumed to be equal to 2150 K as suggested by Solomah [5] and Ramanathan and Modest [18]. This value was formerly found to agree with measurements made during the machining of silicon nitride [31].

Kitagawa and Matsunawa [7] more recently have suggested that in laser machining the evaporation energy is the dominant variable in determining processing conditions. These authors also stated that it is well understood that machining of Si_3Ni_4 is mainly based on the decomposition process. Therefore although the evaporation temperature is in the range of 2700-3300 K, decomposition occurs at a lower temperature namely 2150 K. Machining of silicon nitride can be assumed to occur at temperatures above 2150 K, in the case of mechanical removal (cutting tool or assist gas pressure) but higher temperatures may be required for unassisted machining. The thermal and physical properties of RBSN are listed in Table 3.1.

Table 3.1: Properties of RBSN [15]

Bulk density	2500 kg/m^3
Specific heat	712 J/kgK
Thermal conductivity	13 W/m K
Decomposition temperature	2150 K
Melting temperature	1698 K
Latent heat of vaporization	8.312 x 10^6 J/kg
X-ray analysis	α form 65%, β form 32%, Si_2ON_2 3%
Microporosity	18%
Knoop hardness	1700 kg/m^2
Coefficient of thermal expansion	3 x 10^{-6} sec^{-1}

3.4.2 Laser Milling

The laser milling process is similar to conventional end milling, but the cutting tool is replaced by the laser beam. The process involves impingement of the laser beam normal to the workpiece. In the present work a computer numerical control(CNC) unit was used to control the motion of an X-Y table on which the workpiece was mounted. The CNC motion precisely creates a blind-cut geometry specified by the computer program.

The laser milling system used in this work is illustrated in Figure 3.1. The laser source was a 1.5 kW (maximum), CW CO_2 laser (Rofin Sinar Model 820). The beam was delivered to the workpiece through a beam delivery system with a ZnSe lens of 127 mm focal length. The workpiece was mounted on a CNC X-Y positioning table. Figure 3.2 shows the schematic of the milling procedure in which the laser beam is scanned across the workpiece resulting in multiple, overlapping grooves. Table 3.2 lists the process variables employed.

Table 3.2: Process variables used in the work

Laser	CW CO_2
Wavelength	10.6 μm
Power	500 W, 1000 W
Beam focus	on surface and above surface (6-37 mm)
Focused spot size	0.25 mm
Scan rate	42 mm/sec to 170 mm/sec
Distance between scans	0.05 mm
Coaxial assist gas	oxygen/nitrogen/air
Gas pressure	207 KPa
Processes	Grooving and milling

3.4.3 Measurement and Analysis

Following laser milling, specimens were carefully sectioned using a diamond wheel. The depth of cut was then measured using an optical microscope. Surface roughness (R_a) was measured in the longitudinal (laser scan direction)and transverse direction of the machined surfaces using two surface profilometers (Sheffield QB Model 8 and Dektak-IIA). A scanning electron microscope (SEM) was used to analyze crack formation and the recast layer.

3.5 Thermal Models

3.5.1 Model for Predicting Preheating Temperature

Laser milling is a process that involves the generation of multiple, overlapping grooves. The workpiece temperature increases with an increase in the number of overlapping laser scans; other laser parameters remain constant. The average increase in temperature of the workpiece, represented as preheating temperature, is expected to play a significant role in determining the depth of cut, recast layer and surface roughness. The preheating temperature is computed using a heat conduction model described below.

The following assumptions were made:

1. The decomposition temperature is developed at the laser spot radius
2. There is no loss of heat from the surface by radiation
3. Heat flows in the x and y direction and no heat flow in the z direction (Figure 3.2 a)

4. Thermal property is independent of temperature

5. No phase transformation occurs

6. The substrate is a semi-infinite solid

7. Quasi-steady state

The solution for a moving heat source in the infinite media is well known and is given by [16]:

$$T = \frac{\epsilon P'}{2\pi K} e^{\frac{-vx}{2k}} K_0(\frac{vr}{2k}) + T_0 \tag{3.1}$$

Now consider the linear flow of heat in the region $-\infty$ <x< ∞ with the initial condition; when t = 0.0 sec,$T = f(x)$ where,

$$f(x) = \frac{\epsilon P'}{2\pi K} e^{\frac{-vx}{2k}} K_0(\frac{vr}{2k}) + T_0 \tag{3.2}$$

But when t > 0, the above equation can be written in the integral form as follows[17]

$$T = \frac{1}{2\sqrt{\pi K t}} \int_{-\infty}^{\infty} f(x\prime) \frac{e^{-(x - x\prime)^2}}{4Kt} dx\prime + T_0 \tag{3.3}$$

Consider the laser beam at the spot 'a'(Figure 3.2) moving with a specific velocity v. The time taken to travel the spot 'a-B-C-b' varies between 0.15 sec and 0.60 sec corresponding to beam velocities of 170 mm/sec and 43 mm/sec. As the laser beam moves towards the spot 'b', the preheating temperature surrounding and near to the spot 'b' also contributes temperature towards that spot. The preheating phenomena is very complex, which consists of quasi-steady state heat flow in the semi-infinite region, transient heat flow near to the edge of the plate and no heat flow at a location away from the edge and also the laser beam along the cutting axis contributes

preheating temperature. But for simplicity the preheating temperature is calculated based on under quasi-steady state condition. Hence in practical more preheating temperature is expected than the theoretical calculation. A Fortran program was developed based on equation (3.3) and was used to calculate the preheating temperature corresponding to different times. A detailed program is enclosed herewith in appendix A.

3.5.2 Thermal Modeling for Predicting the Depth of Cut

A theoretical model was formulated to estimate the depth of cut that takes into account chemical decomposition and the preheating due to the overlapping of laser scans.

The following assumptions were made to formulate the problem:

1. The beam intensity is constant during irradiation and is of sufficient magnitude to cause decomposition
2. The beam has a Gaussian energy distribution
3. The vapors created during irradiation are transparent to the laser beam
4. The heat changes associated with the formation and dissociation of the recast layer are neglected
5. Thermal properties are independent of temperature
6. Absorptivity for silicon nitride is taken as 0.3 for grooving [18]

7. Absorptivity for silicon nitride is taken as 0.4 for milling because multiple beam reflections from the walls of grooves as well as preheating temperature from the previous cut

8. The preheating temperature at various speeds due to multiple, overlapping scans is calculated by considering at the laser spot to be at the decomposition temperature

The decomposition reaction can be written as:

$$Si_3N_4(s) \rightarrow 3Si(l) + 2N_2(g)$$

When heated slowly at atmospheric pressure (Si_3N_4) decomposes into silicon and nitrogen gas at a temperature of 2150 K [18]. As the temperature is raised above the decomposition temperature, the decomposition pressure increases and large pores form leading to blistering and bloating. This kind of defect is particularly common when high heating rates are used [19]. Nitrogen has been observed to diffuse through a thin silicon layer at lower temperature but at higher temperature explosive removal of nitrogen takes place. Subsequent removal of the silicon [in the molten state] is accomplished by a high pressure gas jet coaxial or off -axial with the laser beam. If the silicon is not completely removed, it resolidifies to form the recast layer. If oxygen is present, then the silicon reacts with O_2 to form SiO_2.

The physical model considers a distributed heat source coupled to an inward propagation of a moving solid-vapor interface. As a result of decomposition and subsequent vaporization of the silicon, the solid-vapor interface moves in the z-direction (depth direction) at a speed of v. The situation is considered in which a subsurface depth d can be vaporized with a beam of power P moving across a surface with velocity. If the intensity I varies with time, then the depth vaporized can be written

as [20].

$$d = \int_0^{t_p} z\prime(t)\, dt \tag{3.4}$$

where

$$z\prime = \frac{I}{\rho(L_v + CT_v)} \quad \text{Grooving}$$
$$z\prime = \frac{I}{\rho(L_v + C(T_v - T_i))} \quad \text{Milling}$$

and

$$I = 2\frac{P\epsilon}{\pi w^2}$$

This equation is derived, based on the assumption that no recast layer is present along the kerf width. The recast layer is either vaporized or removed from the cutting edge by high pressure assist gas.

3.5.3 Model for Predicting Surface Roughness

The roughness of laser milled surfaces may be predicted using a model that considers the depth of groove, the overlap distance and the beam diameter. The model developed here does not consider the presence of a recast layer and assumes that the groove profile is represented by a triangle (Figure 3.3). The mean depth D$\prime$ is given by Copley et al. [21].

$$D\prime = \frac{D_0}{z}\int_0^z exp(-z^2/2)dz \tag{3.5}$$

where $z = 0.707f/w$ and D_0 is the maximum groove depth

Boothroyd and Knight [22] gave an expression for surface roughness as:

$$R_a = 4\frac{(area\ of\ triangle\ a'b'c')}{f} \tag{3.6}$$

Equation (3.7) may be simplified to:

$$R_a = \frac{|D_0 - D'|}{2} \tag{3.7}$$

If the triangular shape is changed to a Gaussian shape for representing the groove profile, equation (3.8) is approximately given by:

$$R_a = \frac{1.25|D_0 - D'|}{2} \tag{3.8}$$

3.6 Results and Discussion

3.6.1 Laser Grooving Using a Focused Beam

Figure 4 shows the effect of laser power and scan rate on grooving depth. Both high power and low scan rate increased the depth of cut as expected. Figure 4 also shows that the analytical model predicted the groove depth at higher scan rates better than at lower scan rates which can be attributed to the significant radiation loss at the lower scan rate. Deeper cuts (greater than 0.5 mm) are accompanied by visible cracks, thick recast layers and very rough surfaces. Copley and Wallace et al. [23-24] conducted 1 kW CO_2 laser grooving of hot-pressed silicon nitride and reported groove depths 0.01 - 0.5 mm with increasing scan rate. They concluded that polarization is a key factor that affects the shape of the groove. A linearly polarized beam parallel to the scanning direction provided that the groove was straight, narrow and deep. Otherwise the groove shape was skewed towards the polarization direction. In addition to polarization, higher power and lower speed promoted the curvature

of the grooves. In the present work, a circularly polarized beam was used which produced a sharp V-shaped groove.

It was observed in laser grooving that the assist gas-jet could not completely expel the liquid silicon and, as a result, a recast layer of silicon was formed. The groove walls had a much thicker recast layer than the bottom surface. Chryssolouris [25] recommends that an off-axial gas jet oriented at 45^0 to the laser beam can be used to minimize the recast layer. Reduction of the amount of recast layer assists in producing deeper grooves because the recast layer in the liquid state absorbs more laser energy which would otherwise remove additional material [26]. The formation and build-up of the recast layer generates cracks due to thermal expansion mismatch between silicon and Si_3N_4 and also causes development of rough surfaces. In order to eliminate cracking, Firestone and Vesley [26] preheated Si_3N_4 to 1273 K prior to CO_2 laser machining. Although the machining rate was increased by an order of magnitude and visible cracks were not identified, the process of preheating the substrate was expensive and cumbersome.

Crack-free grooving of Si_3N_4 can be achieved when the laser is changed from CO_2 to Nd:YAG. Harrysson and Herbertsson [27] reported that cracks were significantly reduced when a Nd:YAG laser was used (over a CO_2 laser) in the hole drilling of hot isostatically pressed (HIP) Si_3N_4. Although no explanation was provided for this effect, we believe that the lower wavelength Nd:YAG laser is better absorbed by Si_3N_4 which in turn facilitates the decomposition reaction to Si vapor and N_2 gas and thus reduces the recast layer formation. Morita et al. [10] found that pulse duration should be under 65 μs and pulse repetition rate should be under 10 kHz to obtain crack-free processing of Si_3N_4 using Nd:YAG lasers. However the groove depth was

very limited (about 0.3 mm maximum) under these conditions. Islam et al. [28] confirmed that the cracking tendency in ceramics during laser machining is a strong function of pulse duration. Morita et al. [29] investigated Nd:YAG laser machining of Si_3N_4 under water and reported a reduction in cracking and the amount of the recast layer formation possibly due to the prevention of Si vapor reaching the saturation level.

The cracking tendency is also related to the type of Si_3N_4. In the present study, RBSN was used as the substrate which by virtue of its porosity provided relief to thermal stresses during the laser machining and thereby reduced cracking. Thus deeper cuts were made possible without cracking in RBSN compared to hot-pressed Si_3N_4. For example, the maximum crackfree grooving depth was 0.73 mm (in the present study) and 0.6 mm [7] respectively for RBSN and hot pressed Si_3N_4.

3.6.2 Laser Rough Milling using a Focused Beam

Figure 3.5 shows the calculated preheating temperature at a given spot as a function of time. For high-speed processing, the time to reach the given spot is short and hence higher preheating temperature can be achieved. The preheating temperature varies with laser power, scan rate, and number of laser scans. Figure 3.6 shows the experimental data relative to the variation of milling depth with scan rate. A comparison with grooving indicates that milling produces a larger depth of cut which is clearly an effect caused by the preheating of the substrate due to overlapping laser scans. Contrary to the present finding, Wallace and Copley [9] reported that in CO_2 laser machining of Si_3N_4, the material removal rate in milling (overlapping multiple grooves) is equal to grooving. The most interesting observation

in our study of milling was the build-up of the recast layer with increasing number of laser scans. The increase in milling depth due to the preheating temperature is indeed offset to some extent by the increased thickness of recast layers. Figure 3.7 shows that as the number of laser scans was increased to obtain larger area coverage, the milling depth became lower because the build-up of recast layers tended to become excessive. The fact that Wallace and Copley [9] did not observe any difference in the depth of cut between milling and grooving may be attributed to a large number of overlapping scans that produced thicker recast layers and thereby eliminated the effect of preheating.

Laser milling requires successive, overlapping passes. The first pass of the laser cut, contributes to the preheating temperature. Subsequent passes increase the preheating effect on the workpiece. As the number of passes increases, the depth of cut also increases, which is shown schematically in Figure 3.8. The preheating eventually reaches a steady state, after which the depth of cut remains constant. It has also been observed that each laser pass generates a groove and a recast layer, irrespective of the preheating temperature. It is to be noted that there is very little recast layer formation during the first cut. Ridge formation occurs in subsequent laser scans and this can be explained as follows: there is a steep temperature gradient due to the preheating effect which in turn causes a surface tension gradient on the groove. Higher surface tension regions pull the molten layer away from the lower surface tension regions, thereby resulting in ridge formation. As the number of scans increases (i.e. width of the milled surface increases), the preheating temperature also increases, which causes a larger temperature gradient that in turn results in a higher surface tension gradient leading to formation of a thicker recast layer. Hence the depth of

cut gradually decreases.

The experimental and analytical model data for laser milling are plotted in Figure 3.9 which shows that the data are only in fair agreement when compared with the grooving data shown in Figure 3.4. This is explained in terms of the presence of a thick recast layer which is not taken into account in the analytical model. X-ray analysis revealed that the recast layer consisted mostly of silicon (and some SiO_2) as a result of the decomposition of Si_3N_4. Since the melting temperature of silicon (1685 K) is readily obtained in laser machining, lower scan rates that give rise to higher temperatures increased the recast layer thickness. SiO_2 (white layer in Figure 3.10) is not discernible at low scans rate partly due to the unfavorable thermodynamics conditions of Si reacting with O_2 to form SiO_2.

Laser milling using a focused beam was found to produce rough surfaces. The surface profilometer traces, shown in Figure 3.11, show that the surface roughness exceeded the maximum limit (30 μm) of the profilometer (Sheffield QB, Model 8) and that the average peak-to-valley decreased with an increase in scan rate. Copley [30] observed a similar increase in surface roughness when the scan rate was reduced especially to a level that it was smaller than the width of the scan. He explained this to be due to the, "light guiding effect" in which the laser beam is deflected from the side into the bottom of the previous groove.

The type of assist gas introduced coaxially with the laser beam significantly affected the depth of cut, the recast layer and the surface roughness. It was clearly observed in laser grooving that oxygen assist gas increased the depth of cut (in comparison with nitrogen) which may be attributed to the contribution of oxidation in addition to decomposition of Si_3N_4. However in laser milling, the average depth of

cut was found to be lower for oxygen-assist as compared to nitrogen-assist gases. This may be due to the presence of a thick recast layer in oxygen-assisted laser machining. Figure 3.12 is a schematic that demonstrates the effect of oxygen, nitrogen and air on milling depth and recast layer. It should be noted that deeper cuts were obtained in the first and last scan of laser milling. Additionally as the width of the milled surface increased (by increasing the number of laser scans), the depth of cut gradually decreased due to the increased amount of the recast layer.

It is commonly accepted that the material removal in CO_2 laser machining is essentially due to the decomposition of Si_3N_4 in to Si liquid and N_2 gas. In order to expel the liquid Si, a coaxial or offaxial gas jet of oxygen or nitrogen is used. Copley [31] first reported that an oxygen assist gas provided deeper grooves than a nitrogen assist gas in CO_2 laser machining of Si_3N_4. Later Wallace and Copley [32] confirmed that there was no change in material removal rate by changing the gas from oxygen to nitrogen. It appears from their work that oxidation contributes very little or none in laser machining of Si_3N_4. In our work, oxygen played a major role in affecting the depth of cut by providing additional energy in grooving and by allowing recast layer formation in milling (see Table 3.3)

Table 3.3: Effect of the assist gas on grooving and milling depth Power: 500 W, Speed: 170 mm/sec, [ref. Figure 3.12 for milling]

Laser Process	Oxygen	Nitrogen	Air
Grooving	0.56 mm	0.38 mm	0.40 mm
Milling	0.21 mm	0.36 mm	0.24 mm

Visible observation indicated that a better surface finish was obtained in laser milling when nitrogen gas, instead of oxygen gas, was used. This is in sharp contrast to laser cutting where improved surface finish was obtained with oxygen rather than nitrogen [6]. The difference between laser cutting and milling is believed to be due to two reasons: one is that the recast layer is substantially less in laser cutting due to the development of a large pressure gradient (thus the gas-jet is able to push the molten layers through the bottom of kerf) while the second is the increased cutting speed as a result of the additional energy supplied by the exothermic reaction of oxygen with Si_3N_4.

3.6.3 Laser Fine Milling Using Defocused Beams

Laser milling of RBSN was carried out using defocused beams with the aid of oxygen assist gas. Figure 3.13 shows that the depth of cut decreased from 0.48 mm to 0.01 mm as the beam was defocused by the distance 0.0 mm to 37 mm from the workpiece surface. The defocused beam assisted in reduction of the size of the recast layer and also prevented crack formation (Figure 3.14) both of which are attributed to lower temperatures at the cutting front. Defocused beams generated smooth surfaces as can be seen in Figure 3.15 (which shows that the R_a value decreases with an increase in defocusing distance). The analytical model does not predict the surface roughness values partly due to the fact that the recast layer thickness is not taken into account (Figure 3.15). From an examination (Figure 3.16) of the surface roughness profiles in the transverse direction, it is clear that the surface finish obtained (R_a = 0.43 μm, Figure 3.16(b)) was better than that obtained from the diamond-cut sample (R_a = 0.8 μm)(Figure 3.17a).

Copley's study [30] of the laser machining of Si_3N_4 showed that the best surface finish obtained with a focused beam was 7.5 μm RMS. Wallace and Copley [9] reported that the best R_a value obtained in laser milling was 2.9 μm at a traversing speed of 2380 mm/sec (depth of cut 0.19 mm).

In the present work laser milling generated thick recast layers which in turn reduced the depth of cut and increased the surface roughness. A double laser milling procedure in which a focused beam was first used for milling followed by a defocused beam for finishing the milled surface was performed to eliminate the recast layer. This procedure resulted in much smoother finish, (R_a 2.8 μm) for 0.5 mm depth of cut, (Figure 3.17b), especially when compared with the single laser milling procedure using a defocused beam that provided an R_a value of 4.7 μm (Figure 3.16a). In addition, most of the recast layer was removed, while the flaws were healed (Figure 3.18). This may be explained by the increased absorption of laser energy by the recast layer which subsequently vaporized.

3.7 Conclusions

Laser grooving and milling of reaction bonded silicon nitride (RBSN) was carried out using a 1 kW continuous wave CO_2 laser. The phenomena of preheating during laser milling is played a key role for determining the depth of cut. It is expected that the actual preheating temperature is higher than the calculated temperature, where the multiple reflection of the laser beam and the preheating temperature contributed along the cutting edge (but the preheating temperature from the previous path is considered) is not considered. Based on the above assumptions an analytical model was developed to estimate the grooving depth, milling depth and the surface rough-

ness, and the results were compared with experimental data. The major results and conclusions are:

1. For a given set of laser processing conditions, milling produced a larger depth of cut than grooving. This may be attributed to the effect of the preheating temperature and the increased absorptance associated with multiple, overlapping laser scans.

2. In laser milling, the development of a large temperature gradient due to overlapping laser scans promoted a surface tension gradient and thereby assisted in the formation of a thick recast Si-layers. Recast layer thickness increased with an increase in the number of overlapping scans.

3. The increase in depth of cut was larger when nitrogen was used instead of oxygen as an assist gas in laser milling.

4. The best surface finish (R_a 0.43 μm) was obtained with defocused beams at a very low depth of cut (0.01 mm) when using single laser milling procedure. Deeper cuts were accompanied by rougher surfaces. A double laser milling procedure was found to be capable of providing a surface roughness of 2.8 μm for a depth of cut of 0.5mm.

5. In RBSN, microcracks were not identified for depths of cut less than 0.73 mm. For hot pressed Si_3N_4, microcracks were readily obtained when the depth of cut exceeded 0.60 mm [7]. The difference may be attributed to the inherent porosity present in RBSN that allowed a reduction in the magnitude of the thermal stresses developed.

3.8 References

[1] Naeem, M., Preston, M. E., and Tyrer, J. R., "Machining of engineering ceramics with high power CO_2 laser",*Advanced Manufacturing Engineering*, 2, (1990), 27-31

[2] Firestone, R. F., "Laser and other non-abrasive machining methods for ceramics", in *Advanced Ceramics 87 conference*, 17-19 Feb (1987), MR 87-112-6

[3] Sheppard, L. M., "Machining of advanced ceramics", *Advanced Material and Processes Inc., Metal Progress*, 12, (1987), 40-43

[4] Morita, N., "Crack-free processing of hot-pressed Silicon Nitride Ceramics using pulsed YAG laser", *Annals of CIRP*, 87, (1991,) 517-524

[5] Solomah, A. G., "Laser machining of silicon nitride", *Annals of CIRP*, 87, (1991), 543-546

[6] Yamamoto, J., Yamamoto, Y., "Laser machining of silicon nitride", *Proceeding of LAMP* (1987), Osaka, Japan, 297-303

[7] Kitagawa, A., Matsunawa, A., "Three dimensional shaping of ceramics by using CO_2 laser and its optimum processing conditions", *ICALEO*, (1990), 294-301

[8] Ramanathan, S., Modest, M. F., "Measurement of temperature and absorptance for laser processing application", *Journal of Laser Applications*, 6, 1, March (1994), 23-31

[9] Wallace, R. J., and Copley, S. M., "Shaping Silicon nitride with a carbon dioxide laser by overlapping multiple grooves", *ASME Journal of Engineering for Industry*, 111, November (1989), 315

[10] Morita, N., Watanbe, T., and Yoshida, Y., "Crack-free processing of hot-pressed Silicon Nitride Ceramics using pulsed YAG laser", *JSME International Journal*, Series Ill, 34, 1, (1991), 149

[11] Wehner M., and Burstrom, M., "Excimer laser machining of Silicon Nitride", *Ceramic Materials and Components for Engines*, lVth International Symposium, Elsevier Applied Sciences, (1992), 813

[12] Hsu R. K. C., and Copley, S. M., "Producing three-dimensional shapes by laser milling", *ASME Journal of Engineering for Industry*, 112, November (1990), 375

[13] Chryssolouris, G., Sheng, P., and Choi, W., "Three-dimensional laser machining of composite materials", *ASME Journal of Engineering Materials and Technology*, 112, October (1990), 387

[14] Morrell, R., *Hand book of Properties of Technical and Engineering Ceramics* Part 1, Her Majesty's Stationery Office, London, (1985), 50-86

[15] Sheu, C. J., "Thermal Treatment, Polishing and Grinding of Reaction Bonded Silicon Nitride", *M. S. Thesis*, (1990), Iowa State University, Ames, 21

[16] Rosenthal, D., "The Theory of Moving Sources of Heat and its application to Metal Treatments", *Transactions of the ASME*, November (1946), 849-866

[17] Carslaw H. S., & Jaeger, J. G., *Conduction of Heat in solids*, Second Edition, Oxford university press, New York, NY., (1980), 53

[18] Ramanathan S., and Modest, M., "Effects of variable thermal properties on evaporative cutting with a moving cw laser", *ASME Heat Transfer in Space Systems*, (1990), 101

[19] Kingery, W. D., Bowen, H. K., & Uhlmann, D. R., *Introduction to Ceramics*, Second edition, John Wiley & Son, New York, 505

[20] Ready, J. F., "Effects due to absorption of laser radiation", *Journal of Applied Physics*, 36, (1965), 462

[21] Copley S. M., et al., "Chapter 6 in Laser Materials Processing", *Materials Processing Theory and Practice*, 3, Volume Editor:M. Bass, (1983), 298

[22] Boothroyd, G., and Knight, W., *Fundamentals of Machining and Machine Tools*, Second Edition, Marcel Dekker, (1989), 167

[23] Copley, S. M., "Shaping ceramics with lasers, Interdisciplinary issues in Materials Processing and Manufacturing", *ASME*, 2, (1987), 631

[24] Wallace, R. J., Bass M., and Copley, S. M., "Curvature of laser machined grooves in silicon nitride", *Journal of Applied Physics*, 59, 10, (1986), 3555

[25] Chrryssolouris, G., *Laser machining: Theory and Practice*, Springer Verlag, New York, NY., (1991), 236-237

[26] Firestone, R. F., and Vesley, E. J. Jr., "High power laser beam machining of structural ceramics", *ASME Symposium on Machining of Advanced Ceramic Material and Components*, Chicago, II , November 27, (1988)

[27] Harrysson R., and Hebertsson, H., "Machining of high performance ceramics and thermal etching of glass by laser", *Proceedings of the 4th International Conference on Lasers in Manufacturing*, May (1987)

[28] Islam, M. U., McGregor, G., and Campbell, G., "Laser rough and finish machining of hard materials", *U.S. Patent No. 5,138,130*, (1992)

[29] Morita, N., Watanabe, T., and Yoshida, Y., "Pulsed laser processing of ceramics in water", *Applied Physics Letters*, 52, 23, (1988)

[30] Copley, S. M., "Laser shaping of materials", *Lasers in Materials Processing, Proc. of ASM Conference*, Los Angeles, CA, Jan 24-26, (1983)

[31] Copley, S. M., "Laser machining of ceramics", *Proceedings of the first international Laser Processing Conference*, Anaheim, CA, Nov. 16-17, (1981)

[32] Wallace R. J., and Copley, S. M., "Laser machining of Silicon Nitride", *Energetics, Advanced Ceramic Material*, 1, 10, (1986), 3555

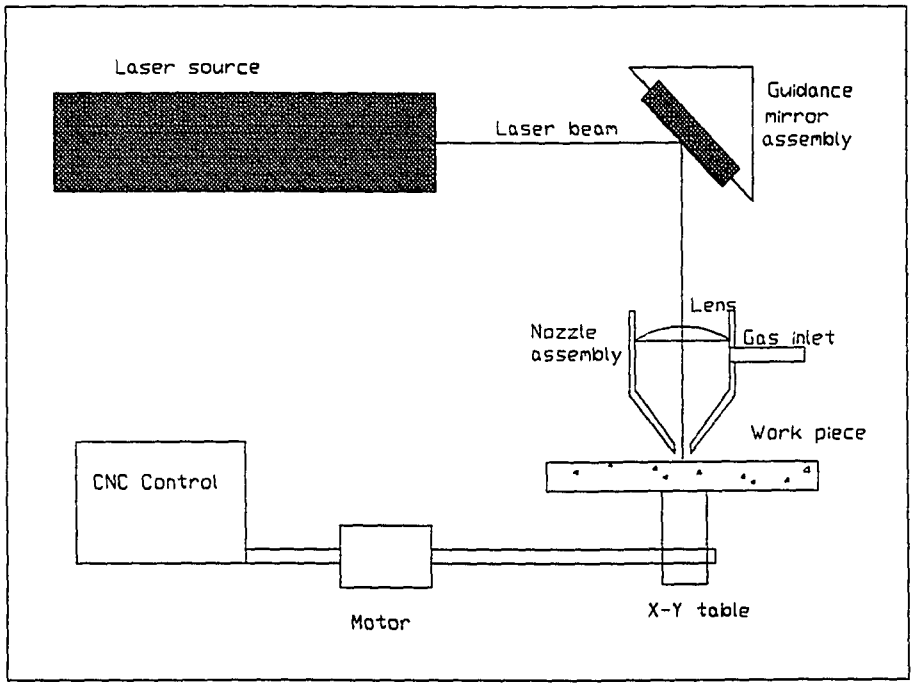

Figure 3.1: A Schematic of the Laser Milling Machine Tool employed in this Study

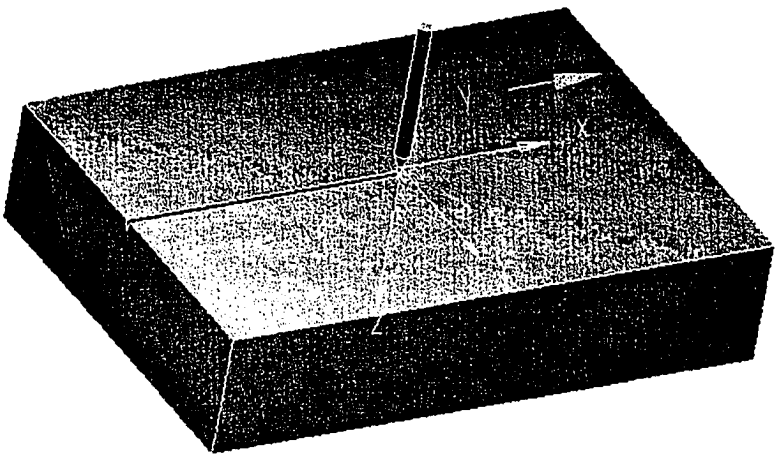

(a)

Laser Scan Process Parameters

Scanning Length AB:	37.00 mm
Distance between a-B-C-b:	12.50 mm
Scanning Pitch BC:	00.05 mm

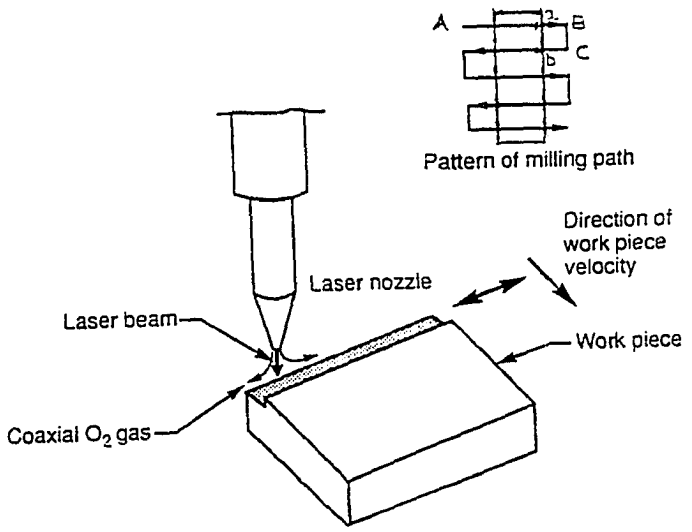

(b)

Figure 3.2: (a)Direction of Moving Heat Source, (b) A Schematic Showing the Laser Milling Procedure

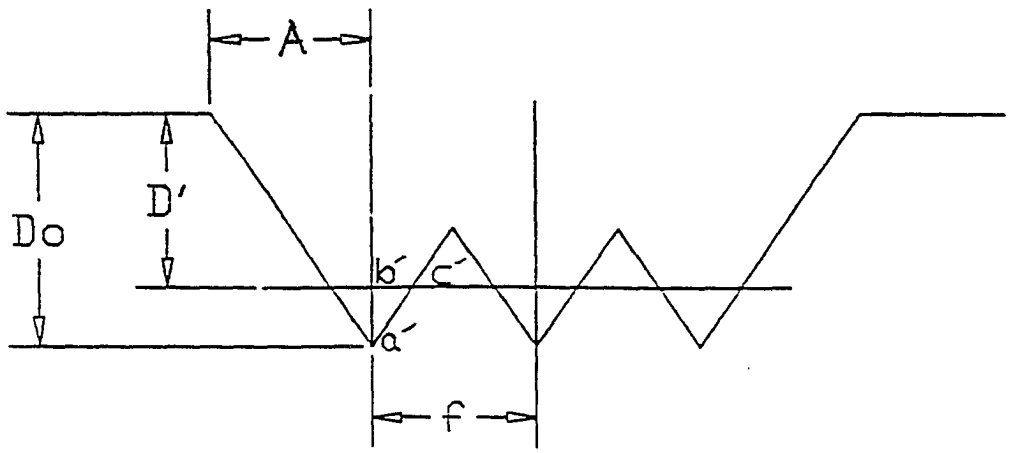

Figure 3.3: A Schematic Representation of Grooves in Laser Milling

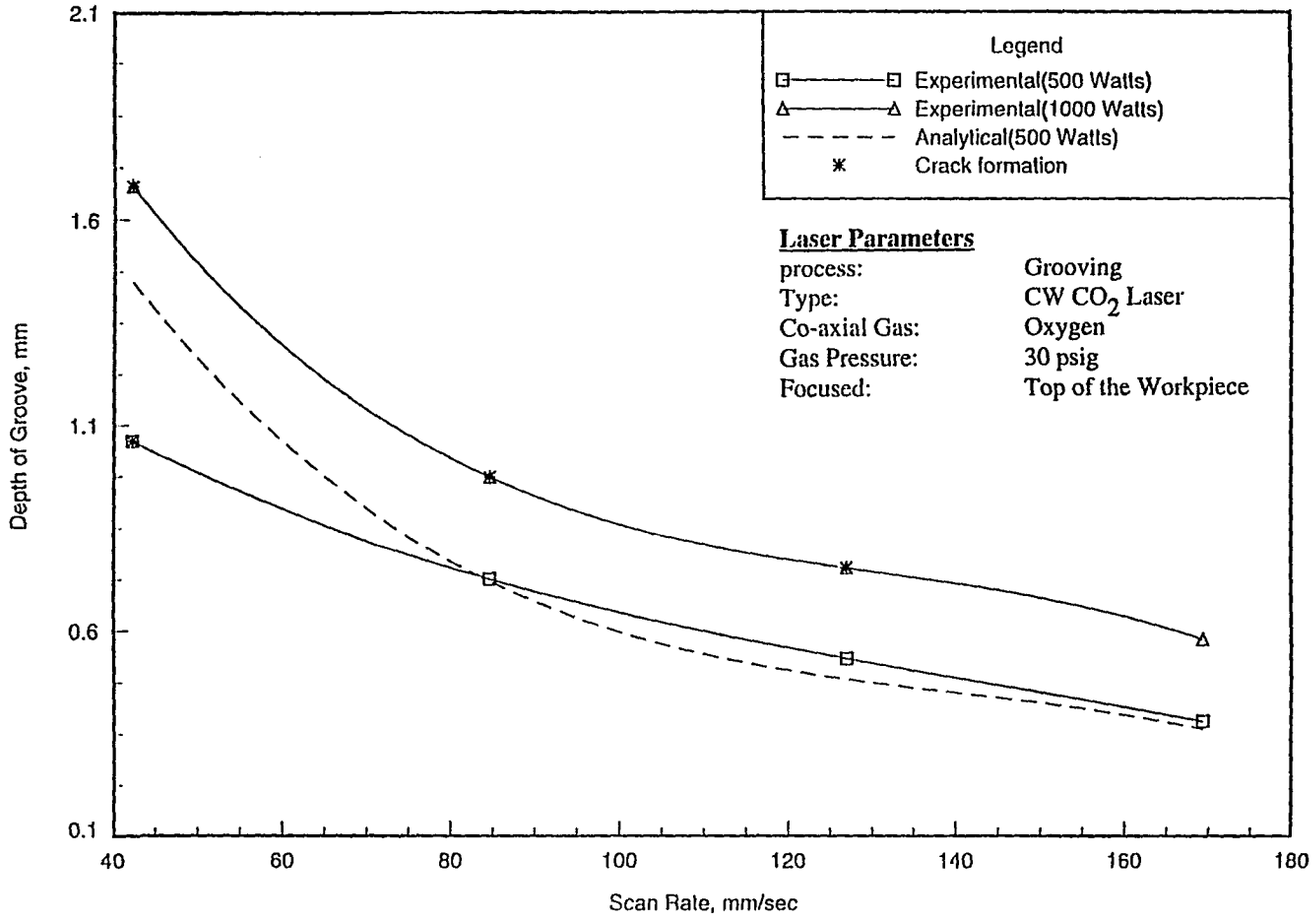

Figure 3.4: Effect of Laser Power and Scan Rate on Groove Depth

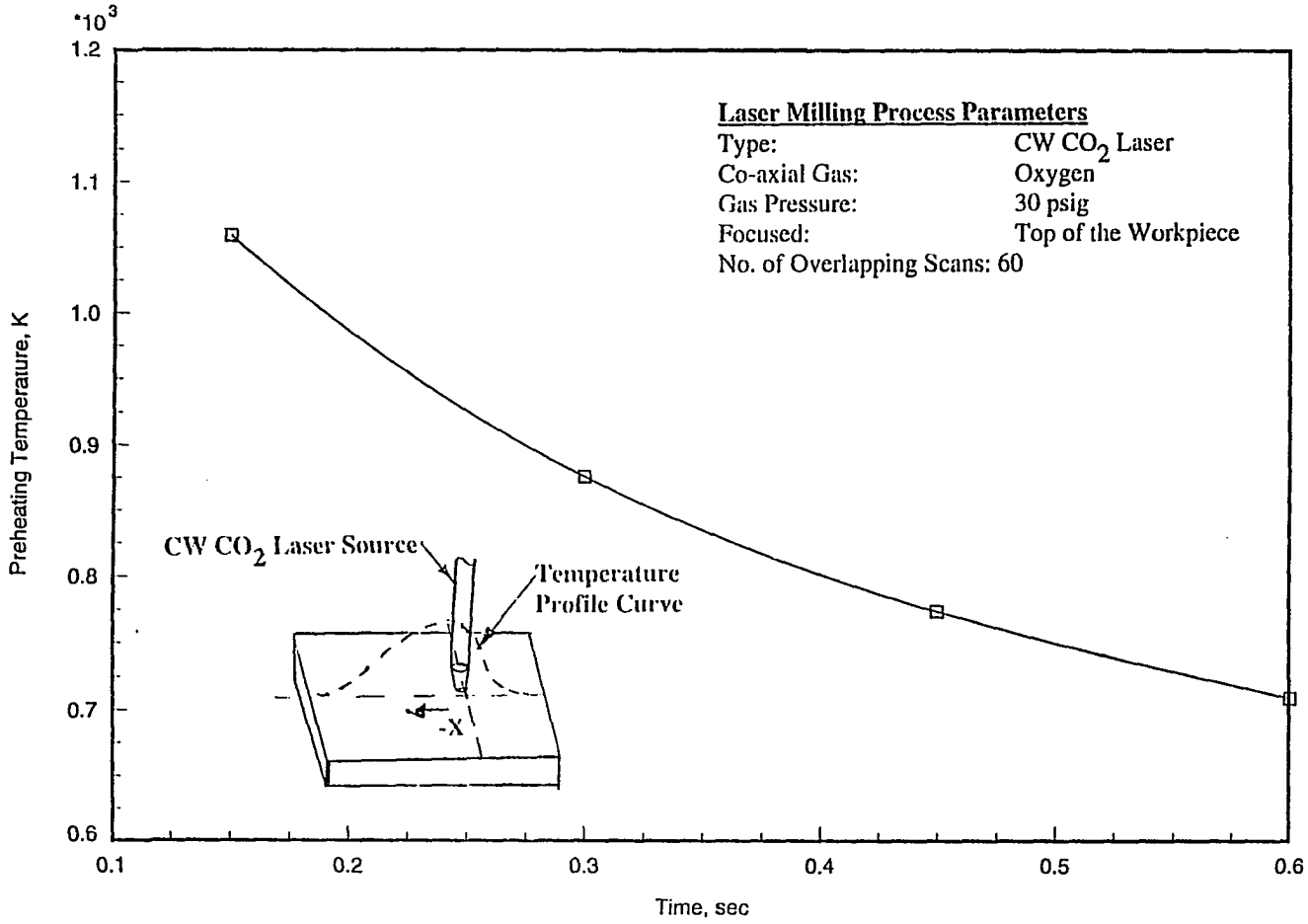

Figure 3.5: Temperature Distribution at Different Time for Determining Preheating Temperature

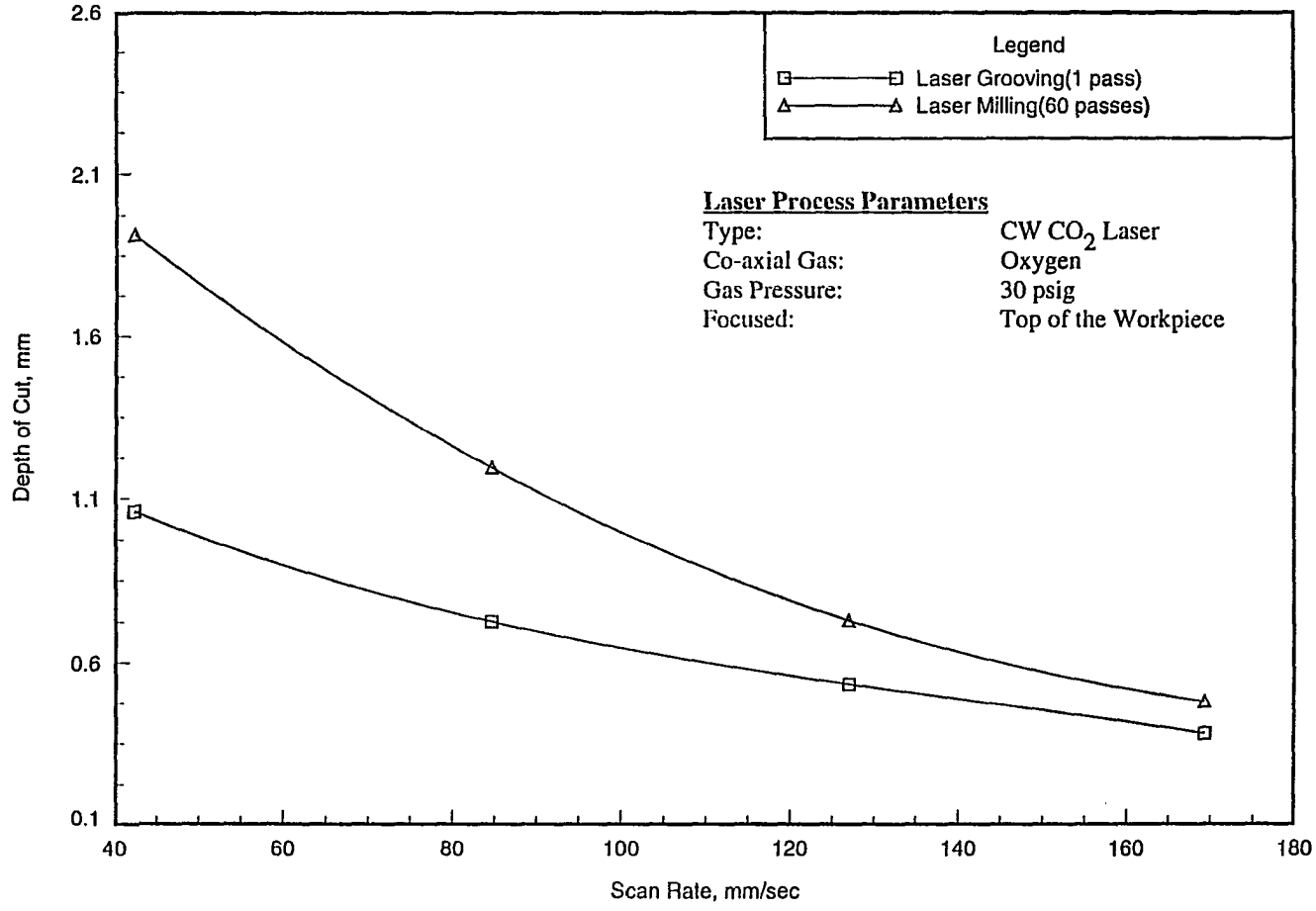

Figure 3.6: A Comparison of Depth of Cut between Grooving and Milling

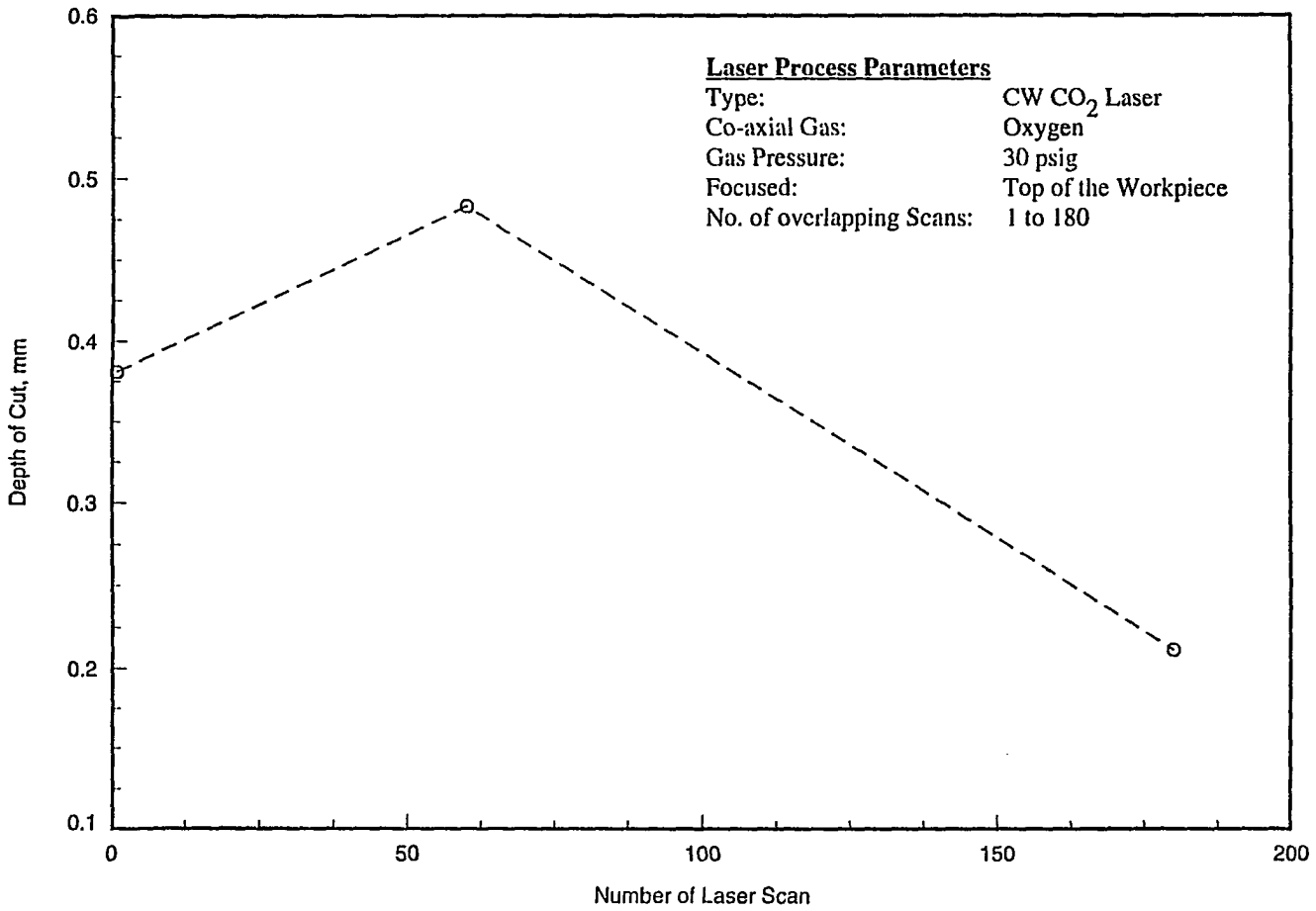

Figure 3.7: Effect of Laser Scan on Depth of Cut

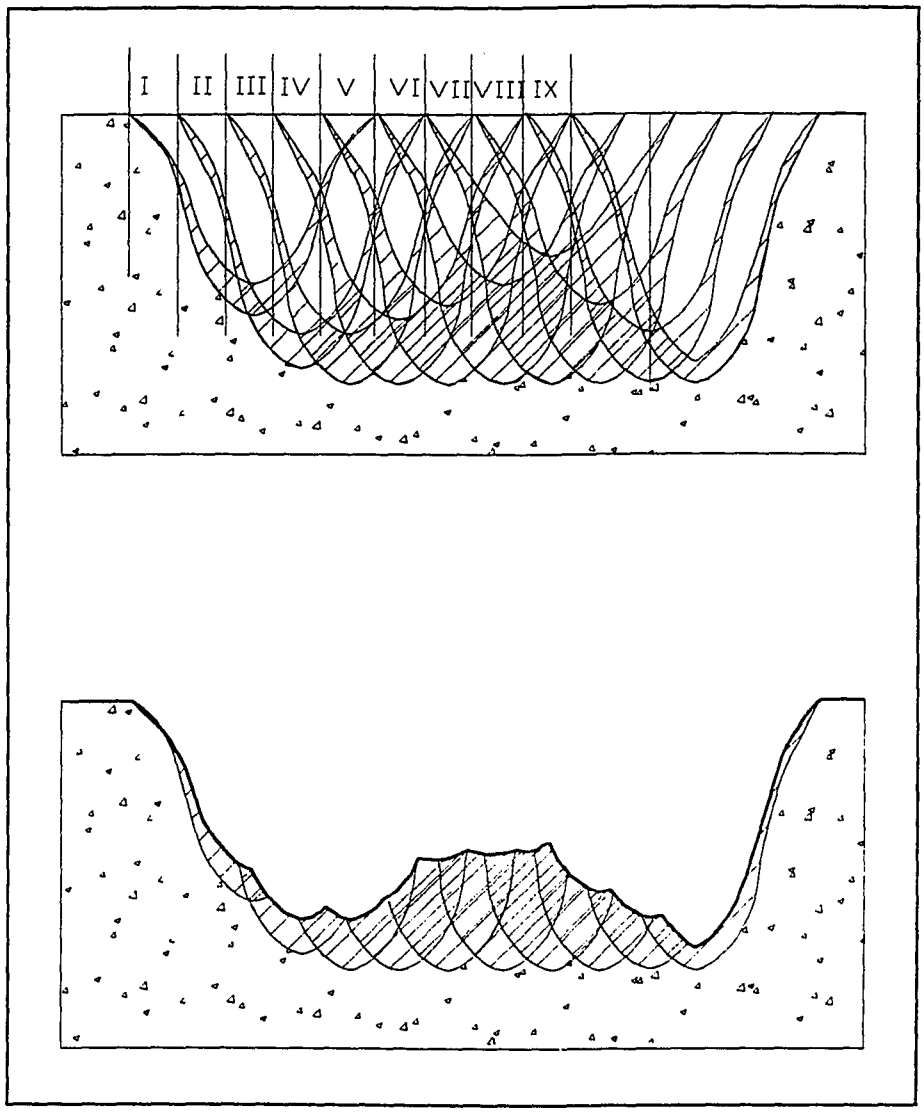

Figure 3.8: (a) Milling Path with Overlapping Distance, (b) Milling Contour with Recast Layer Buildup

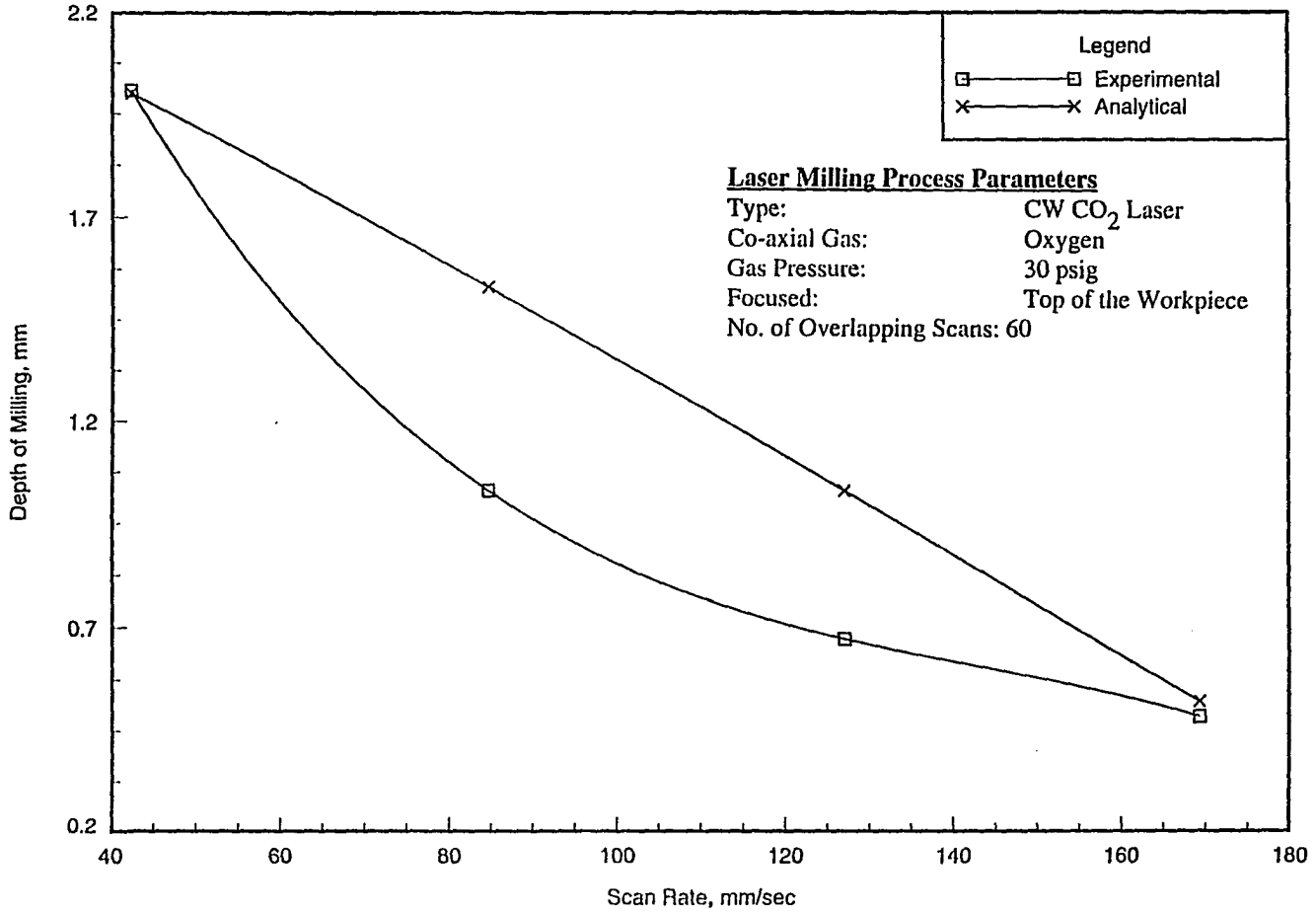

Figure 3.9: Effect of Scan Rate on Milling Depth

Figure 3.10: Scanning Electron Micrograph of Laser Rough-Milled Surfaces Processed at Scan Rate of 170 mm/sec (Assist Gas: Oxygen)

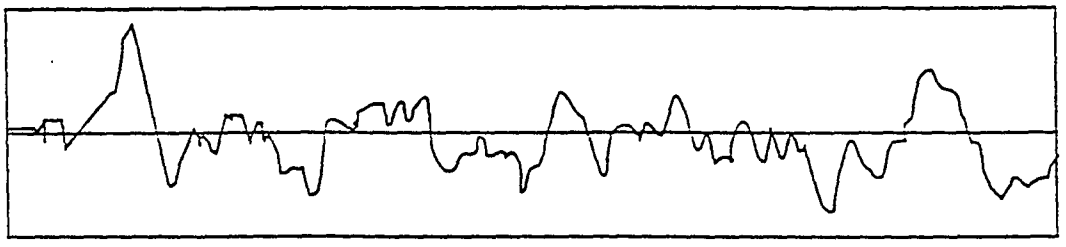

Power = 500 W, laser beam speed = 200 in./min
Ave. peak-to-valley distance = 7.4(relative value)

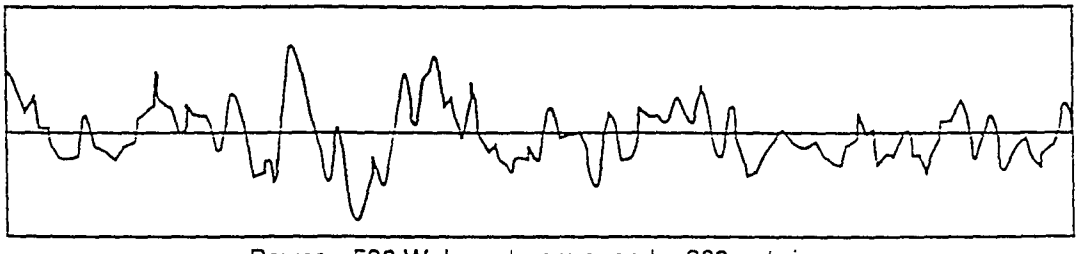

Power = 500 W, laser beam speed = 300 in./min
Ave. peak-to-valley distance = 6.95(relative value)

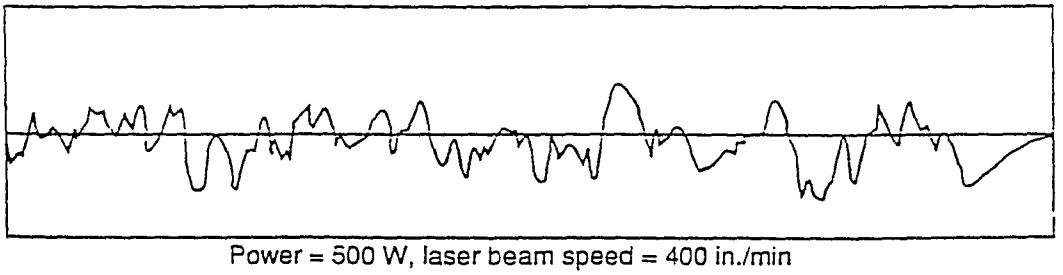

Power = 500 W, laser beam speed = 400 in./min
Ave.peak-to-valley distance = 4.6(relative value)

Figure 3.11: Surface Profile Traces of Laser Rough-Milled Surfaces at Different Scan Rates

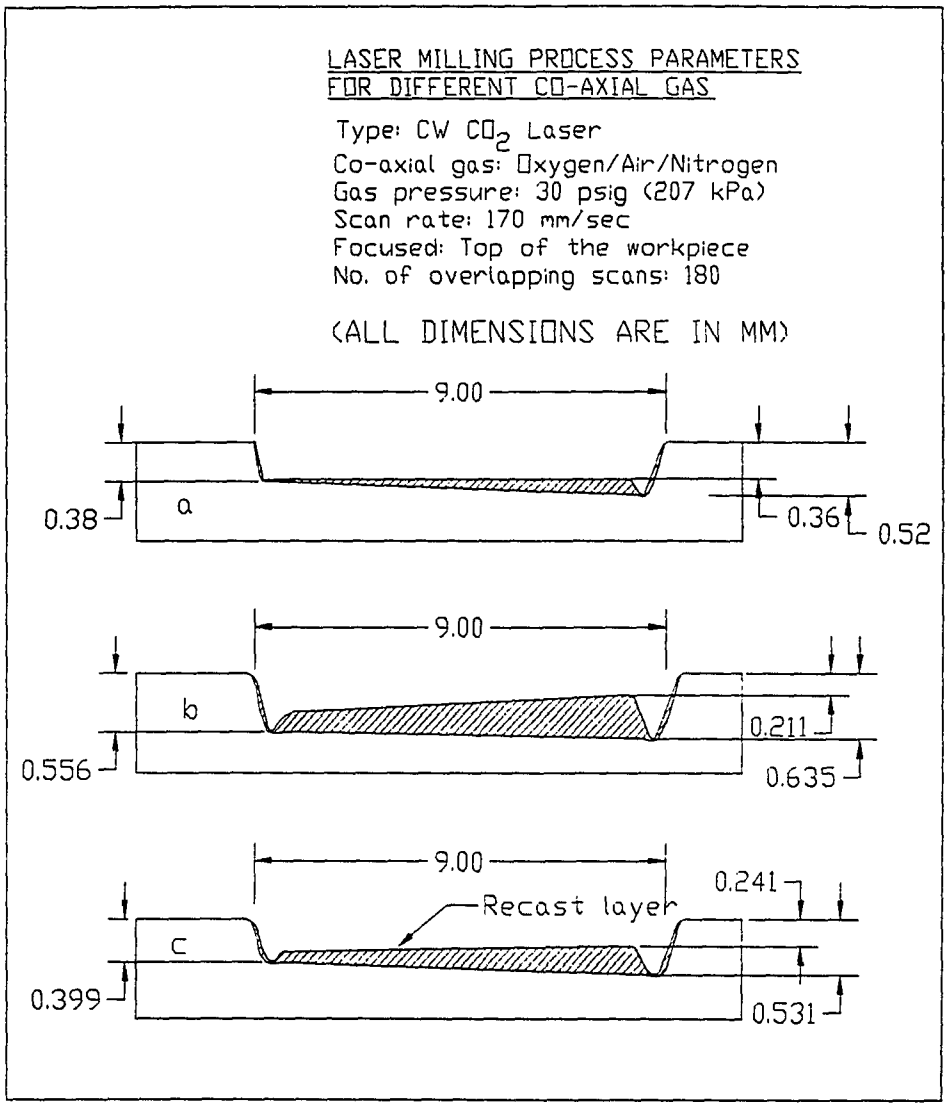

Figure 3.12: Milling Depth with Recast Layer with Assist Gas (a) Nitrogen, (b) Oxygen and (c) Air

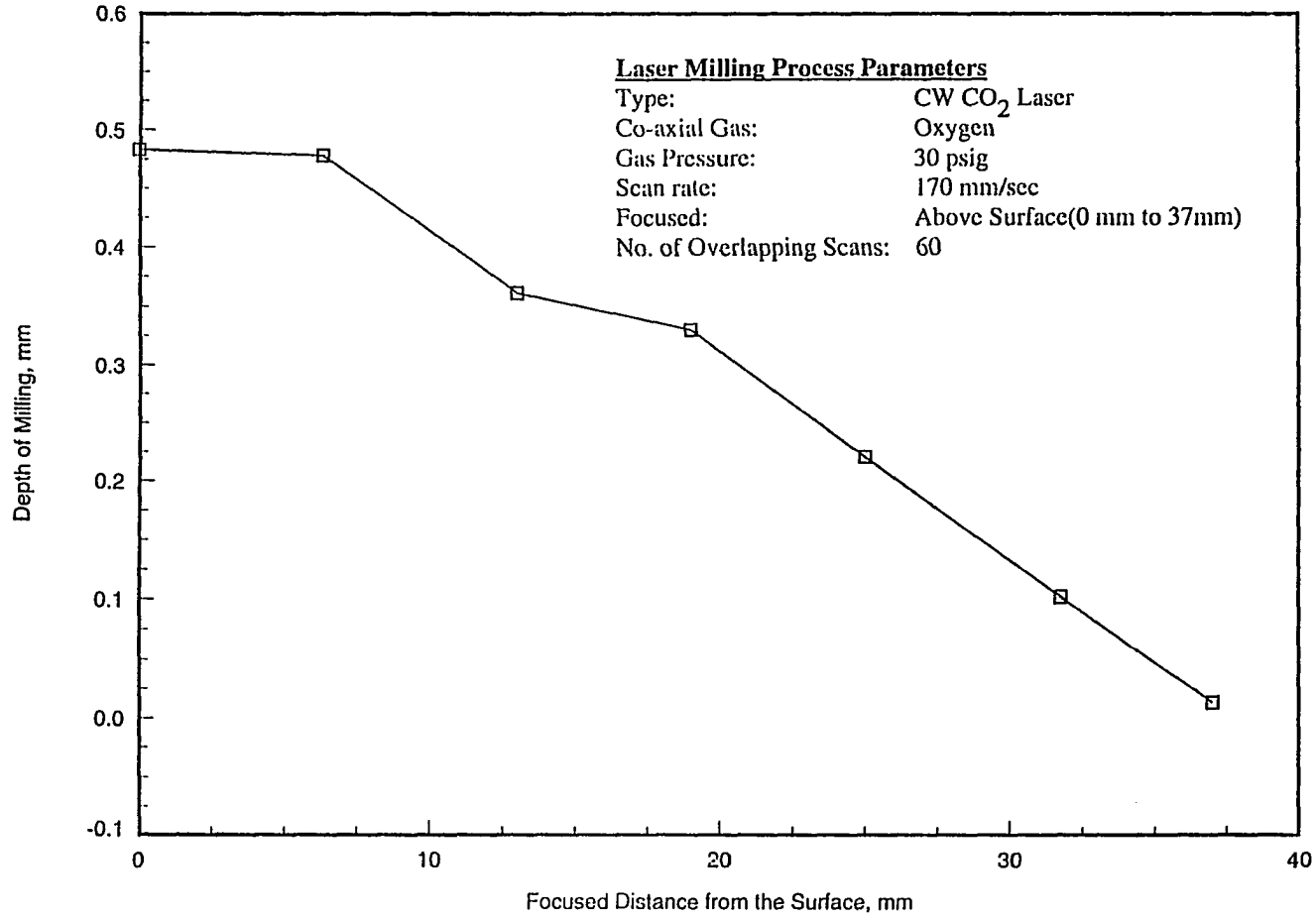

Figure 3.13: Effect of Defocusing on the Depth of Milling

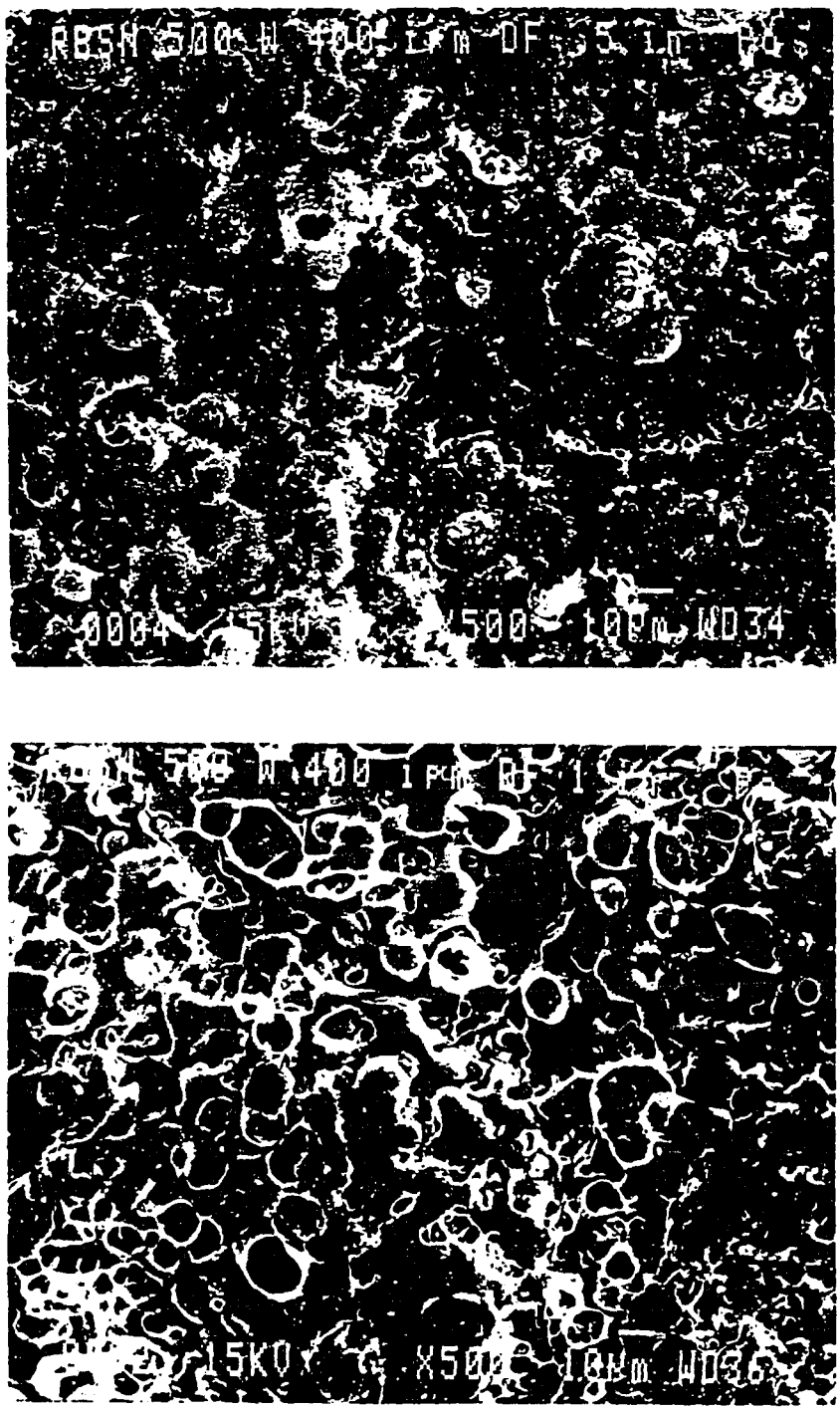

(a)

(b)

Figure 3.14: Scanning Electron Micrographs of Laser Fine-Milled Surfaces. Defocusing Distance: (a) 12 mm and (b) 25 mm

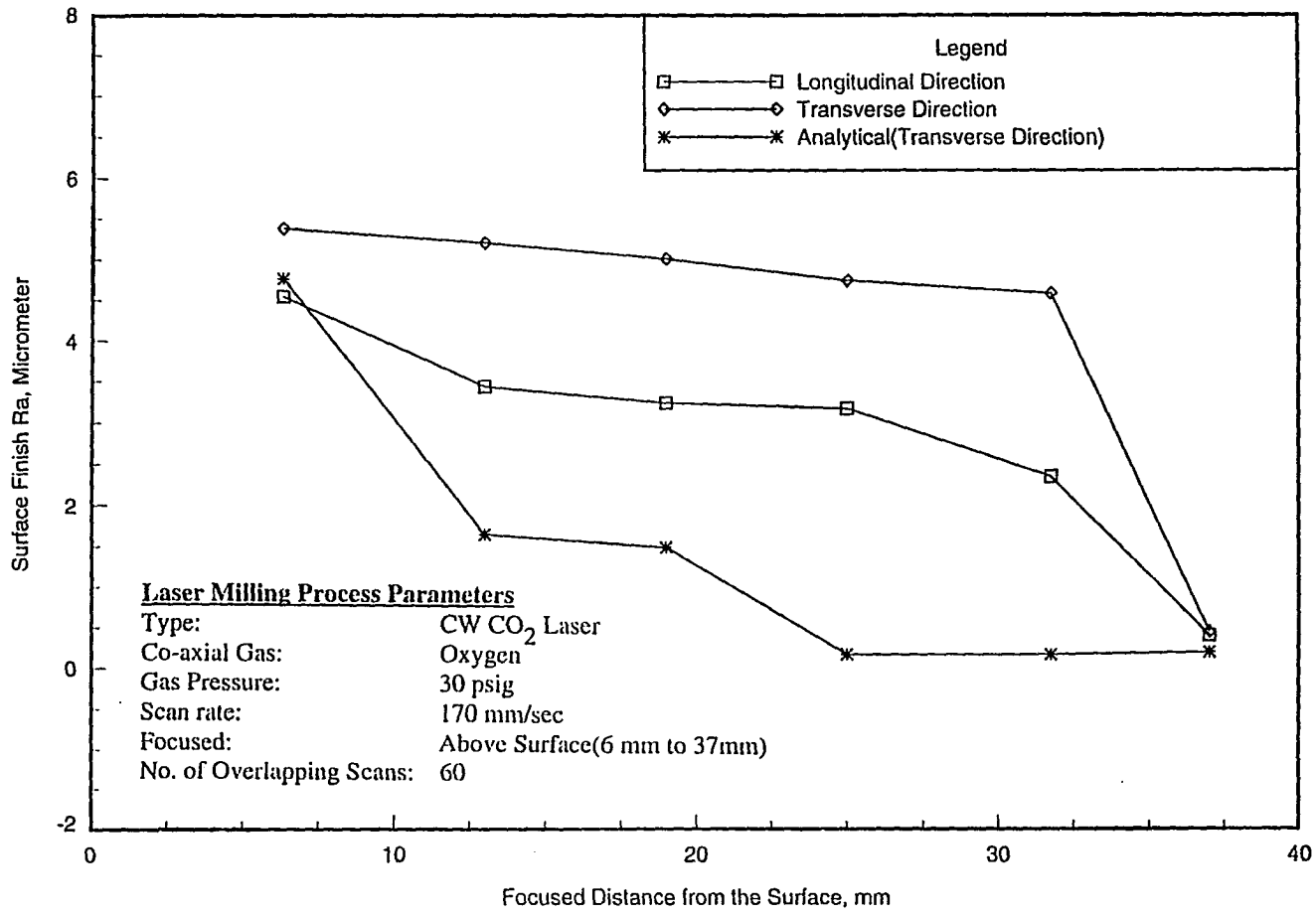

Figure 3.15: Effect of Focusing Distance on the Surface Roughness, R_a

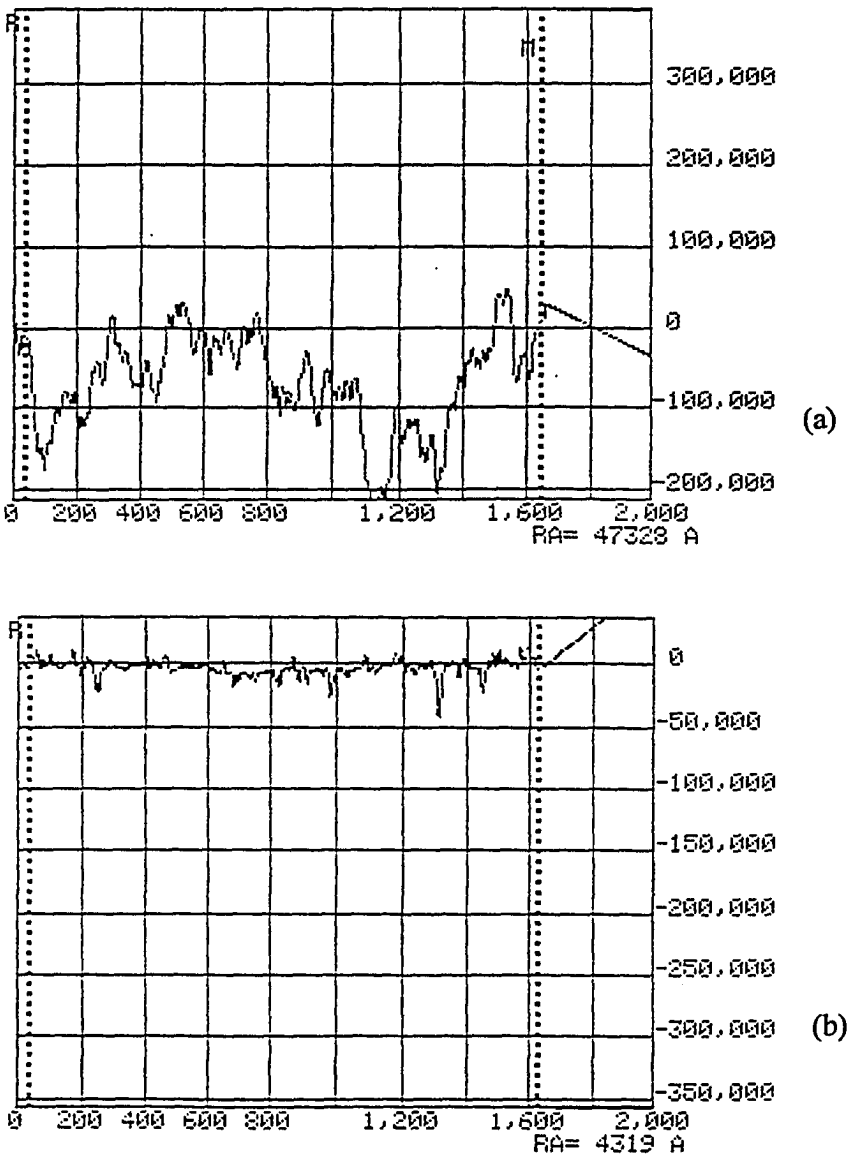

Figure 3.16: Surface Profiles of Laser Fine-Milled Samples at (a) 25 mm Defocused Distance and (b) 37 mm Defocused Distance

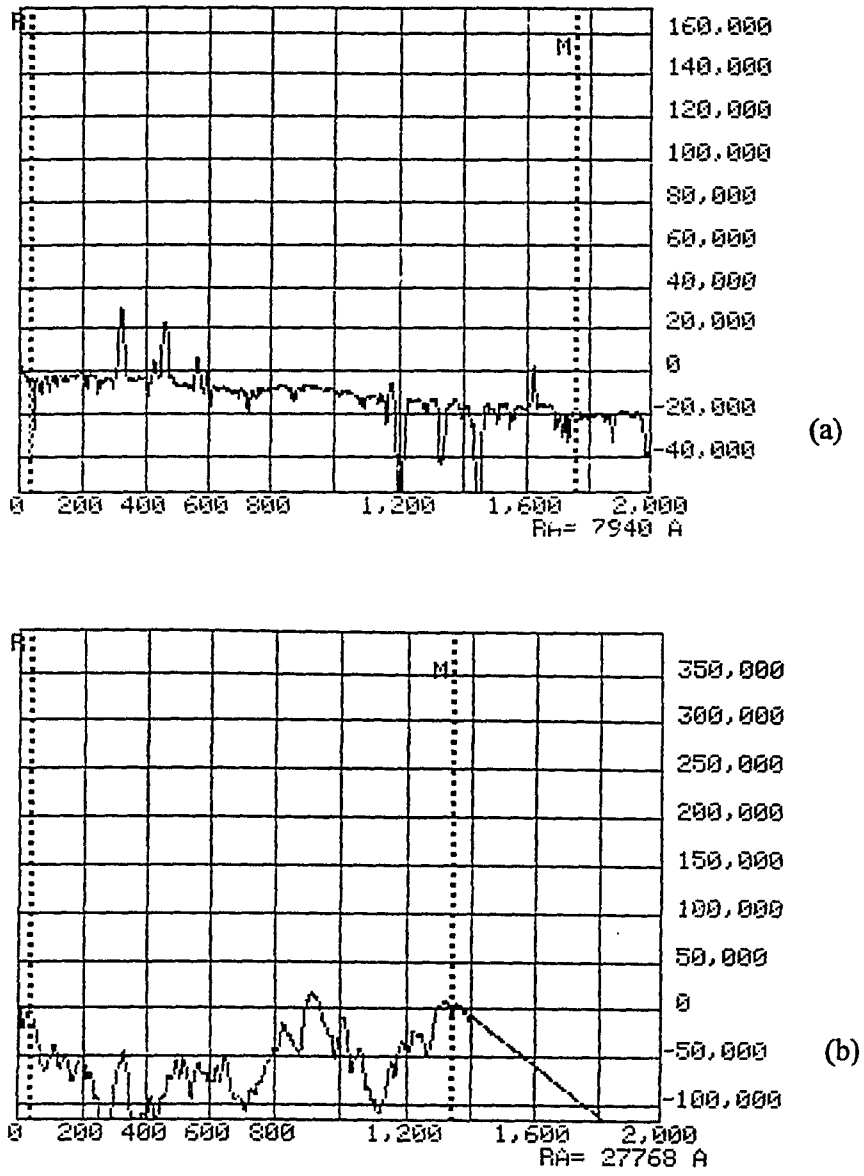

Figure 3.17: Surface Profile of (a) Diamond cut Surface and (b) Combined Laser Rough (Focused Beam) and Fine Milled (25 mm Defocusing Distance) Surface

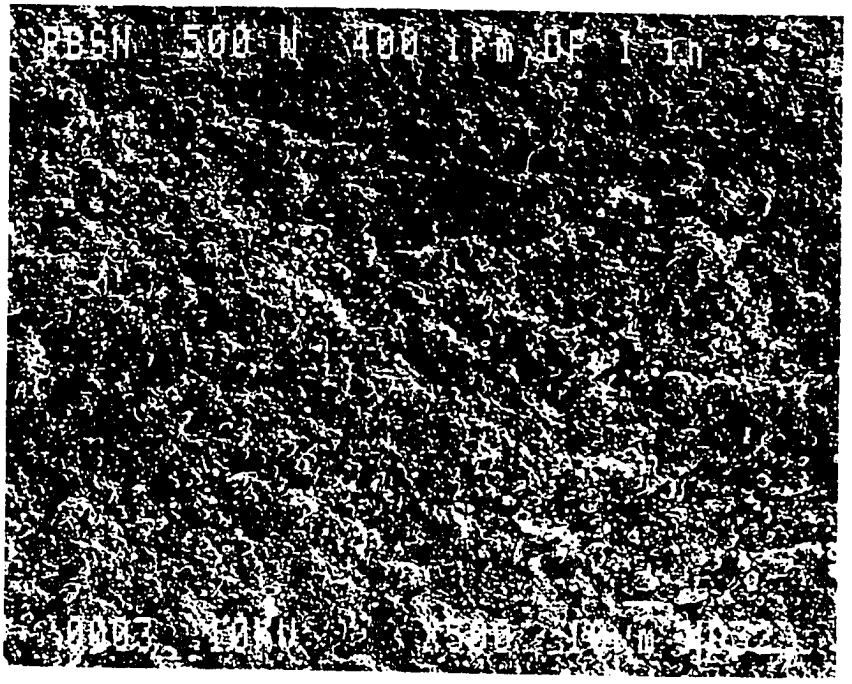

Figure 3.18: Scanning Electron Micrographs of the Sample Shown in Figure 3.17(b)

4. RECAST LAYER FORMATION AND ITS EFFECTS IN LASER MACHINING, ON HOT ISOSTATICALLY PRESSED SILICON NITRIDE

A paper to be submitted to the International Journal
of High Technology Ceramics, Leeds, United Kingdom.

Aloke Ray*, P. A. Molian*, M. F. Berard†

4.1 Abstract

In laser machining of ceramics, recast layer formation is a potential problem that is responsible for initiating cracks, degrading the surface finish and lowering the depth of cut. In this paper, an investigation was undertaken to examine the formation of the recast layer in the laser machining of hot isostatically pressed silicon nitride. A 500 watt continuous wave CO_2 gas laser was employed to generate grooves and milled cuts on silicon nitride specimens. The size, composition and location of the recast layer were evaluated as a function of travel speed (scan rate), number of laser passes (successive, overlapping passes with an overlap of 0.05 mm) and assist gas velocity. The effects of the recast layer on surface finish and crack formation were determined.

*Department of Mechanical Engineering, Iowa State University
†Department of Engineering Fundamental & Multidisciplinary Design, Iowa State University

Experimental results show that the recast layer size (height and width) increased with an increase in the number of laser passes (up to 75) after which it remained constant. Recast layer height varied as a hyperbolic tangent function of number of laser passes. Recast layer size was reduced by an increase in assist gas velocity at the exit of the nozzle. Finite element modeling verified that the assist gas flow in the kerf plays a significant role in determining the height and width of the recast layer in laser milling. The recast layer which is a mixture of Si and SiO_2 , caused the milled surface roughness to exceed $R_a = 30$ μm and aided in crack initiation. Chemical etching of laser milled surfaces reduced the size of the recast layer and improved the surface finish to about $R_a = 10$ μm.

4.2 Introduction

Due to their high hardness and brittleness ceramics are difficult to machine by conventional techniques. Laser machining is an excellent method for producing holes, grooves and odd-shaped cavities in ceramics. However, a major limitation is the formation of a recast layer that adversely affects surface finish and depth of cut, and is responsible for crack formation on the machined surfaces. Condensation of vaporized material and solidification of the molten layer constitute the recast layer. In this work, recast layer formation is investigated as a function of gas flow rate and the number of overlapping passes.

Silicon nitride has numerous applications including high-performance bearings, low-inertia turbocharger components, high temperature gas turbine rotor, shroud, piston inserts and cylinder liners, most of which require machining at one or other stages during their fabrication. Laser machining of silicon nitride has been investi-

gated by several researchers [1-14] but limited data is available concerning the mechanics of recast layer formation. During laser machining, silicon nitride decomposes into Si which subsequently melts and resolidifies as the recast layer. In the presence of oxygen, molten silicon oxidizes to form SiO_2 which contributes to the increased amount of the recast layer.

In laser hole drilling of ceramics, due to the limited size of the hole, most of the molten material is not blown away by the assist gas, hence it resolidifies quickly (due to high thermal diffusivity) across the hole and increases surface roughness.

Maruo et al. [7,8] studied the mechanisms of material removal during laser machining of silicon nitride using continuous wave (CW) CO_2 and pulsed excimer lasers. They observed that the wavelength of the laser beam had a significant effect on the decomposition of silicon nitride and, consequently, on the formation of the recast layer. In CO_2 laser machining, due to the longer wavelength (λ=10,600 nm), silicon nitride decomposed in to liquid silicon in the form of droplet which then adhered to the walls of the machined surface. On the contrary, silicon nitride dissociated in to silicon vapors in excimer laser wavelength (λ=248 nm) processing resulting in a much "cleaner" machining. However the material removal rate in excimer laser machining is substantially lower than in CO_2 laser machining.

Morita et al. [9,10] carried out laser machining of hot-pressed silicon nitride using both normal pulsed (msec) and Q-switched (nsec) Nd:YAG (1064 nm) lasers. They found that the laser parameters including pulse duration, peak power, and pulse repetition rate, largely determine the formation of the recast layer. Both the recast layer and the occurrence of cracking were reduced by reducing the pulse length from msec to nsec and decreasing the pulse repetition rate from 50 kHz to 0.1 kHz. Studies

with the normal pulsed Nd:YAG laser showed that for pulse durations above 10^{-4} sec and for laser powers up to 4 kW, both the recast layer thickness and associated crack density were increased. In addition, pulse repetition rates higher than 10 kHz increased the crack density and thickened the recast layer. These workers concluded that crack formation is essentially caused by the thermal expansion mismatch between the recast layer and the silicon nitride substrate. They believed that the material removal mechanism in Nd:YAG laser machining involves the decomposition of silicon nitride into silicon vapor which saturates in the hole and condenses to liquid form. Morita [11] carried out Nd:YAG laser machining of silicon nitride under water and observed the formation of a recast layer as well as cracks when longer pulses were used.

Solomah [12] investigated the laser cutting of hot-pressed silicon nitride using an oxygen- assisted CW CO_2 laser and reported that the recast layer, mostly consisted of SiO_2 and had a thickness of 150 μm to 350 μm. Yamamoto et al. [13] performed laser machining of silicon nitride using nitrogen and oxygen as assist gases. X-ray analysis of the recast layer revealed that only silicon was present when nitrogen was used as an assist gas while a mixture of Si and SiO_2 were identified when oxygen was used. Ray et al. [14] made a detailed study of grooving and milling of reaction bonded silicon nitride using a CW CO_2 laser and observed that the recast layer was much thicker in milling than when grooving and substantially reduced the depth of cut.

In the present study, an investigation was undertaken to examine the recast layer formation in laser grooving and milling of hot isostatically pressed silicon nitride as a function of assist gas pressure and the number of successive, overlapping laser passes.

4.3 Recast Layer Formation in Laser Machining

The formation of a recast layer in laser machining of a material depends on several factors including:

1. oxidation, decomposition and melting of the material
2. viscosity and surface tension of the molten layer
3. type of machining (drilling, grooving, cutting), and
4. assist gas flow parameters (pressure and flow rate)

Figure 4.1a is a schematic of blind hole drilling using a pulsed laser. The initial pulses generate a shallow blind hole within which the flow rate of the assist gas is high enough that most of the molten layer is blown away. However as the number of pulses increase or as the depth of hole increases, the assist gas flow rates in the hole cavity are reduced (pressure gradient becomes lower), allowing more recast layer to form, until a through hole is achieved, after which the assist gas can readily eject most of the molten layer through the bottom of the hole (Figure 4.1b).

Grooving differs from blind hole drilling in that, an open channel is left in the wake of the moving laser beam. This less confined geometry provides a ready pathway for assist gas flow and allows more effective removal of molten slag and less recast layer formation than during drilling to the same depth (Figure 4.1c). As the depth of grooving is increased, gas flow become progressively more restricted by the sidewall of the groove, leading to formation of a thicker recast layer on the sidewall.

Laser cutting is a process that combines drilling to produce a through hole and grooving to produce a trailing open cut (Figure 4.1d). In this case, the less confined

geometry for the cut results in assist gas flow rates that are too low to completely remove the molten slag. Also, because the liquid wets and adheres to the parent material, it produces a rougher surface finish than for simple drilling. If the thickness of the workpiece being cut is increased, the flow rate of the assist gas through the cut is further reduced, and more recast layer is observed along the sidewall of the cut.

Figure 4.2 illustrates the progress of the milling cut as the laser moves toward the left of the figure. During the first pass of the laser, the depth and width are very small and, due to high assist gas flow rates in the shallow groove, most of the molten slag is blown out of the groove. During the next few passes, the combined effects of preheating from the previous passes and multiple reflection of the beam from both groove walls produce a deeper cut. Because of its close proximity to the cutting beam, the surface of the right hand side (RHS) groove wall is melted on each of these early passes and a shallow curvature for the RHS wall results. Once a steady state temperature has been reached, the depth of cut stabilizes and remains constant thereafter. For each subsequent laser pass, the molten slag is blown by the assist gas toward the RHS of the groove, since this is the least constrained direction for gas flow. As the number of laser passes increases, the width of the milled groove increases causing a decrease in the flow rate of the assist gas in the widening groove to the point where molten slag is not completely blown out of the groove, and recast layer formation takes place toward the RHS of the groove. On each pass, molten material is blown toward the RHS and deposits on top of the previous recast layer, producing the maximum depth on the RHS of the growing recast layer.

The viscosity of the molten layer plays a very important role in recast layer formation. As the process is continued in the left hand side (LHS) direction, the

maximum temperature occurs at the groove surface being cut (LHS) and then gradually decreases in the RHS direction. Hence the lower the temperature, the higher the viscosity obtained. In this process, newly formed molten silicon with low viscosity adheres to highly viscous solid silicon and gradually form a ridge, where the influence of the assist gas is minimal. Hence a rougher surface is expected.

4.4 Material and Methods

4.4.1 Material

The material used in this investigation was hot isostatically pressed silicon nitride (HIPSN) which has a unique combination of excellent high-temperature mechanical properties as well as resistance to oxidation and thermal shock. There are three major types of silicon nitride named after the fabrication process: reaction bonded, hot-pressed and hot- isostatically pressed. HIPSN is the most dense of all three forms and is usually produced under conditions of high temperature and high pressure with the aid of sintering additive such as yttrium oxide. The additive plays a significant role in the densification process by reacting with a silica film and silicon nitride to form an inter-granularΦ liquid phase such as Y-Si-O-N which consolidates the powder compact [15].

In the present work HIPSN was obtained from Norton Company (Grade: NCX-5102) in the form of a 75 mm x 75 mm square, 6 mm thick disc. The composition and relevant properties of NCX-5102 are given in Table 4.1. The surface roughness of the as-received silicon nitride, measured using a profilometer, was $R_a = 0.8\ \mu m$.

Table 4.1: Properties of HIPSN [16] [18]

PROPERTY	VALUE
Bulk density (kg/m^3)	3230
Specific heat (J/kgK)	1294.5
Thermal conductivity (W/m K) at 300 K	38
Decomposition temperature (K)	2150
Melting temperature (K)	1698
Latent heat of vaporization (J/kg)	6.206×10^6
Hardness (GPa), Vickers	16.1

4.4.2 Laser Machining

Figure 4.3 shows the experimental arrangement used for laser machining. The workpiece was mounted on an X-Y table controlled by a computer numerical control (CNC) unit. A continuous wave CO_2 laser was focused on the workpiece surface. The beam was circularly polarized and was incident normal to the workpiece surface. Oxygen gas, coaxial with the laser beam, was blown into the machining zone through a gas-jet nozzle. The distance between the nozzle and workpiece was kept constant. Laser machining parameters and process variables are listed in Table 4.2.

Two types of laser machining processes, grooving and milling, were employed. Grooving, a single-pass laser process, was carried out at three different speeds: 42 mm/s, 84 mm/sec and 170 mm/s. Oxygen gas pressure in the nozzle was 193 kPa (28 psig). Milling, a successive overlapping laser pass process, was performed at a specific speed of 170 mm/s with nozzle pressure of 97 and 193 kPa. The distance between successive laser passes was held constant at 0.05 mm. Laser milling was investigated as a function of the number of passes (25, 50 and 100) and nozzle gas

Table 4.2: Process variables used in the work

Laser	CW CO_2
Wavelength	10.6 μm
Power	500 W
Beam focus	on the surface
Focused spot size	0.25 mm
Coaxial assist gas	oxygen
Nozzle diameter	2.5 mm
Nozzle-workpiece distance	1 mm

pressures 97 and 193 KPa (14 psig and 28 psig). The velocity of gas flow at the exit of the nozzle was measured using flowmeters and was 387 m/sec for 193 kPa (28 psig) and 314 m/sec for 97 kPa (14 psig).

4.4.3 Chemical Etching

Following laser machining, some specimens were chemically etched in a 3:1 mixture of concentrated nitric acid and hydrofluoric acid. The specimens were placed in the acid medium and ultrasonically vibrated for two hours to cause complete reaction. The purpose of chemical etching was to remove the recast layer. It is well known that a HNO_3/HF mixture can selectively dissolve the Si/SiO_2 recast layer without affecting the silicon nitride substrate [17]

4.4.4 Measurement and Analysis

Laser machined as well as chemically etched specimens were sectioned using a diamond wheel. Some of the cutting oil used during diamond cutting was trapped in the specimen and was removed by immersing the substrate in acetone. The specimens

were then examined with an optical microscope and with a scanning electron microscope (SEM) to determine the following: depth of cut, recast layer thickness, crack formation. A wavelength dispersive X-Ray probe attached to the SEM was used to identify the composition of the recast layer and the chemically etched surface. The surface roughness of the laser milled and chemically etched surfaces was measured using a surface profilometer (Dektak-IIA). Thermal conduction and energy balance models, described in a previous study [14], were employed to predict the depth of cut after laser grooving and milling of the material (HIPSN).

4.5 Results and Discussion

4.5.1 Laser Grooving and Milling

Figures 4.4-4.6 show the transverse sections of laser generated grooves before and after chemical etching. The following facts may be inferred from these figures.

1. An increase in scan rate reduced the groove depth and width as well as decreased the thickness of the recast layer on the side wall. The build-up of recast layer with increasing groove depth may be explained by the reduction in gas flow rate which in turn did not permit sweeping the molten material out of the groove.

2. Chemical etching of the laser machined grooves was very effective in eliminating the recast layer.

3. The fact that groove depth remained the same before and after chemical etching regardless of scan rate suggests that the recast layer did not form at the bottom of the groove. The scouring action of the direct impingement of the assist gas

on the bottom of the cut seems to be very effective in sweeping away the molten material.

4. The Recast layer mostly formed on the walls of the groove because the assist gas, due to its degraded flow rate along the walls, was unable to eject the highly viscous molten layer. The high viscosity of the molten Si-layer is due to its contact with the cold wall and its oxidation of silicon to form viscous SiO_2. The net result is the formation of a recast layer that has an increasing thickness toward the top of the groove.

Table 4.3 verifies that the analytical model, which is based on the assumptions of chemical decomposition and evaporation of silicon nitride and described in Reference 14, predicts slightly higher values of groove depth than the experimental data obtained.

Figures 4.7 and 4.8 are the transverse sections of laser milled and chemically etched specimens as a function of number of laser passes. Assist gas pressure and scan rate of laser beam were held constant at 193 kPa(28 psig) and 170 mm/sec (400 in/min) respectively. A comparison of milling with grooving clearly indicated that the depth of cut was substantially higher for milling which was attributed to the preheating of the substrate (due to overlapping laser passes) and multiple reflections of the beam from the side walls. Deepening of cut appears to have occurred in the first few laser passes. There was no change in the depth of cut as the number of laser passes was increased from 50 to 100 (compare Figures 4.7 and 4.8) . However the recast layer height and width increased with an increase in the number of laser passes. Figure 8 depicts the contours of laser milling cuts for 50 and 100 laser passes. It is evident that the recast layer starts building up in height at a distance of about

0.3 mm from the first laser pass. In addition, a ridge of recast layer can be seen to have formed on the top surface of the specimen next to the first laser pass (see Figure 4.9). Wavelength dispersive X- ray analysis (WDS) revealed that the recast layer consisted of a mixture of Si, SiO_2 and Y_2O_3 (Figure 4.10).

Table 4.3: Comparison of experimental and theoretical groove depths

Laser power: 500 Watts, Absorptivity: 0.3, Spot size: 0.25 mm, Assist gas: Oxygen at 193 kPa (28 psig)

Scan rate mm/sec	Experimental Groove Depth, mm	Analytical Groove Depth, mm
42	1.15	1.22
84	0.53	0.59
170	0.28	0.32

As expected, chemical etching of laser milled cuts removed the recast layer (Figures 4.7 and 4.8). WDS analysis of chemically etched surfaces, shown in Figure 4.11, indicate a reduced Si-content and the absence of carbon, oxygen and nitrogen when compared with as-laser milled cut surfaces. However the Y -concentration was increased. Cracks were not readily observed in the as-laser milled surfaces. But chemical etching of the recast layer revealed crack formation (Figure 4.12).

The resulting laser milled surfaces exhibited very high surface roughness (R_a > 30 μm) essentially due to the recast layer. Subsequent chemical etching reduced the surface roughness to R_a 10 μm in the longitudinal direction (laser machining direction) and to R_a 14 μm in the transverse direction. Surface roughness data after chemical etching are displayed in Figure 4.13.

Results described so far clearly demonstrate that the recast layer formation is strongly dependent on the number of laser passes during milling. Figure 4.14 schematically illustrates the recast layer formation for increasing number of laser passes. Note that both the height and width of the recast layer increases with an increase in number of laser passes. Figure 4.15 shows that during the first 25 laser passes, the recast layer height was not measurable and after 75 laser passes, it remained constant. Experimental results indicated that the recast layer height follows a shape that may be approximated by a"tanh"function. An iterative procedure gave the following general equation that describes the relation between number of laser pass and recast layer height:

For $25 < N < 75$ laser pass

$$H = H_0 - A\ tanh[B(N - C)] - D \tag{4.1}$$

where

H	=	Recast layer thickness for any intermediate laser pass
H_0	=	Maximum recast layer thickness
$A, B, C,$ and D	=	constants depending upon input gas velocity, nozzle size and distance between nozzle and specimen

It is believed that the assist gas flow conditions inside the milled cut account for the variation of recast layer height with the number of passes. During the first 25 passes, the gas velocity is high enough to eject the molten silicon out of the kerf. As the number of laser passes increases, the width becomes larger leading to a loss in gas flow rate and hence recast layer build up occurs. It was further observed that

for a given number of laser passes, the assist gas flow conditions such as pressure and velocity affect the formation of the recast layer. Figure 4.16 shows that for lower assist gas velocity, the recast layer height and width are larger thereby suggesting that the assist gas flow plays a critical role in laser milling.

4.5.2 Finite Element Analysis of Recast Layer

A finite element modeling (FEM) approach was employed by using the "Algor" steady state fluid flow analysis package to predict the recast layer formation in laser milling. The FEM predicted formation of a jet structure in the kerf that matched the recast layer shape. From this observation, it was conjectured that the jet structure controls the formation of the recast layer. The same jet structure in the kerf was obtained using slip boundary condition. In the FEM analysis, it was assumed that the assist gas was fully responsible for the removal of the recast layer from the kerf. Figure 4.17 shows a schematic of gas flow along with boundary conditions. The objective was to determine the magnitude and pattern of velocity distribution across the kerf as a function of gas flow velocity input (387 and 314 m/sec) and number of laser passes. The following assumptions were made:

1. two-dimensional steady state compressible flow exists
2. temperature inside the kerf is assumed to be equal to the decomposition temperature of silicon nitride (2150 K)
3. density, dynamic viscosity and temperature in the kerf are constant
4. slip boundary conditions exist on the milled contour (i.e. only $U_z = 0$)

The following continuity and momentum equations were considered in the finite element analysis:

$$\nabla \cdot \vec{u} = 0 \tag{4.2}$$

$$\frac{\partial \vec{u}}{\partial t} + \vec{u} \cdot \nabla \vec{u} = -\frac{1}{\rho}\nabla p + \frac{\mu}{\rho}\nabla^2 \vec{u} \tag{4.3}$$

where

$\vec{u}$ = Laser scan rate , mm/sec

ρ = Density of the material, kg/m^3

∇p = Pressure gradient, Pa/m

μ = dynamic viscosity, N.s./m^2

The values used in the FEM were: gas velocity = 314 m/sec and 387 m/sec, nozzle diameter = 2.54 mm, gas dynamic viscosity at 2150 K = 7.5 x 10^{-3} N.s./m^2 [19], distance between nozzle and specimen surface = 1 mm.

Figures 4.18 and 4.19 depict the FEM velocity profiles obtained for 50 laser passes at an input gas velocities of 387 m/sec (gas pressure: 193 kPa) and 314 m/sec (gas pressure: 96.5 kPa) respectively. At the location of maximum height of recast layer (obtained from the experimental data shown in Figure 4.16), the gas velocity is about 120 m/sec. It appears that for a gas velocity less than 120 m/sec, flow is insufficient to remove the recast layer.

Figures 4.20 and 4.21 show the velocity profiles for 100 laser passes at input gas velocities of 387 m/sec and 314 m/sec respectively. Again the diagrams illustrate that at the location of maximum height of the recast layer (from Figure 4.20), the gas velocity is about 250 m/sec. A comparison with Figures 4.18 and 4.19 shows that the threshold gas velocity for removal of recast layer increases with an increase in number

the of laser passes. From the above observation, it can be concluded that the recast layer formation is much higher at low assist gas pressure. As the number of passes increases, the recast layer formation gradually increases up to a certain level, after which the thickness remains constant. This may be attributed to the fact that for a larger number of passes, the molten slag must travel a longer path, which requires a higher gas velocity, before the molten slag is ejected from the milled contour.

4.6 Conclusions

A study was undertaken to examine recast layer formation and its effects in laser grooving and milling of a specific ceramic material namely hot pressed silicon nitride (HIPSN). Major conclusions drawn from this study include:

1. Laser grooving (single laser pass) generated a shallow depth of cut and a thin recast layer that is mostly deposited on the walls of the groove

2. Laser milling (multiple, overlapping passes) produced deeper cuts and thicker recast layers. The size of the recast layer (height and width) increased with an increase in the number of laser passes.

3. Recast layer caused the roughness of laser milled surfaces to exceed 30 μm (Arithmetic Average). Chemical etching following laser machining improved surface finish to 10 μm (Arithmetic Average) by eliminating recast layer.

4. Both experimental results and finite element modeling demonstrated that the assist gas flow conditions play the key role in affecting the size of the recast layer in laser milling.

4.7 References

[1] Affolter, P., and Schmid, H. G.,"Processing of New Ceramic Materials with Solid State Laser Radiation", *SPIE - High Power lasers and Their Industrial Applications*, 801 (1987), 120-129

[2] Hamann, C. and Rosen H.,"Laser Machining of Ceramic and Silicon", *SPIE - High Power lasers and Their Industrial Applications*, 801 (1987), 130-137

[3] Harrysson, R. and Herbertsson H., "Machining of High Performance Ceramics and Thermal Etching of Glass by Laser", *Proceedings, Fourth International Conference on Lasers in Manufacturing*, 1987, 211-220

[4] Laudel, A., "Laser Machining of Ceramic", DOE Rept. No. BDX-613-2507, 1987

[5] Powell, J., Ellis, G., Menzies, I. A. and Scheyvaerts, P. F., "CO_2 laser cutting of Non-Metallic Materials", *Proceedings, Fourth International Conference on Lasers in Manufacturing*, 1987, 69-82

[6] Chryssolouris, G., "Laser Machining, Theory and Practice", Springer-Verlag, New York, NY, 1991

[7] Maruo, H., Miyamoto, I., and Ooie, T., "Processing Mechanism of Ceramics with High Power Density Lasers", in *Proceeding of LAMP* (June 1992) Nagaoka, Japan, 293-298

[8] Maruo, H., Miyamoto, I., and Ooie, T. and Horiguchi, Y., "Laser Machining of Ceramics-Machining Mechanism and Quality", in *Advanced Technology in Welding, Materials Processing and Evaluation*, 5th International symposium in J. W. S., Tokyo (April, 1990), 251-256

[9] Morita, N., "Crack-free processing of hot-pressed Silicon Nitride Ceramics using pulsed YAG laser", *Annals of CIRP*, 87 (1991) 517-524

[10] Morita, N., Watanbe, T., and Yoshida, Y.,"Crack-free processing of hot-pressed Silicon Nitride Ceramics using pulsed YAG laser", *JSME International Journal*, Series Ill, 34, 1, (1991) 149

[11] Morita, N., Watanabe, T., and Yoshida, Y., "Pulsed laser processing of ceramics in water", *Applied Physics Letters*, 52, 23, (1988)

[12] Solomah, A. G.,"Laser machining of Silicon Nitride", *Annals of CIRP*, 87 (1991) 543-546

[13] Yamamoto, J., Yamamoto, Y.,"Laser machining of Silicon Nitride", *Proceeding of LAMP* (1987) Osaka, Japan, 297-303

[14] Ray, Aloke, Molian, P. A., Scrutton, R. F., and Mitra, A. K., "Carbon-dioxide Laser Milling of Reaction Bonded Silicon Nitride", *International Journal of Ceramics*, U. K., Submitted on Dec'94

[15] Schneider, S. J. Jr., "Engineered Materials Handbook", Vol. 4, ASM International, The Materials Information Society, 1992

[16] "Properties of HIPSN, (NCX - 5102)", Manufactured by Norton Company, Massachusetts, MA

[17] Morrell, R., "Hand book of Properties of Technical and Engineering Ceramics", Part 1, Her Majesty's Stationery Office, London, (1985)

[18] Ramanathan S., and Modest, M., "Effects of variable thermal properties on evaporative cutting with a moving cw laser", *ASME Heat Transfer in Space Systems*, (1990), 101

[19] White, F., "Viscous fluid flow", 2nd edition, McGraw-Hill Inc., New York, (1991), 28-29

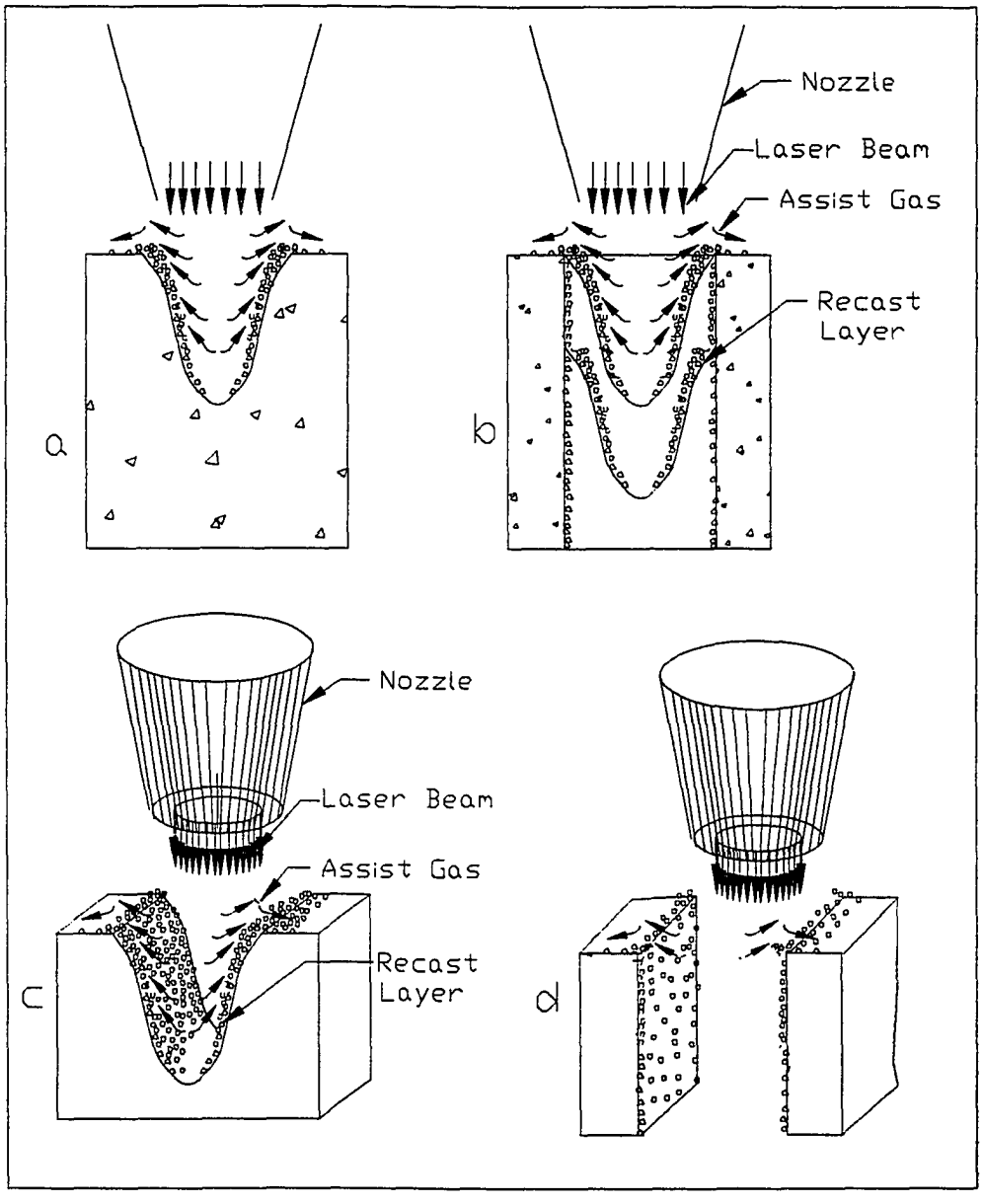

Figure 4.1: Formation of Recast Layer for a) Laser Drilling of a Blind Hole, b) Laser Drilling of a Through Hole, c) Laser Grooving and d) Laser Cutting

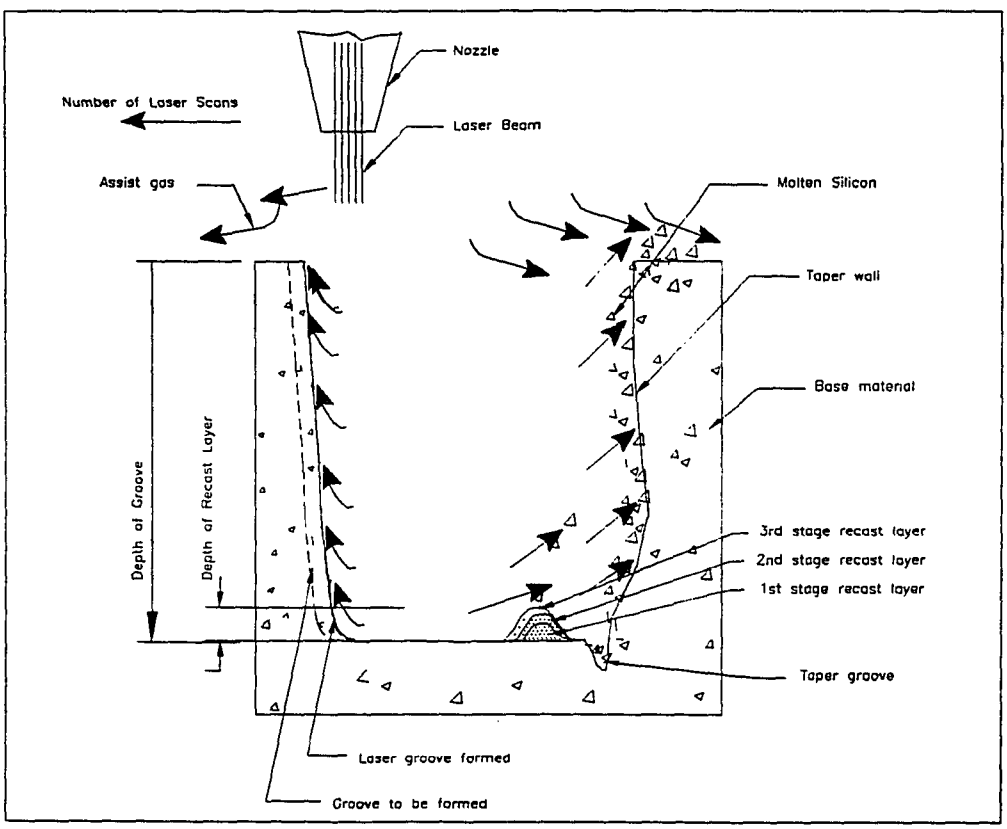

Figure 4.2: Formation of Recast Layer during Laser Machining

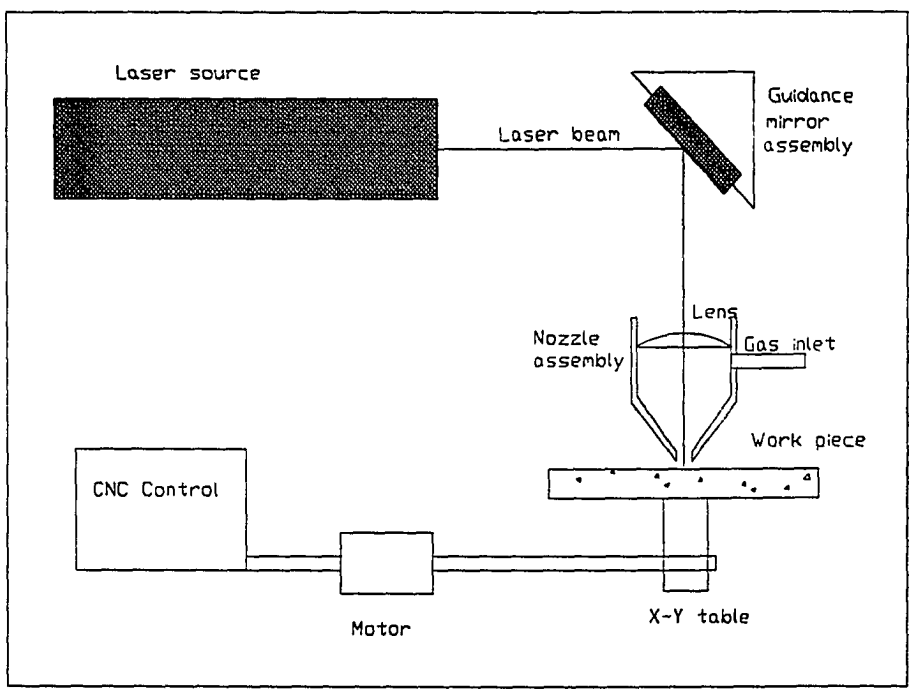

Figure 4.3: A Schematic of the Laser Milling Machine Tool Employed in this Study

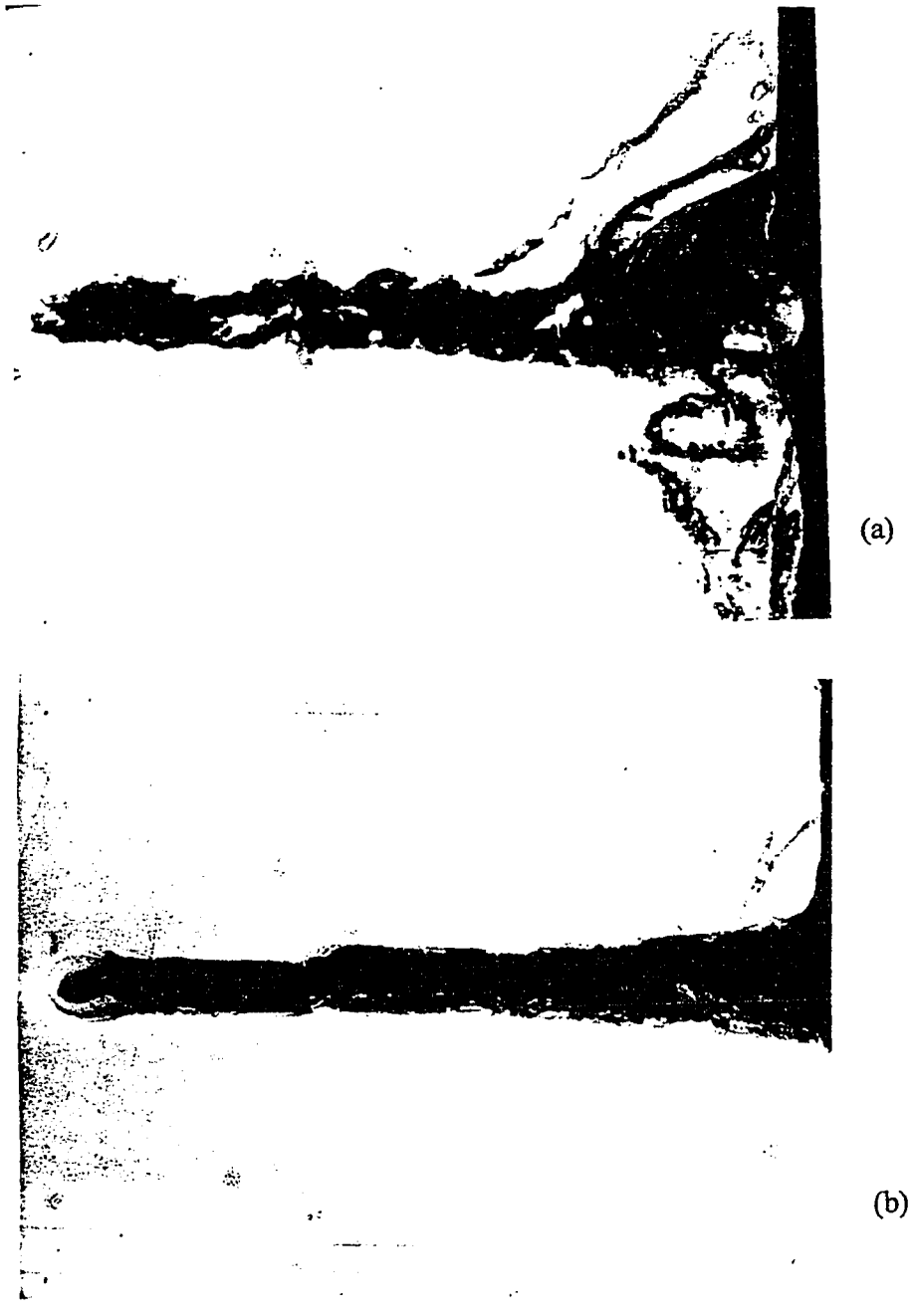

Figure 4.4: Transverse Section a) As Laser Grooved at 42 mm/sec, Assist Gas Pressure 193 kPa, b) After Chemical Etching

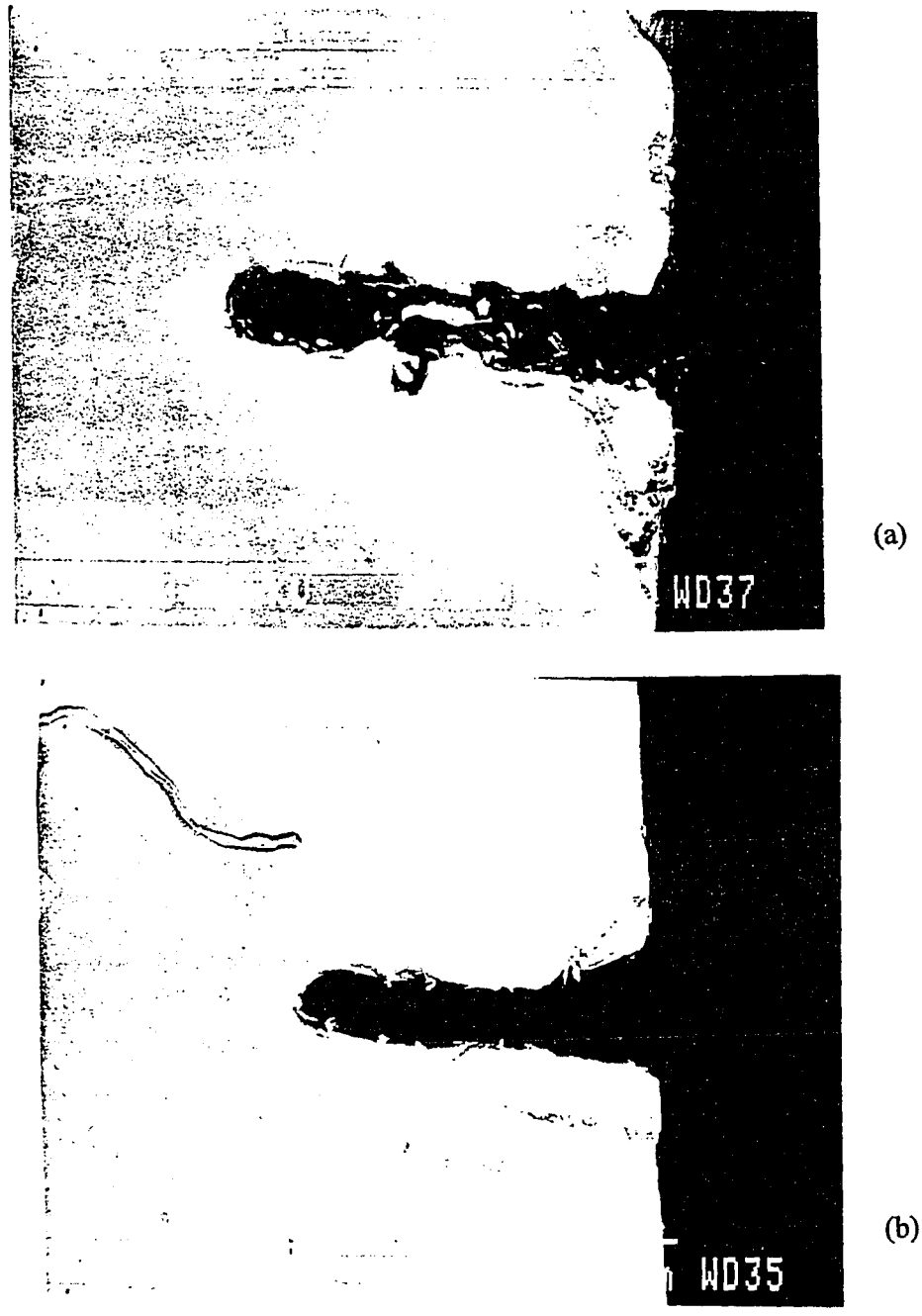

Figure 4.5: Transverse Section a) As Laser Grooved at 84 mm/sec, Assist Gas Pressure 193 kPa, b) After Chemical Etching

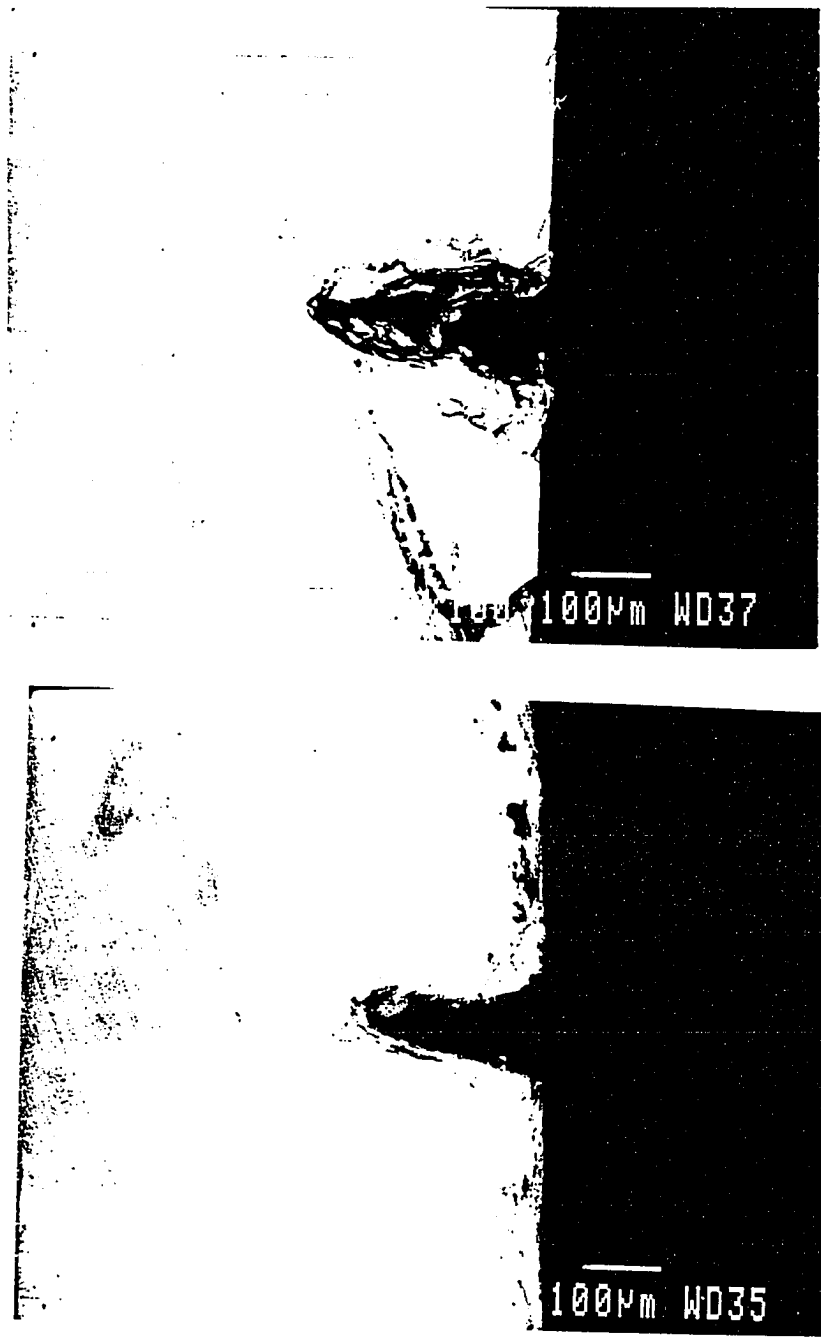

(a)

(b)

Figure 4.6: Transverse Section a) As Laser Grooved at 170 mm/sec, Assist Gas Pressure 193 kPa, b) After Chemical Etching

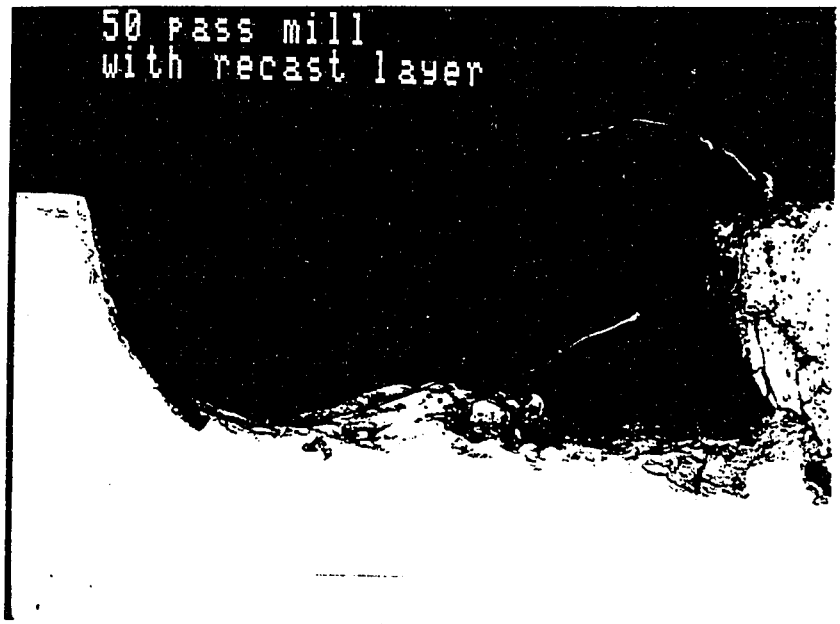

(a)

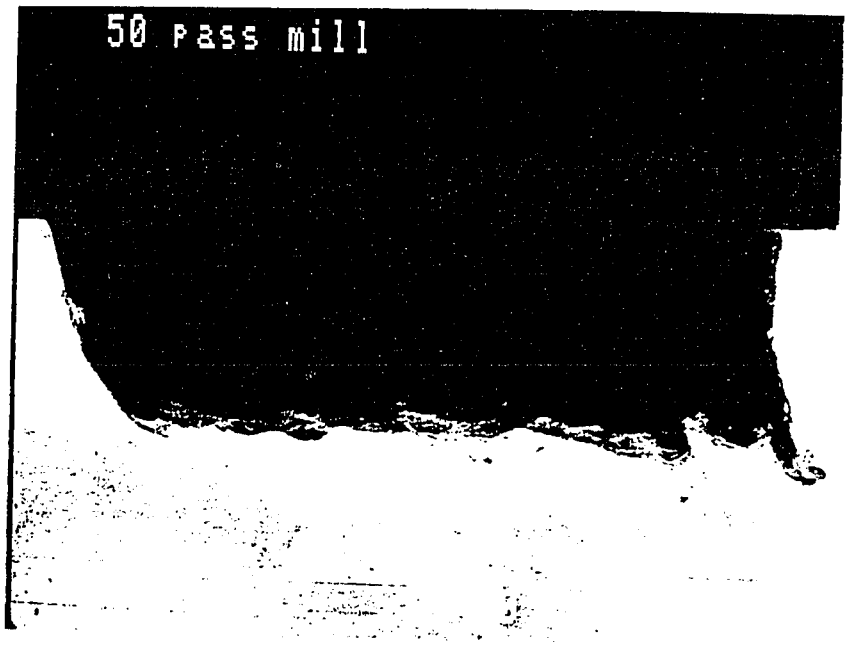

(b)

Figure 4.7: Transverse Section a) 50 Pass as Laser Milled Surface b) 50 pass Laser Milled and Chemical Etched

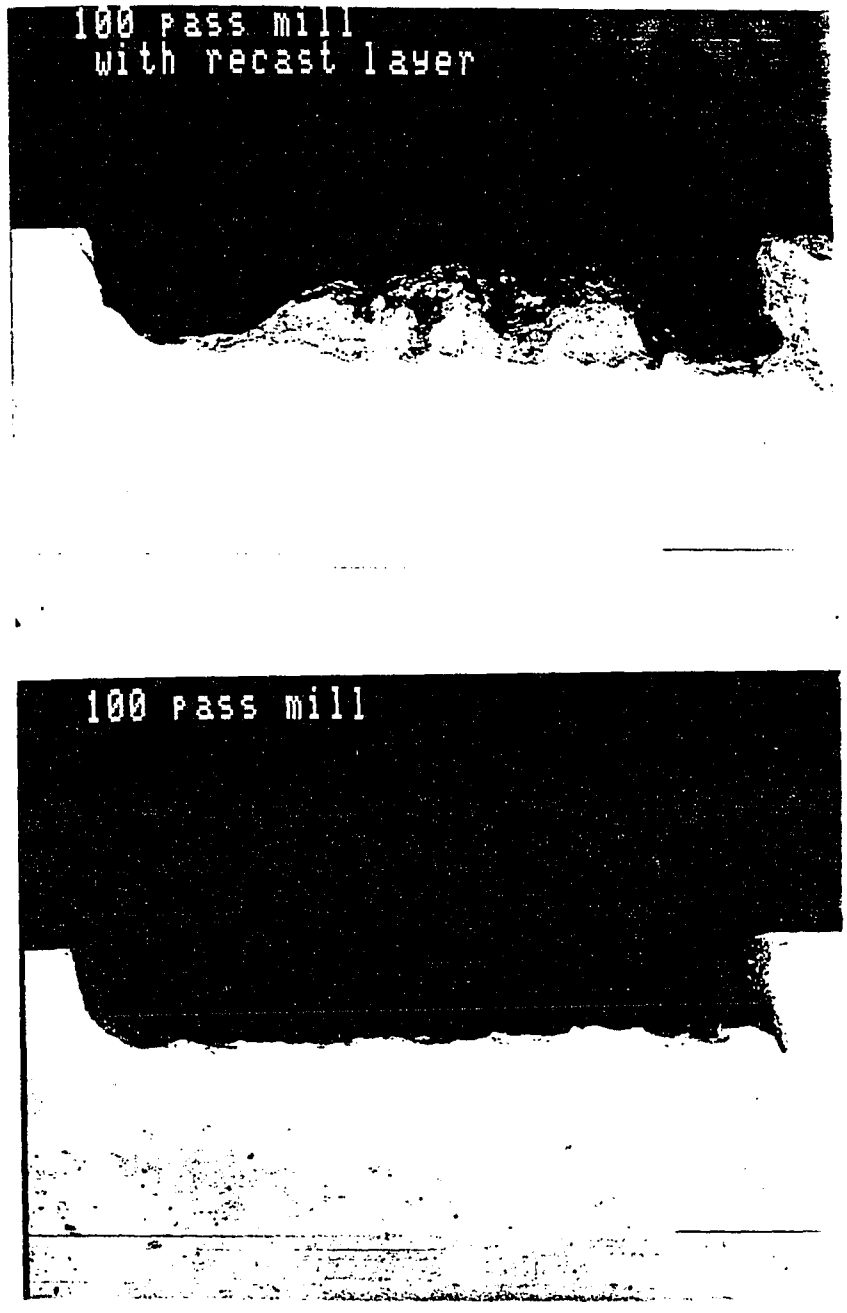

Figure 4.8: Transverse Section a) 100 Pass as Laser Milled Surface b) 100 Pass Laser Milled and Chemical Etched

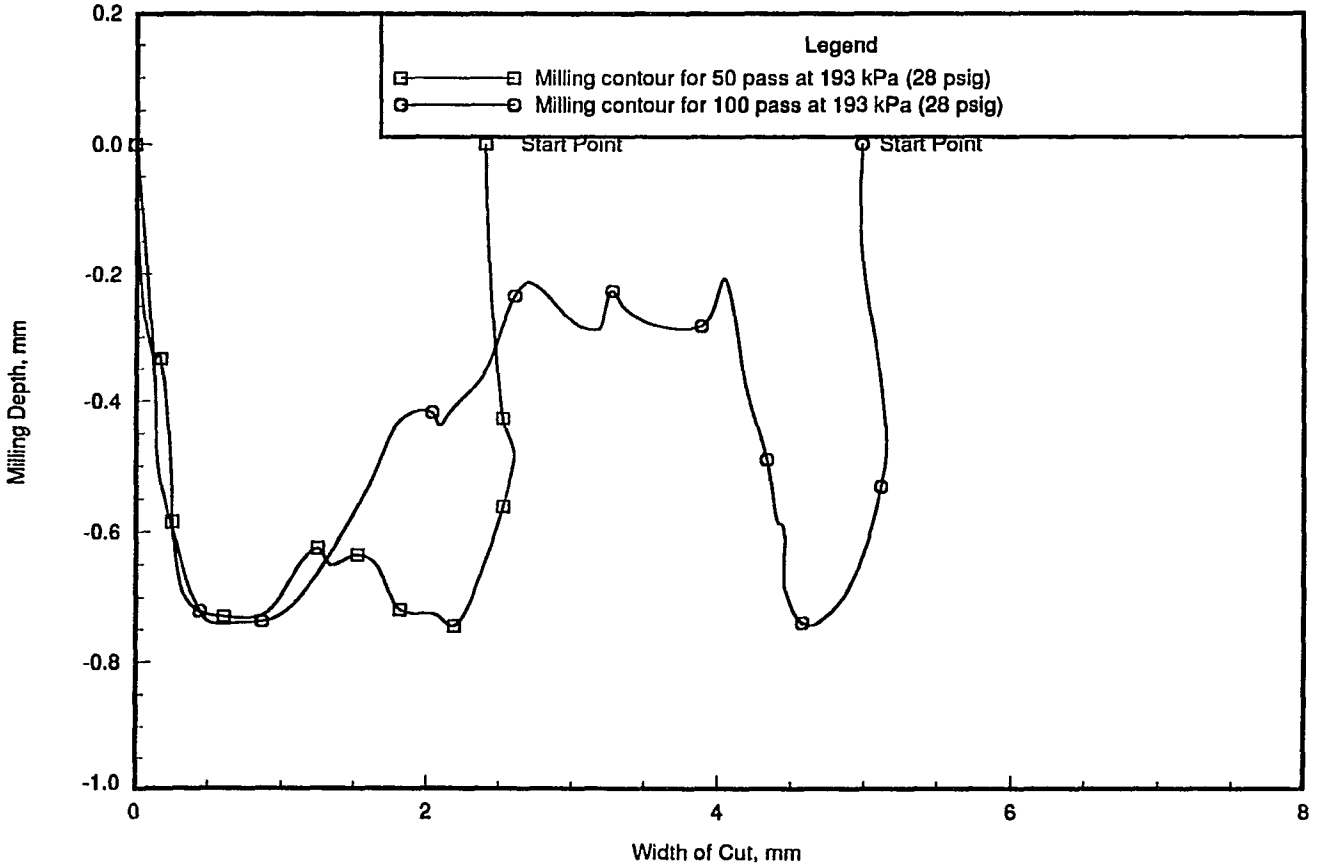

Figure 4.9: Depth of Milled Contour for 50 and 100 Passes before Chemical Etching

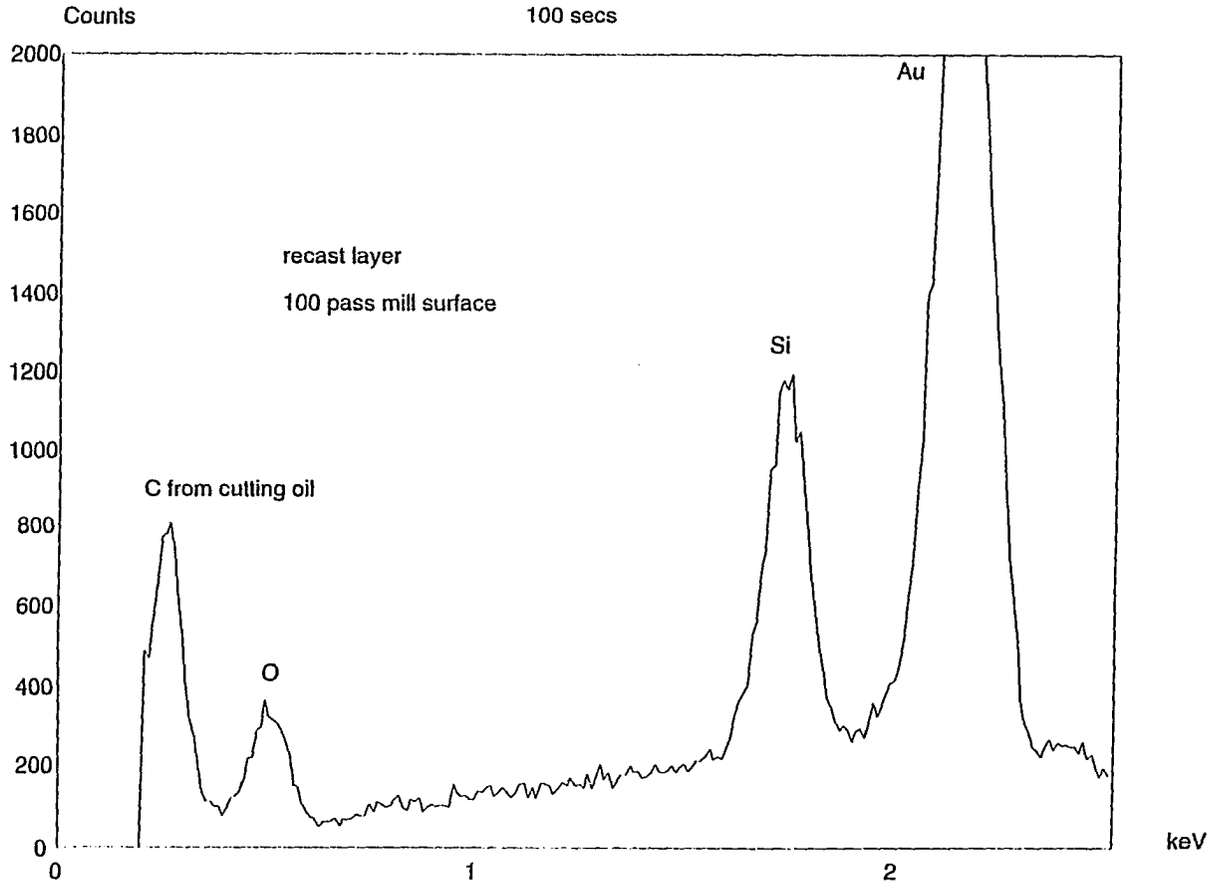

Figure 4.10: WDS X-ray Spectrum on the as-Laser Milled Contour

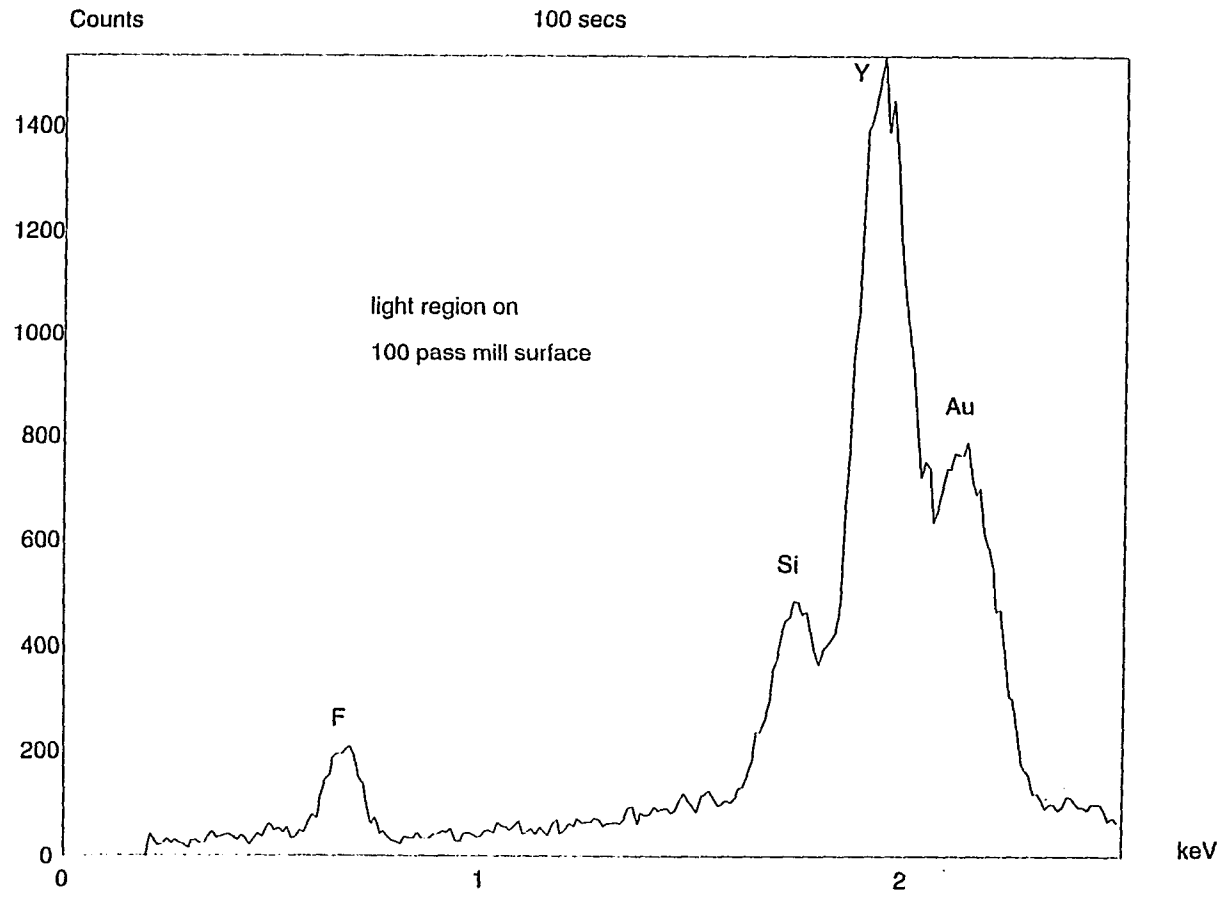

Figure 4.11: WDS X-ray Spectrum on the Laser Milled and Chemically Etched contour at 100 Passes

Figure 4.12: SEM Micrograph showing the Cracks for 100 Passs Milled Surface after Chemical Etching

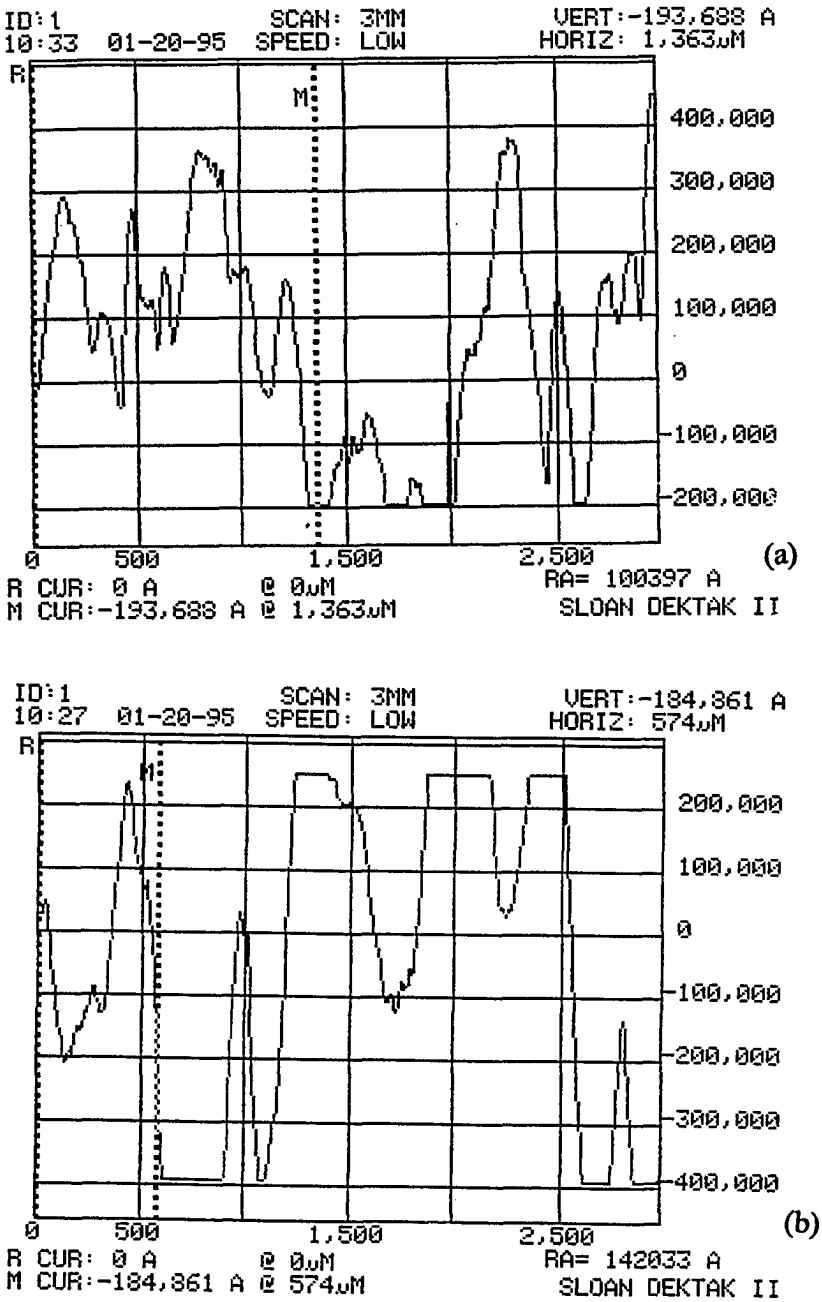

Figure 4.13: Surface Roughness along a) Longitudinal and b) Transverse direction of Laser Milled and Chemically Etched Specimen

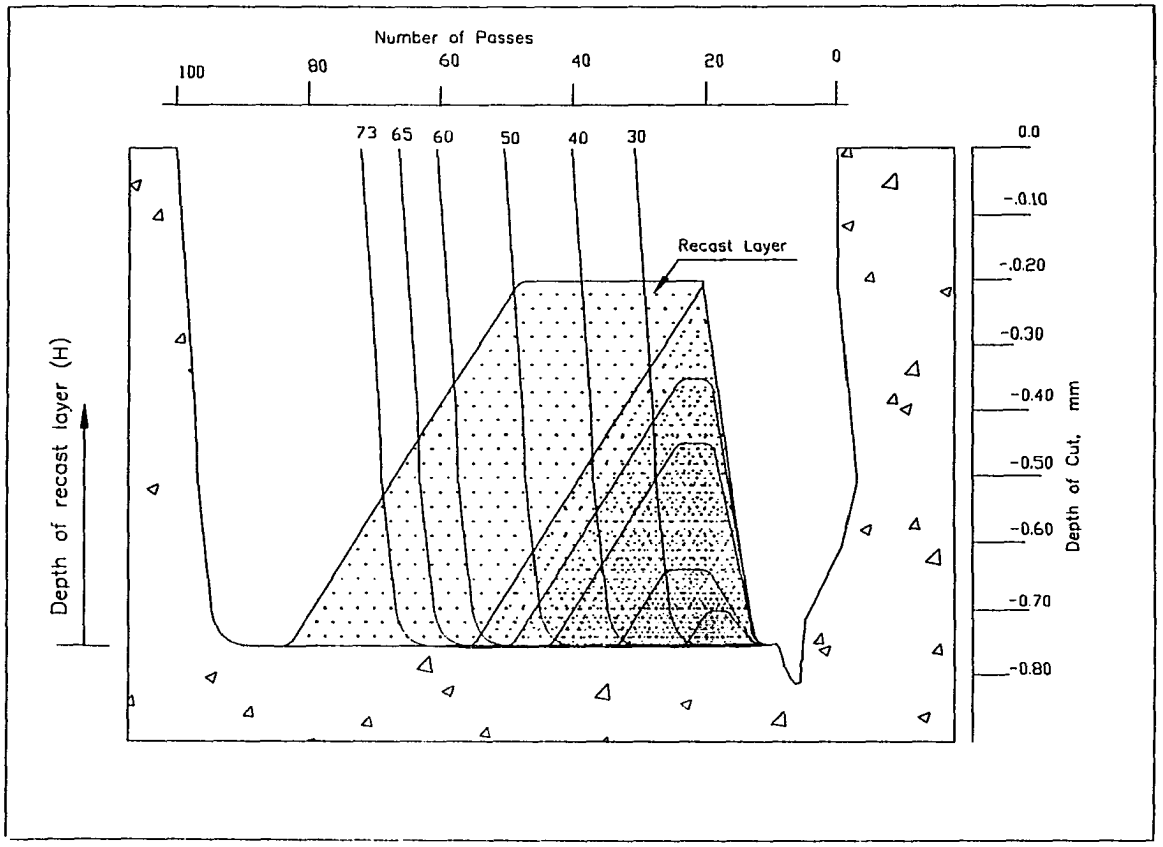

Figure 4.14: Schematic Representation of Sequence of Recast Layer Formation from 0 to 100 Passes during Laser Milling Process

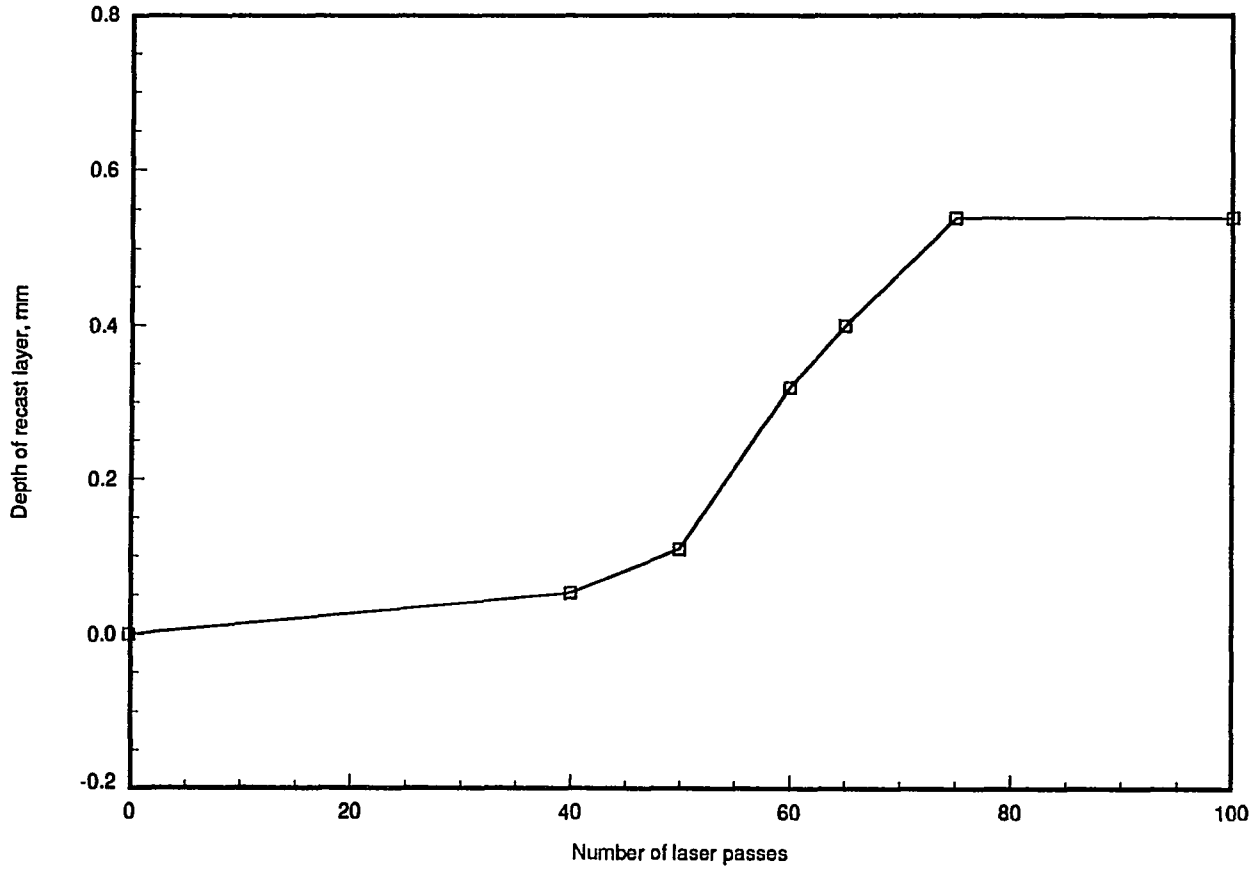

Figure 4.15: Depth of Recast Layer formation at Various Passes, (Assist Gas Pressure 193 kPa)

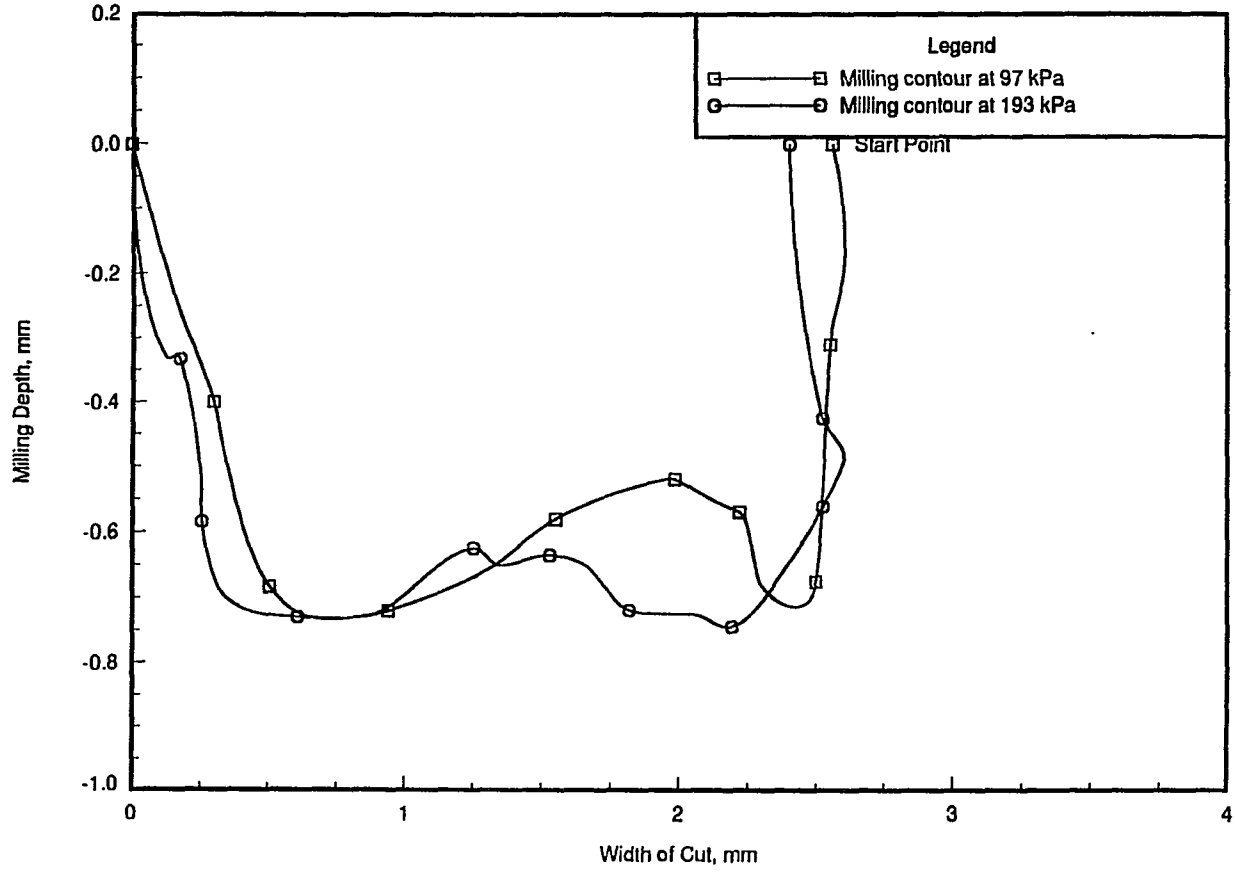

Figure 4.16: Comparison of Depth of Milled Contour at 97 kPa and 193 kPa Assist Gas Pressure for 50 Passes

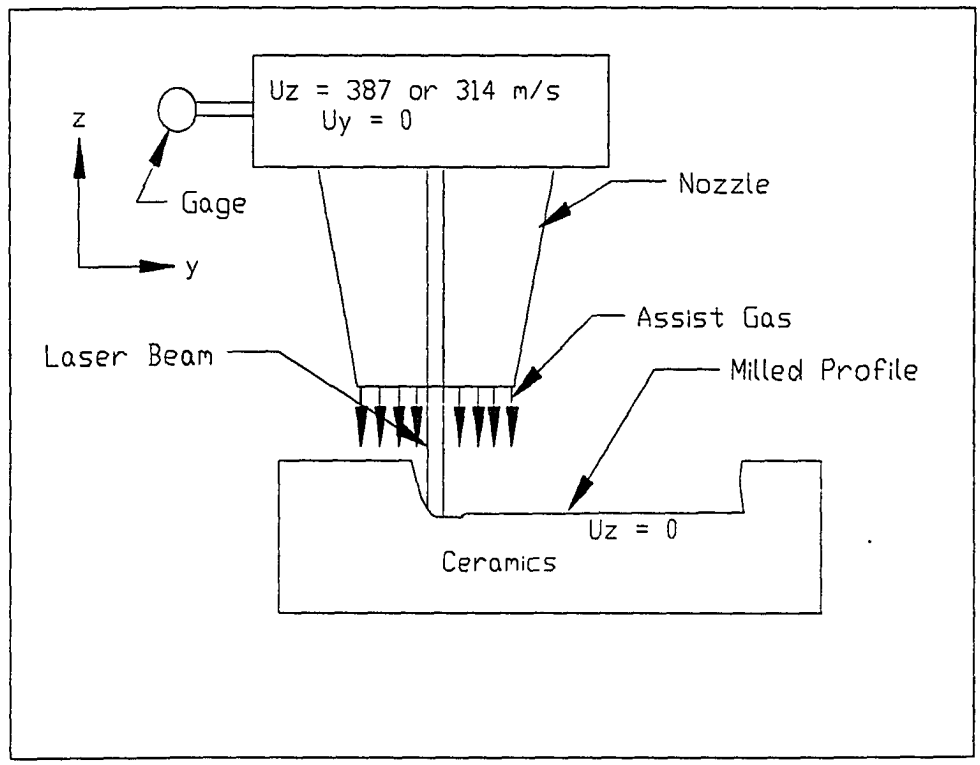

Figure 4.17: Schematic Representation of Gas Flow for Finite Element Modeling

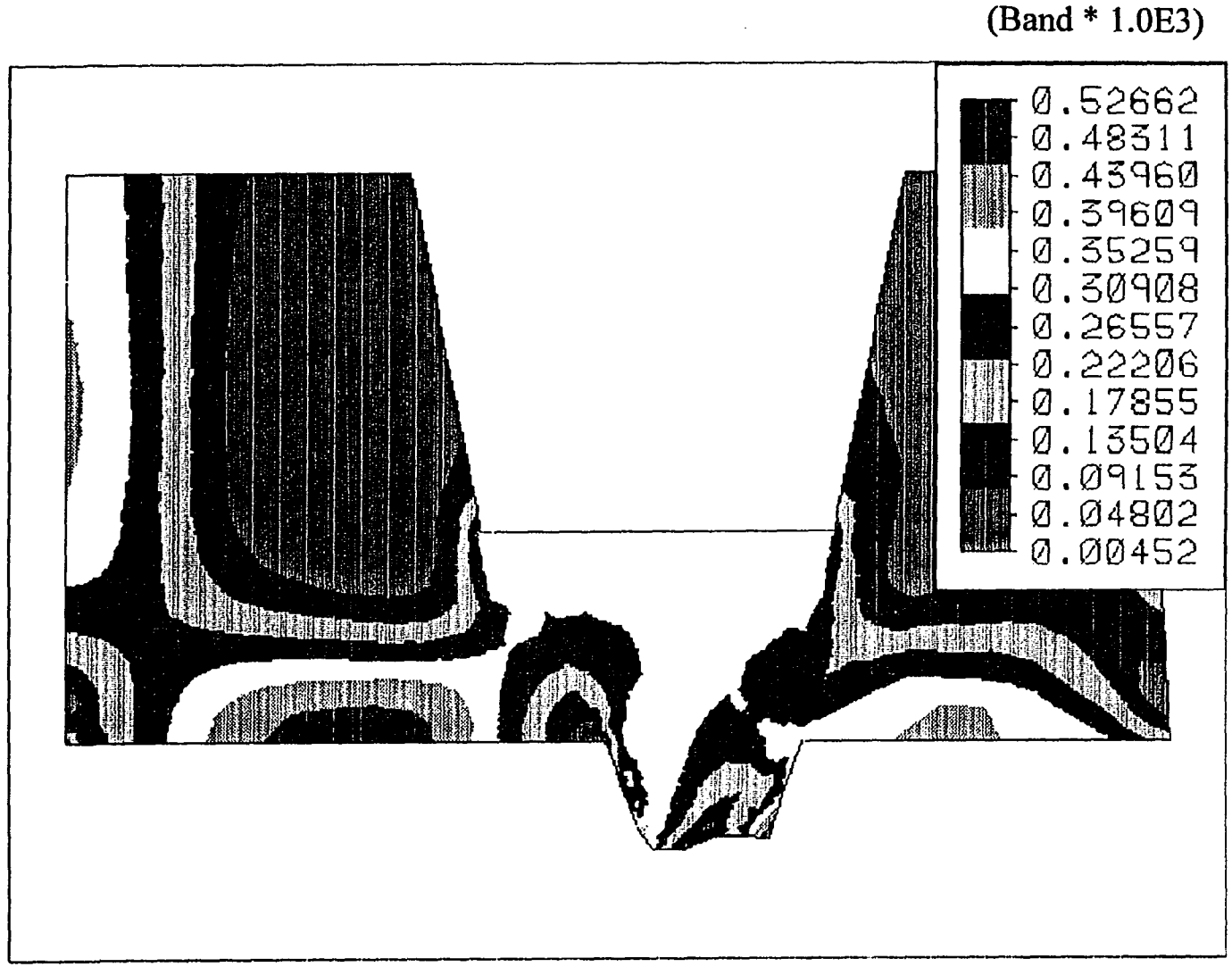

Figure 4.18 Velocity profile curve for 50 pass by finite element analysis for 314 m/sec nozzle exit velocity

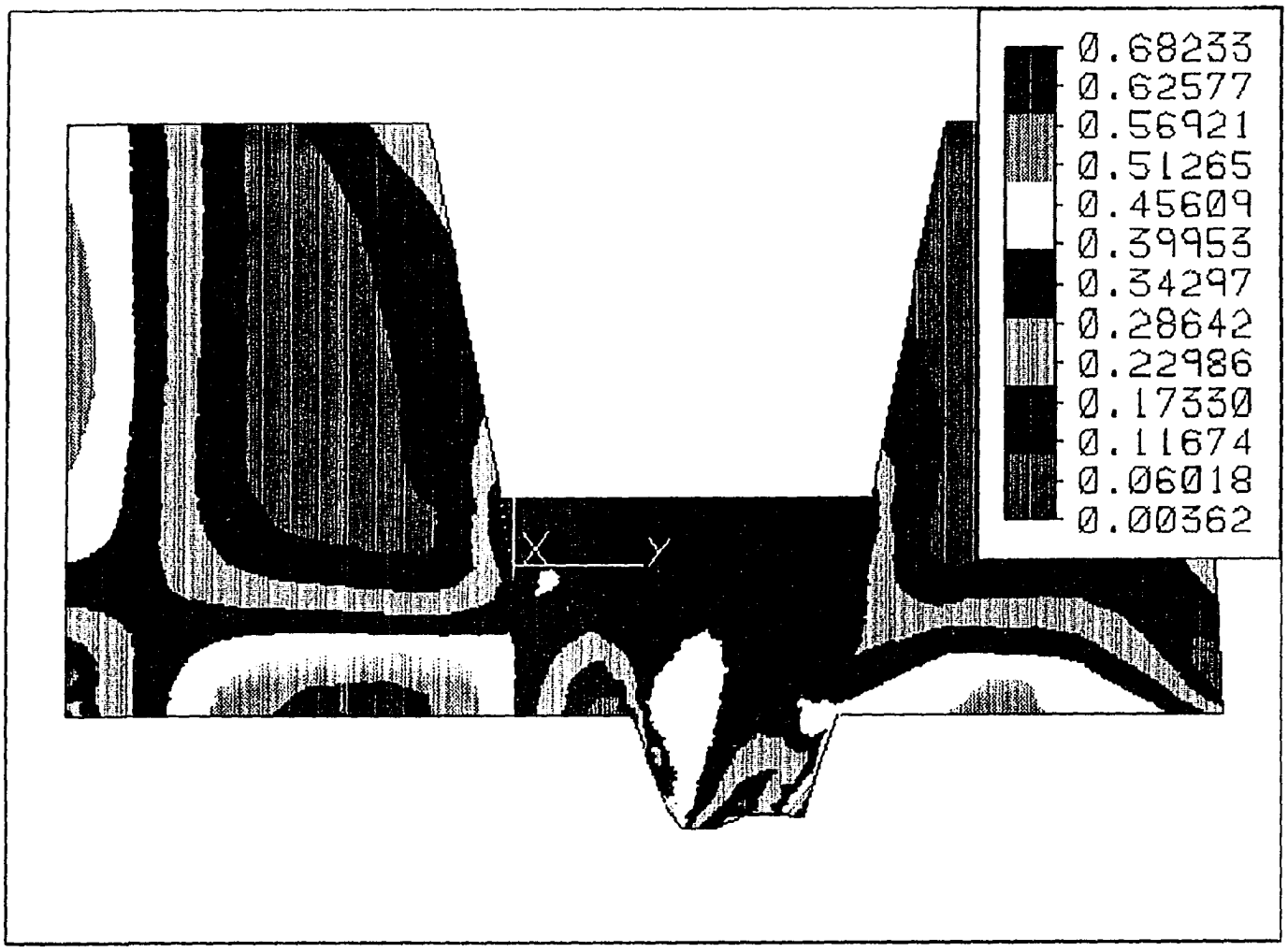

Figure 4.19 Velocity profile curve for 50 pass by finite element analysis for 387 m/sec nozzle exit velocity

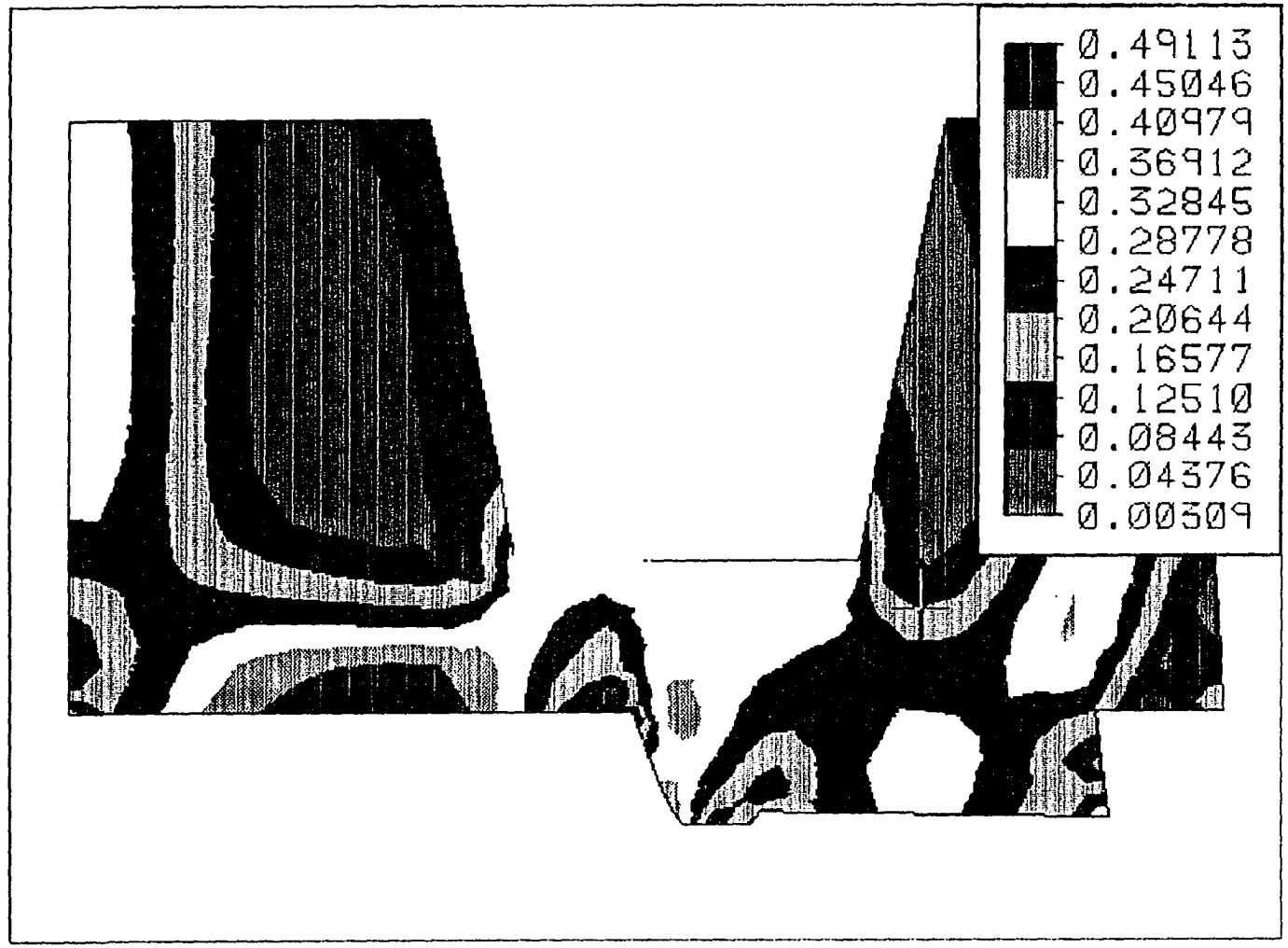

Figure 4.20 Velocity profile curve for 75 pass by finite element analysis for 314 m/sec nozzle exit velocity

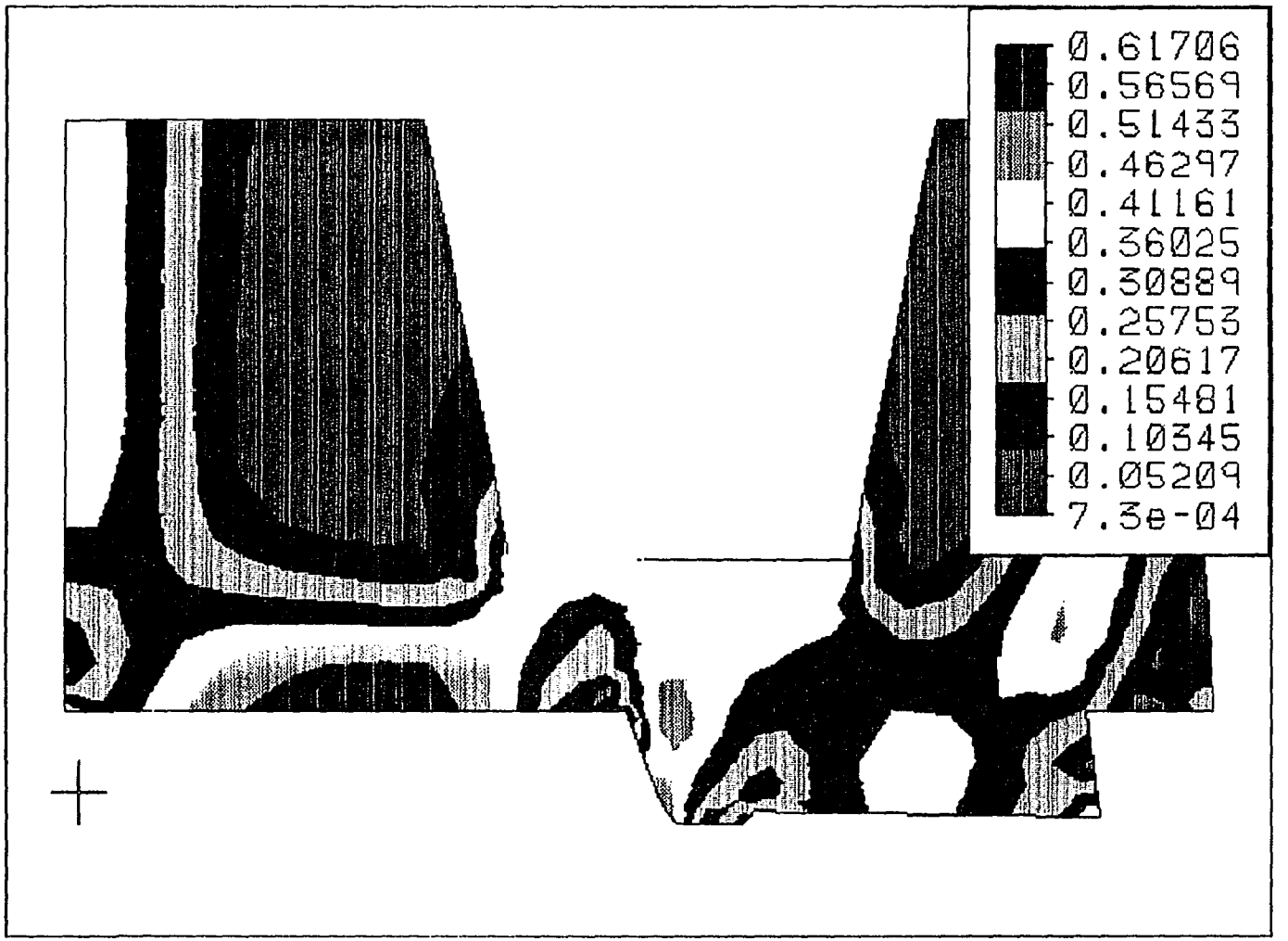

Figure 4.21 Velocity profile curve for 75 pass by finite element analysis for 387 m/sec nozzle exit velocity

5. A MODEL FOR THE PREDICTION OF DIMENSIONAL TOLERANCES OF LASER CUT HOLES

A paper to be submitted to the International Journal of Production Research, United Kingdom.

Aloke Ray*, R. F. Scrutton†, P. A. Molian*and J. L. Hall*

5.1 Abstract

Dimensional variation in laser cutting of sheet metals depends on two factors: the accuracy and repeatability of the positioning system, and the thermal effect of the laser beam on the workpiece material. In this work, a physical model was formulated to estimate the dimensional accuracy of holes due to the occurrence of thermal shrinkage following the laser cutting of steel plates. The model included the assumption that the layer adjacent to the hole is plastically deformed and contains residual stresses of amount equal to the yield strength. The model was used to calculate the size of the holes and cut-out disks of varying radii in steel plates with thicknesses of 3.2 mm and 6.4 mm. The model-predicted data was verified with the experimental data obtained using a 1 kW continuous wave CO_2 laser. Results indicated that there

*Department of Mechanical Engineering, Iowa State University
†Department of Industrial and Manufacturing System Engineering, Iowa State University

is an excellent correlation between the model and the experimental data.

5.2 Nomenclature

T	Temperature, K,
t	Time, sec,
k	Thermal diffusivity, m^2/sec,
K	Thermal conductivity, W/m K,
ϵ	absorptivity of the material
r	$\sqrt{(x^2+y^2)}$ or the radius of hole or disk, m,
P	Laser power, watts,
δ	Material thickness, m,
v	Cutting speed, m/sec,
d	Half width of the Heat Affected Zone(HAZ), m,
σ_r	Radial stresses, MPa,
σ_θ	Circumferential stresses, MPa,
σ_y	Yield stresses of the material, MPa,
E	Young's Modulus, MPa,
ν	Poisson's ratio

5.3 Introduction

Laser systems are finding increasing use in manufacturing industry for sheet metal cutting applications because of the increased awareness among engineers and managers of the capabilities of laser processing and the rapid progress in the technology of laser systems. In addition, the ease of interfacing a laser with CAD/CAM tools allows cost-effective manufacturing of parts and quick changes in design.

Laser cutting offers several benefits: higher material removal rates than conventional processes; narrow kerf; non-contact processing; and the possibility of cutting soft as well as hard materials. Laser cutting is a precision process in which the kerf width is typically in the range 0.15 and 0.25 mm while the taper is about 1 to 2 degrees. Features can be produced with a minimum (web) spacing of about 0.3 times the sheet thickness because the distortion accompanying the process is generally small.

Laser cutting is used to produce many features (various geometries) on large sheets of metal. Although dimensional tolerances and surface finish are generally satisfactory, there still exists a clear need for holding tighter tolerances especially if the feature density is high and the spacing between features is small. The process capability defined in terms of dimensional tolerance of a feature is dependent on several factors including laser cutting parameters, material thickness and properties, accuracy of the positioning machine such as a CNC (computer numerical controller) or robot, the feature size and shape, and the laser-material interaction phenomena. Excellent positioning accuracy (about 0.005 mm) of the motion system may be obtained by using modern servo-mechanisms, high speed CNC, and light but rigid tables. However thermal expansion and shrinkage of the workpiece during laser cutting can cause distortion and thereby affect the process capability. It has been demonstrated [1] that

for long lengths of cut in a sheet metal laser-cut shrinkage strains are higher in magnitude than the expansion strains resulting in a net thermal shrinkage. In order to obtain the best possible accuracy, the part program must accordingly be modified to compensate for this net thermal shrinkage. The objective of the present study was to determine the thermal shrinkage associated with the laser cutting of mild steel plates as a function of feature shape and size, and also to suggest methods for improving dimensional accuracy.

A review of the literature concerning the process capability of laser cutting resulted in very little information [2-7]. Hoffman et al. [1] reported that the dimensional accuracy of laser cut parts of carbon steel, stainless steel, aluminum, titanium and composites can be held to $\pm$ 0.013 mm and surface roughness to 0.8 μm R_a. They determined that laser power and spot size, travel speed and type of assist gas were the key variables that control the accuracy.

Thermal effects are common when cutting thick steel plates, where heat build-up occurs, resulting in a rough, wide kerf. Pulsing the beam reduces the thermal effects but at the expense of reduced cutting speed. Amada laser systems [2] used water assistance during laser cutting to obtain better surface finish and accuracy. Water was sprayed in the form of a mist on the cut edge thus preventing heat build-up. The type of assist gas was found to have a key role in improving the accuracy and surface finish. Nitrogen and argon were the best choices for laser cutting of stainless steel and titanium respectively. Shimizu et al. [3] made a systematic study of the effects laser power and cutting speed on process capability and reported that the dimensional accuracy for cutting of 1.2 mm steel sheet was better than $\pm$ 0.02 mm while the surface roughness was 5 μm (maximum peak-to-valley distance).

Nuss and Geiger [4] conducted a detailed study of the beam polarization effect on precision when laser cutting steel and superalloy. Correlations between tolerances and direction of beam polarization were established. It was concluded that circularly polarized light must be used if tight tolerances are to be held. Osada [5] described an experimental study of the ultra-fine cutting of steel plates by a CO_2 laser. A shorter focal length lens, a smaller incoming beam diameter, and less degradation of optical components are essential to obtain precision laser cutting. Studies showed that the best accuracy obtained was $\pm$ 0.01 mm for 10 mm diameter holes cut with a distance of 100 mm apart.

Dilthey et al. [6] demonstrated that the accuracy of laser cutting is improved if the laser beam has a Gaussian energy distribution. They further showed that dross formation affects precision in laser cutting. For example, the laser cutting of stainless steel exhibited poorer dimensional accuracy than carbon steel due to the excessive formation of viscous dross clinging to the walls of the cut. Petring et al. [7] obtained smooth surfaces and good rectangularity with very little thermal distortion in the 5 kW laser cutting of 15 mm thick stainless steel under optimum conditions.

5.4 Thermal Models

5.4.1 Thermal Model for Prediction of Dimensional Accuracy

Laser cutting of sheet metal causes non-uniform heating in the zone adjacent to the kerf that in turn resists uniform thermal expansion and leads to thermal stresses. This is a physical situation which is similar in most respects to that which occurs in the arc welding and plasma cutting processes. The thermal cycling and accompanying expansions, contractions and elastic and plastic deformations which occur have been

analyzed in detail by many workers including Mitsubushi [10] and Okerblom [8]. More recent computer analyses have become extremely complex so that in the present the simpler analysis of Okerblom [8] will be used. In this theory, it is assumed that a region near to the heat source becomes heated to the extent that the yield flow stress becomes negligibly small. Plastic flow occurs under the action of thermal stresses, resulting in permanent shape change. On cooling, residual stresses (on the order of the yield strength at ambient temperature) develop in and around the region which formerly deformed plastically. The thickness of the region stressed to the yield point value therefore determines the final degree of distortion. In Okerblom's [8] theory it is also assumed that the line heat source is formed instantaneously (very large welding speed). Okerblom [8] assumes that the thickness of the layer stressed to the yield point is approximately equal to twice the thickness of material heated above the recrystallization temperature. He also neglects the possible effects of volume change accompanying phase transformation. The final distortion analysis is carried out on the body after it has cooled to room temperature. The general usefulness of Okerblom's 8] theory has been validated by the work of Bibby and Goldak [9].

Let us consider the laser beam moving on a long plate as shown in Figure 5.1. As it travels along the -x-axis, the heat source produces a steady temperature field which exhibits hot and cold portions surrounding the beam. The temperature gradients generate longitudinal and transverse stresses. The hot zone (eventually the kerf in laser cutting) begins to expand but the surrounding cold zone prevents it from expanding thus causing the development of compressive stresses in the hot zone and tensile stresses in the cold zone. During cooling (after laser cutting is completed), the stress pattern is reversed the plate is also less constrained due to the presence of the

kerf. This will in turn produce smaller tensile residual stresses in the zone adjacent to the kerf.

Typical physical and thermal properties of mild steel plate are listed in Table 5.1.

Table 5.1: Properties of typical Mild Steel Plate [10]

Bulk density	7860 kg/m^3
Specific heat	420 J/kgK
Thermal conductivity	45 W/m K
Melting temperature	1700 K
Thermal diffusivity	13.6 x 10^{-6} m^2/s
Yield strength	205 MPa
Young modulus	205 x 10^3 MPa
Poisson's ratio	0.3

Consider the laser cutting of a hole using a stationary laser beam and moving workpiece in x and y directions. The temperature rise during laser heating may be assumed to follow Okerblom's [8] equation given below which assumes the following:

$$T = \frac{\epsilon P\sqrt{k}}{2K\delta\sqrt{\pi v r}} e^{\frac{-v(x+r)}{2k}} \tag{5.1}$$

1. The temperature distribution over the thickness is uniform
2. The beam is treated as a line heat source
3. Bessel function is approximated
4. High cutting speed
5. Heat evolution due to phase change is neglected

For mild steel when the temperature reaches 873 K, the yield strength reduces to zero [8]. Hence plastic deformation in the HAZ can occur from the cut edge to the point where the temperature is 873 K. An estimate of the width of the heat affected zone, d, in which plastic deformation may take place is made from the above equation. It is expected that phase transformation of austenite to pearlite (or martensite) also occurs in the HAZ which involves expansion during cooling. We assume that the volume increase accompanying phase change contributes little to the dimensional inaccuracy as compared with the distortion caused by the residual stresses.

The values of HAZ (d) for steel plates of varying thickness are listed in Table 5.2.

Table 5.2: Calculated values of width of HAZ (d) for varying thicknesses of steel plates

Laser power (P): 1000 watts, Diffusivity (k): 13.6 x10^{-6} m^2/s
Conductivity (K): 45 W/m k, x = 0.0
and y = d, absorptivity (ϵ): 0.8 [11]

Plate thickness (δ) mm	Cutting speed (v) m/sec	Width of HAZ (d) mm
3.20	0.0508	0.2900
6.40	0.0254	0.2650

Radial displacement is now determined using the equations developed by Timoshenko and Goodier [11]. In doing so, the stresses are assumed to be symmetrical about the center of the hole in the semi-infinite plate. This is equivalent to Okerblom's original assumption that the linear weld bead is laid down in an incrementally short time interval.

The stress distribution symmetrical about an axis is given by the following ex-

pressions [8]

$$\sigma_r = \frac{A}{r^2} + B(1 + 2logr) + 2C \tag{5.2}$$

$$\sigma_\theta = -\frac{A}{r^2} + B(3 + 2logr) + 2C \tag{5.3}$$

where A, B and C are the constants and σ_r and σ_θ are corresponding radial and circumferential stresses.

Figures 5.2 and 5.3 depict the laser-cut hole and disk in a semi-infinite plate respectively. R and d are the radius and the width of the region stressed to the yield point respectively. It should be noted that d is very small compared to R. Equations 5.4 and 5.5 along with the boundary conditions listed in Table 5.3 were applied to evaluate the constants A, B, and C for the hole and disk.

Table 5.3: Boundary conditions for hole and disk

Condition	Hole	Disk
r = R	$\sigma_r = 0$	$\sigma_r = 0$
r = R	$\sigma_\theta = \sigma_y$	$\sigma_\theta = \sigma_y$
r = R + d	$\sigma_\theta = \sigma_y$	—
r = R - d	—	$\sigma_\theta = \sigma_y$

Once the values of all the constants are known, the displacement u, in the radial direction may be calculated as follows [11]:

$$u = \frac{1}{E}\left[-\frac{(1+\nu)}{r}A + 2(1-\nu)Br\log r - B(1+\nu)r + 2C(1-\nu)r\right] \tag{5.4}$$

The difference in thickness of the stresses layers between 3.2 mm and 6.4 mm thick plate is so small (see Table 5.2) that it does not contribute any significant

Table 5.4: Diametral Displacement ($U_T = 2$ u)

Diameter of Hole or Disk, mm	Displacement U_T, mm
50.80	- 0.0163
76.20	- 0.0317
101.6	- 0.0450

difference in the shrinkage in our application. The diametral displacement (shrinkage) is same for both the hole and the disk. Table 5.4 lists the displacement (shrinkage) data.

5.5 Experimental method

In the present work, accuracy and repeatability of the X-Y table was measured using a precision dial indicator. The results are shown in Table 5.5. The repeatability of the X-Y table was found to be 0.0127 mm.

The manufacturer's figures for the repeatability and the positioning accuracy

Table 5.5: X-Y Table Positioning Accuracies at a Speed 42.33 mm/sec.

Length of Travel mm	Travel(X-dir.) mm	Accuracy mm	Travel(Y-dir.) mm	Accuracy mm
06.35	06.3246	-0.0254	6.3246	-0.0254
12.70	12.6746	-0.0254	12.6746	-0.0254
19.05	18.9992	-0.0508	18.9992	-0.0508
25.40	25.3492	-0.0508	25.3492	-0.0508

[For length of travel $\geq$ 25.4 mm, the accuracy remained constant]

Table 5.6: Repeatability and Positioning Accuracies for Xcel 765 CMM Machine.

Repeatability	0.0035 mm
Positioning Accuracy(X-axis)	+ 0.0040 mm
Positioning Accuracy(Y-axis)	+ 0.0040 mm

of the Co-ordinate Measuring Machine(CMM) are shown in Table 5.6 (Model Xcel 765, Manufacturer: Brown and Sharpe, in accordance with ANSI/ASME B89.1.12M National Standard)

5.5.1 Experimental Setup and Measurements

In the laser cutting experiments 3.2 mm and 6.4 mm thick low carbon steel plates were used. The laser cutting system used in this work is illustrated in Figure 5.4 The laser source was a 1.5 kW (maximum), CW CO_2 laser (Rofin Sinar Model 820). The beam was circularly polarized and delivered to the workpiece through a beam delivery system with a ZnSe lens of 127 mm focal length. The workpiece was mounted on a CNC X-Y positioning table. Figure 5.5 shows the schematic of the cutting procedure in which the laser beam was scanned across the workpiece resulting in the cutting of a disk or the cutting of a hole in the workpiece. Table 5.7 lists the process variables employed.

5.5.2 Experimental Measurement

The minimum and maximum sizes of the kerf width were measured using an optical microscope and are given in Table 5.8. The co-ordinate measuring machine

Table 5.7: Process variables

Laser	CW CO_2
Wavelength	10.6 μm
Power	1000 Watts
Beam focus	on the surface
Focused spot size	0.25 mm
Scan rate	25.4 mm/sec (6.4 mm) and 50.8 mm/sec (3.2 mm)
Distance between scans	0.05 mm
Coaxial assist gas	oxygen
Gas pressure	97 kPa (6.4 mm) and 138 kPa (3.2 mm)

(CMM) was used to measure the diameters of the holes and disks by registering 20-50 points around the circumference. The maximum and minimum sizes were considered to be the upper and lower limits of the diameter. The numerical data values are listed in Appendix B.

Table 5.8: Kerf Width for 1020 Steel Plate

Thickness(mm)	Minimum Width(mm)	Maximum Width(mm)
3.20	0.2134	0.2337
6.40	0.2692	0.2972

5.6 Results

Once the experimentally determined positioning accuracies and repeatabilities, experimental kerf widths and theoretically determined thermal displacements were obtained, the total dimensional inaccuracies could be estimated and are shown in Figures 5.6 through 5.9. Comparison of experimental and analytical data is also

shown in Table 5.9, and the difference in experimental and analytical data is shown in Table 5.10.

Departures from nominal dimension are shown plotted against diameter in Figures 5.6 and 5.7 (for the disk) and Figures 5.8 and 5.9 (for the hole). Differences between calculated and theoretical values exhibit one pattern for the hole and the opposite pattern for the disk. Overall, large diameters are produced equally accurately as smaller ones in terms of (Dhole - Dnom.), (Ddisk - Dnom.). However, expressed as a percentage, larger holes are produced more accurately.

Regarding overall accuracy of cutting it is clear that the maximum error that might be expected is $\pm$ 0.1mm for the holes or the disks. It is observed that, disks are produced more accurately than holes. Also holes and disks in thicker sheet are generally produced less accurately than in thinner sheet.

5.7 Conclusion

Given the natural variation in edge roughness texture, and the errors implicit in the motion of the X-Y table and the CMM that were used, it can be concluded that the theory of Okerblom [8] can provide a reasonable estimate of the dimensional errors which might be expected in the laser cutting of thin low carbon steel sheet.

In our calculation we have considered 20 points to 50 points along the circumference for determining hole or disk diameter. The selection of the number of points, in the present situation is based on standard practice. This calls for the creation and implementation of statistical data which can produce more accurate results. Based on our analytical calculations as well as from experimental observation, it can be concluded that a good prediction of sizes can be made. This analysis is completely

Table 5.9: Experimental and Analytical Data for Laser cut Disk and Holes

Thickness in(mm)	Nominal Size (Dnom) of the cut(mm)	Disk(mm)(Ddisk)		Hole(mm)(Dhole)	
		Experimental	Analytical	Experimental	Analytical
3.20	50.8	50.540	50.532	50.941	50.979
–	–	50.548	50.552	50.969	50.999
3.20	76.2	75.953	75.947	76.420	76.394
–	–	75.970	75.968	76.447	76.415
3.20	101.6	101.312	101.361	101.746	101.808
–	–	101.378	101.381	101.757	101.828
6.40	50.8	50.462	50.468	50.967	51.035
–	–	50.515	50.496	50.981	51.063
6.40	76.2	75.975	75.884	76.411	76.450
–	–	76.007	75.912	76.450	76.478
6.40	101.6	101.264	101.2970	101.734	101.863
–	–	101.323	101.325	101.808	101.891

[Data includes x-y Table positioning accuracy of - 0.0508 mm but excludes CMM accuracy of + 0.0040 mm]

Table 5.10: Difference in Experimental and Analytical Data for Laser cut Disk and Holes

Thickness in(mm)	Nominal Size (Dnom) of the cut(mm)	Diff. in Disk(mm)(Ddisk)		Diff. in Hole(mm)(Dhole)	
		Experimental	Analytical	Experimental	Analytical
3.20	50.8	0.009	0.020	0.028	0.020
3.20	76.2	0.017	0.021	0.027	0.021
3.20	101.6	0.066	0.020	0.011	0.020
6.40	50.8	0.052	0.028	0.014	0.028
6.40	76.2	0.033	0.028	0.039	0.028
6.40	101.6	0.059	0.028	0.074	0.028

[Data includes x-y Table positioning accuracy of - 0.0508 mm but excludes CMM accuracy of + 0.0040 mm]

restricted to circular hole or disk made of thin mild steel plate.

5.8 References

[1] Grigoryants, "Basics of Laser Material Processing", Chapter 5, *Mir Publishers*, CRC Press, 1994

[2] Hoffman, D. J., Migliore, L. R.,"Advanced Laser Cutting", in *Proc. Conference*, Reno Neveda, 1-3 Nov. 1987, 252-262

[3] Shimizu, T., Asao, F., Masuo, Y. and Nishimoto, I., "CO_2 laser Cutting of Steels and Ceramics" methods for ceramics', in *Nagoya-shi Kogyo Kenkyusho Kenkyu Hokoku (Res. Rep. Nagoya Munic. Ind. Res. Inst.)*, Vol. 72, 1987, 1-4

[4] Nuss, R., Geiger M., "Laser Beam Cutting of Thin sheet: Process Quality and Technical Aspect. I. Influence of the Machine and the Beam Polarization", *Werkstattstechnik*, Oct 1988, 78(10), 565-568

[5] Osada, H., "Ultra fine Cutting by CO_2 Laser", Focus on Laser Materials Processing -6th .*International Congress on Applications of Lasers and Electro-optics - ICALEO'87*, SanDiego, CA, 8-12 Nov. 1987, 157-162

[6] Dilthey, U., Faerber, M., Weick, J.,"Laser Cutting of Steel-cut Quality Depending on cutting parameter", *Riv. ital. Saldatura*, Sept-Oct 1992, 44(5), 449-453

[7] Petring,D., Zeffererer, H., Beyer,E., Uhlig, G. and Behr, F., "Laser Beam Fusion Cutting of Stainless Steels with CO_2 Laser", *Stahl*, 15 March, 1992(1), 71-76

[8] Okerblom, N. O."The calculations of Deformations of Welded Metal Structure". Her Majesty's Stationery Office, London, 1958, 13-33

[9] Bibby, M. J., and Goldak, J. A., " Weld Induced Camber in Structural Sections" 101-115 (page), *Weldments: Physical Metallurgy and Failure Phenomena"*, Proceedings of the Fifth Bolton Landing Conference, Aug 1978. Edited by : Christoffel, R. J., Nippes, E. F., and Solomon, H. D., Published by: General Electric Co., Schenectady, NY.

[10] Mitsubushi K., "Residual Stress and Distortion", *Metal Handbook*, Society of Metal, Ohio, 9th edition, 6, (1983), 856-894

[11] Timoshenko, S. P., Goodier, J. N., *"Theory of Elasticity"*, 3rd edition, McGraw Hill Book Company, New York, 1970

[12] Wilson, J., Howkes, J. F. B., *"Lasers Principles and Applications"*, Prentice Hall International Series in Optoelectronics, 1987, 174

[13] Schuoker, D., "Proceedings of Society of Photo Instrumentation Engineers", Vol.952,(Society of Photo Instrumentation Engineers, 1988), 592-599

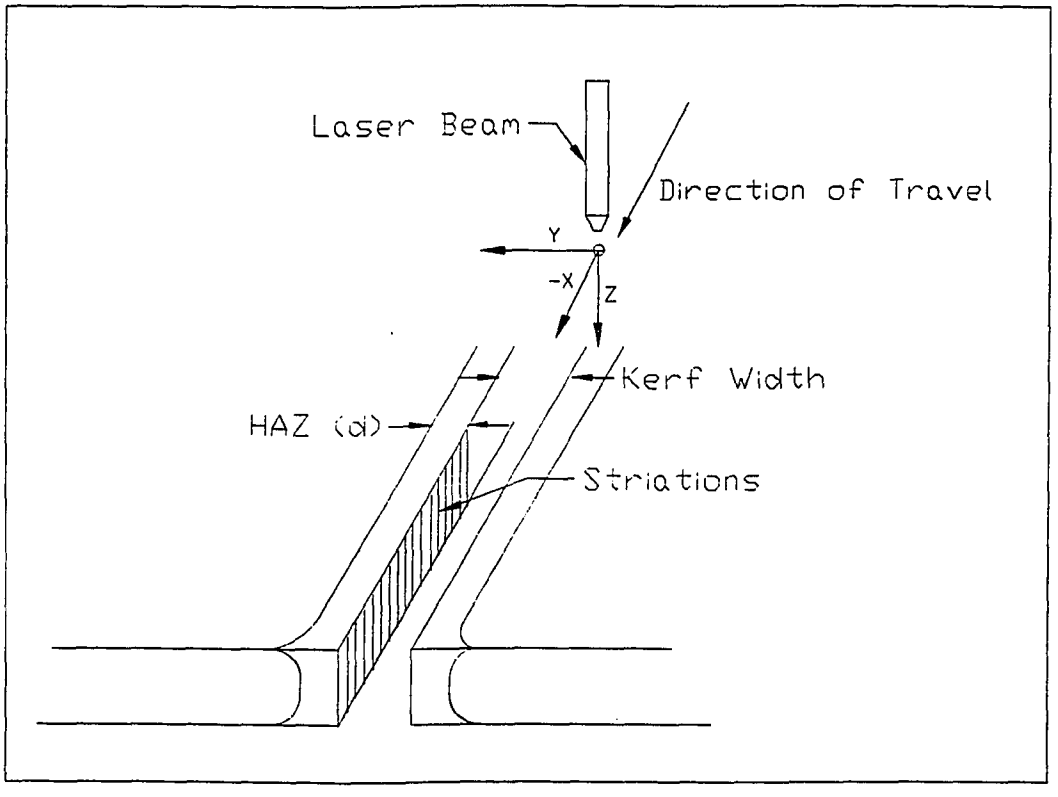

Figure 5.1: A schematic representation of Laser cutting process

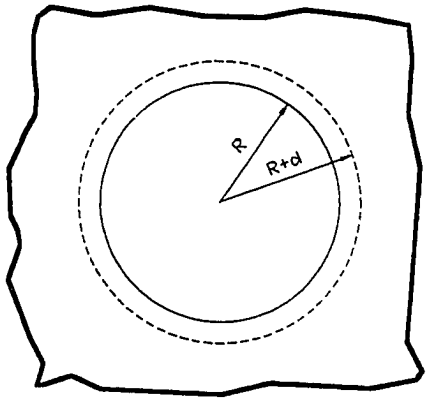

Figure 5.2: Hole in a semi-infinite plate with (HAZ)

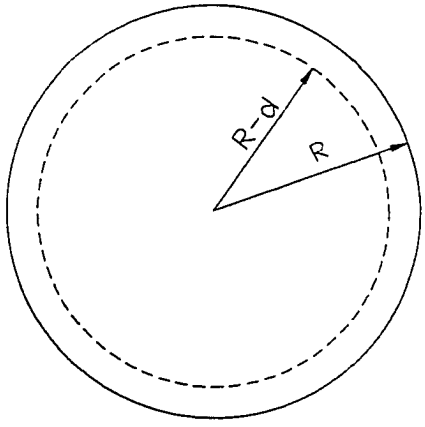

Figure 5.3: Cut-out solid disk with (HAZ)

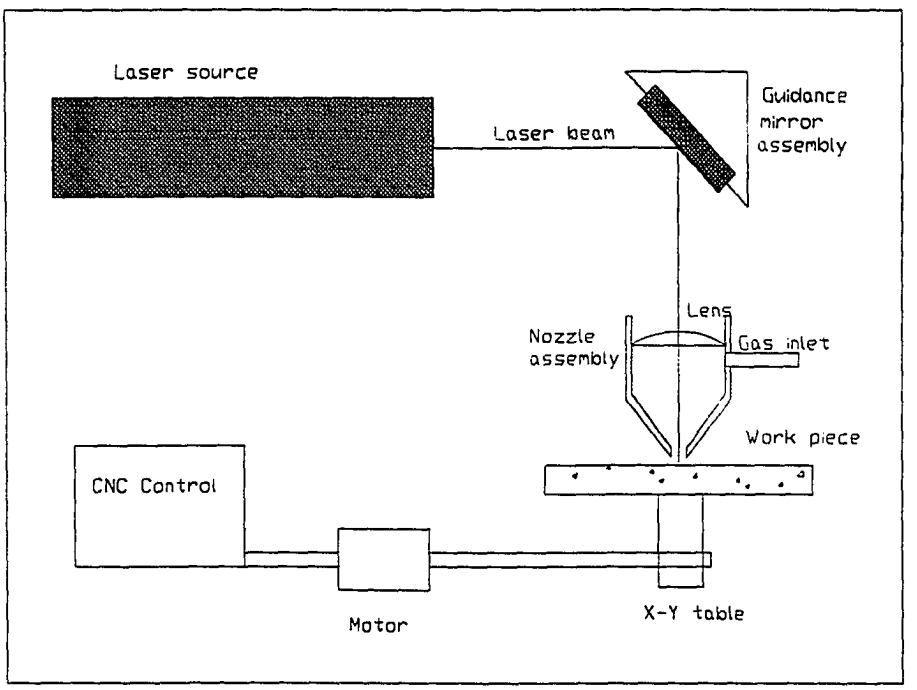

Figure 5.4: A schematic of the laser cutting system employed in this study

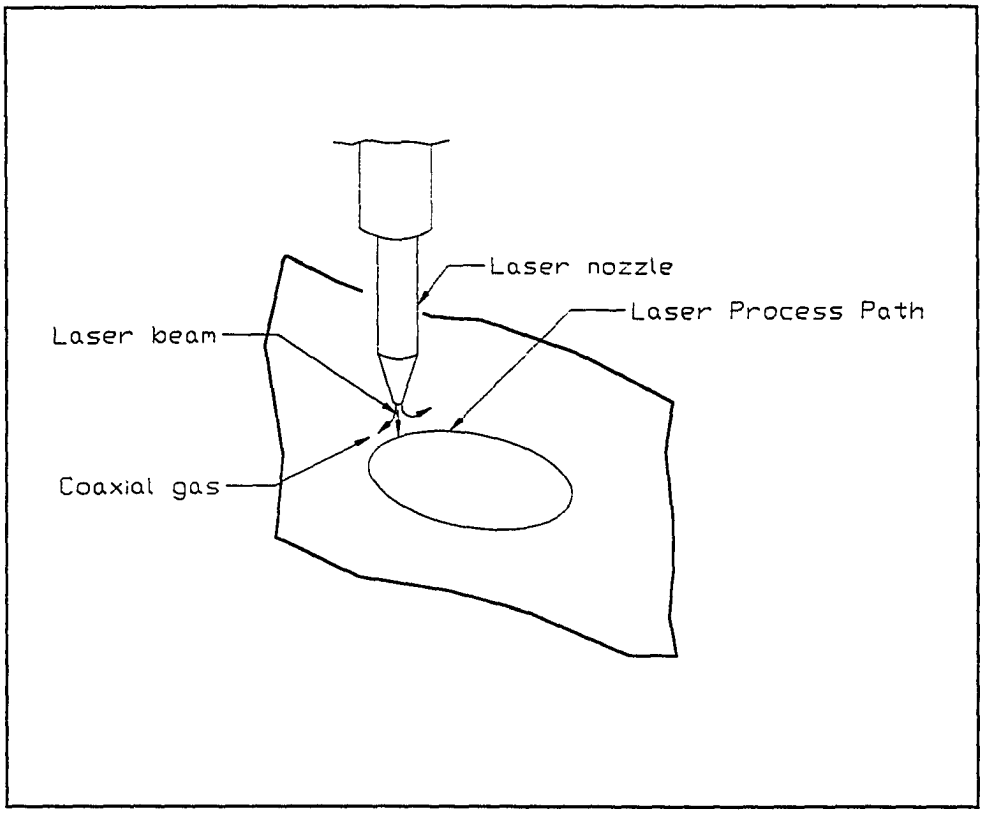

Figure 5.5: A schematic showing the Laser Cutting procedure

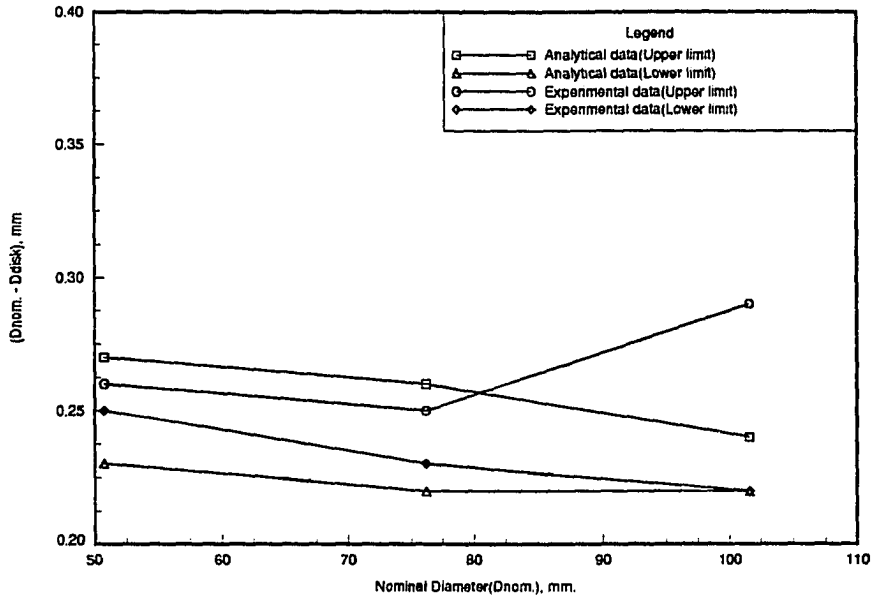

Figure 5.6: Accuracy VS. Nominal dia. for 3.20 mm Steel Plate, for the disk [Data includes positioning table inaccuracy]

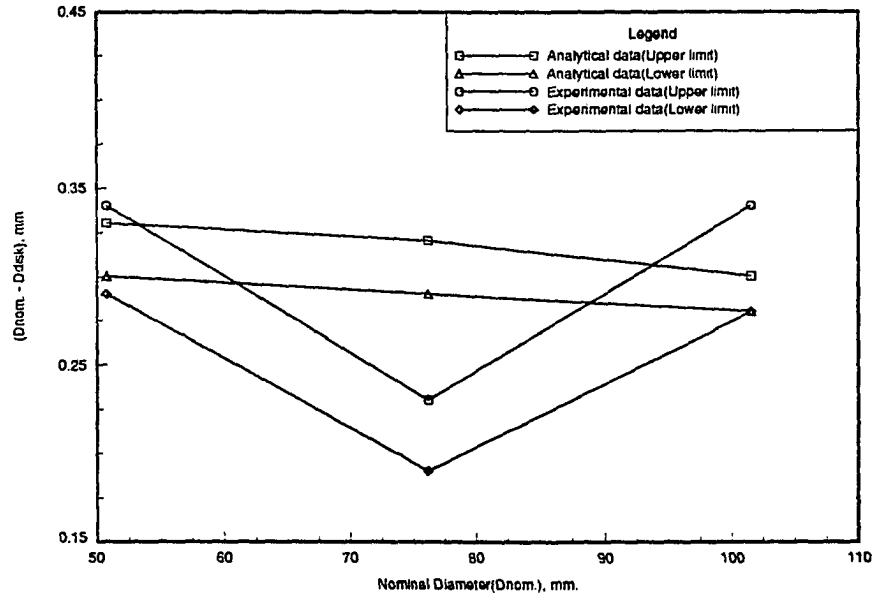

Figure 5.7: Accuracy VS. Nominal dia. for 6.40 mm Steel Plate , for the disk [Data includes positioning table inaccuracy]

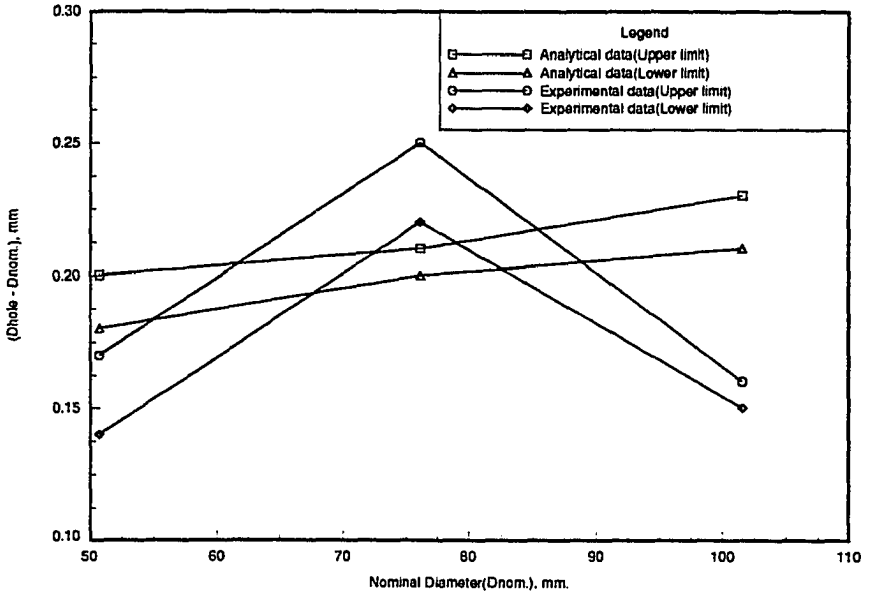

Figure 5.8: Accuracy VS. Nominal dia. for 3.20 mm Steel Plate for the Hole [Data includes positioning table inaccuracy]

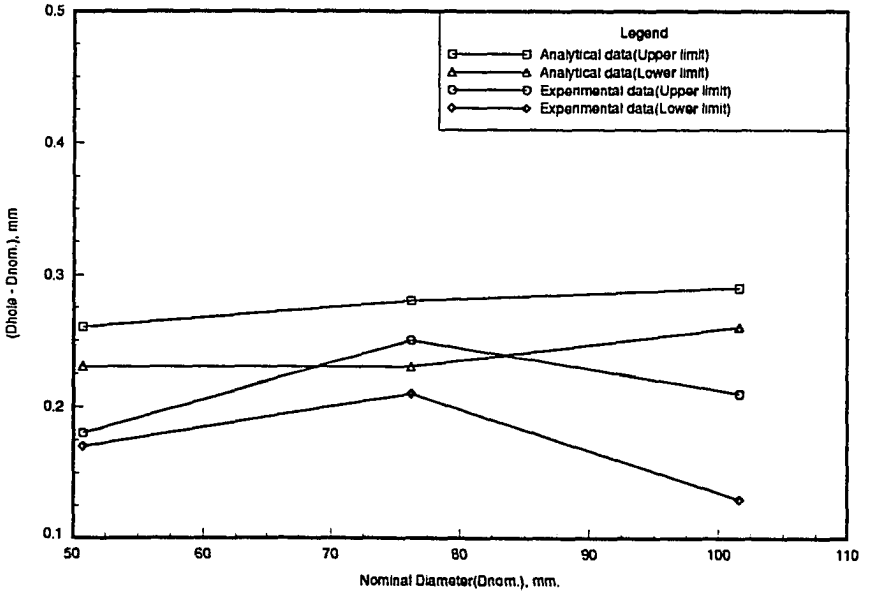

Figure 5.9: Accuracy VS. Nominal dia. for 6.40 mm Steel Plate for the Hole [Data includes positioning table inaccuracy]

6. GENERAL CONCLUSIONS

In the present investigation, we have studied laser-material interaction with ceramics and metals. The study of laser milling was focused on the experimental methods and thermal modeling of material removal aspects such as depth of cut, temperature of the workpiece, and the quality of the milled surface of silicon nitride. A parametric study involving laser power, spot size, travel speed and type of assist gas and its flow was carried out. The potential problem in laser milling of silicon nitride is the formation of recast layer which in turn responsible for initiating cracks, degrading the surface finish and lowering the depth of cut.

It is observed that, the influence of assist gas plays very important role. In case of laser cutting of ceramics, type of assist gas such as O_2 produced deeper cut, but on the other hand during laser milling process more depth of cut is obtained with more recast layer, hence overall depth of milling is greatly reduced. Oxygen produced exothermic reaction during laser material interaction, hence deeper cut with more recast layer is expected. In case of nitrogen as an assist gas produces less depth of cut during cutting, but in milling produces less recast layer , hence overall depth of milled surface is much higher with less cracks compared to oxygen. Porosity in ceramics absorbs energy, which helps for deeper cut with less cracks on the top surface.

The preheating temperature is also one of the key issue for determining depth of cut in case of laser milling. Higher the speed more the preheating temperature is expected on the cutting zone due to overlapping laser scans, where the heat radiation from the surface is minimum. More preheating temperature contributes towards deeper cut with more recast layer on the surface. If the assist gas pressure is not high enough to blow away most of the molten slag, which gets redeposited on the milled surface, thus reducing surface finish.

In case of laser interaction with mild steel, the presence of oxygen produces exothermic reaction, hence deeper cut is expected and also less kerf width is observed during high speed laser cutting process. It is experimentally found that as the thickness of the plate increases, the kerf width also increases. During laser cutting process as the size of the cut (bigger dia hole) increases more thermal shrinkage in the surrounding edge is expected, which adversely effects the overall dimensional tolerances.

A thorough investigation is necessary to understand laser-ceramics interaction, so that deeper milled contours can be produced with less recast layer and minimum thermal damage on the surface. In case of dimensional tolerances, the prediction of size of various different shapes with different material have left for future investigation.

REFERENCES

[1] Sanderson, R. J., "Lasers in Metalworking, a summary and Forecast", Tech. Tran Corp., Naperville, IL, 1983, 48

[2] Chryssolouris, G., "Laser Machining - Theory and Practice", Springer-Verlag, 1991, New York, NY

[3] Steen, W. M., "Laser Material Processing", Springer-Verlag, 1991, NEW YORK, NY

[4] "Guide for Laser Materials Processing", Laser Institute of America, 1993, p. 93

[5] Natarajan, R., "An Experimental and Theoretical Study of Heat Transfer Effects During a Laser-Cutting Process", *Ph. D Thesis, Iowa State University*, Ames, IA, 1990

[6] Hsu, M. J., "Analytical and Experimental Studies of Advanced Laser Cutting Techniques", *Ph. D Thesis, Iowa State University*, Ames, IA, 1992

[7] Yilbas, B. S., "Study of Affecting Parameters in Laser Hole Drilling of Sheet Metals", *ASME Journal of Engineering Materials and Technology*, vol. 109, Oct. 1987, 282-285

[8] "Technical Note, CO_2 Laser Cutting", Spectra Physics, Industrial Laser Division, Farmington Hills, MI

[9] Powell J., "Guidelines and Data for Laser Cutting",*Industrial Laser Annual Handbook*, 1990, 56-66, Liverpool, U. K.

[10] Ray, Aloke, Molian, P. A., Scrutton, R. F., Mitra, A. K., "Carbon-dioxide Laser Milling of Reaction Bonded Silicon Nitride", Submitted to *International Journal of High Technology Ceramics*, 1995, Leeds,U. K.

[11] Smith, W. F., "Structure and Properties of Engineering Alloys", McGraw Hill Book Company, New York, 1981, 28-29

[12] Watu, D., "Laser Hole Drilling under nonlinear Liquid Mediums", *M. S. Thesis, Iowa State University*, Ames, IA, 1993

[13] Powell, J., Ivarson, A., Kamalu, J., Broaden G., Magnusson, C., "The role of Oxygen Purity in Laser Cutting of Mild Steel", *ICALEO*, 1992, 433-442

[14] Gabzdyl, J. T., Morgan, D. A., "Assist Gases for Laser Cutting of Steels", *ICALEO*, 1992, 443-448

[15] Neill, W. O., Gabzdyl, J. T., Steen, W. M., "The Dynamical behoΦavior of Gas jets in Laser Cutting", *ICALEO*, 1992, 449-458

[16] Wallace, R. J., and Copley, S. M., "Shaping Silicon nitride with a carbon dioxide laser by overlapping multiple grooves", *ASME Journal of Engineering for Industry*, III, November (1989) 315

APPENDIX A. SOURCE CODE FOR ESTIMATING PREHEATING TEMPERATURE

```
      program aloke1
c     ------------------------------------------------------------------
c     Program for predicting Preheating temperature
c     ------------------------------------------------------------------
      implicit real*8(a-h,o-z)
      external func
      common/var1/x(400),t(400),tn(400)
      common/var2/dt,time
      common/intg/i,nx
      common/spl/s(400),ind(400)
c
      pi = 4.0*datan(1.0d0)
c
c     read in test condition
c
      read(1,*)nx,nstep
      read(1,*)tau,dt
c
c     generate a grid with pack
c
      xd = 12.5
      xc = 11.0
      call pack(nx,xc,xd,tau,x,400)

      do i=1,nx
         x(i) = x(i)-11.0
      enddo
```

```
c     ------------------------------------------
c     initialize temperature distribution
c     ------------------------------------------
      do i=1,nx
         r = abs(x(i))
         tmp1 = dexp(-116.0*(x(i)+r))
         if(abs(x(i)) .le. 0.0125)then
            t(i) = 2150.0
         else
            t(i) = 240.6/sqrt(r)*tmp1 + 300
         endif
         write(10,*)x(i),t(i)
      enddo
c
c     set integration limit
c
      xb  = x(1)
      xe  = x(nx)
      acc = 1.0d-3

      time = 0.0
      do n=1,nstep
         time = time + dt
         call spcoef(nx,x,t,s,ind)
         do i=1,nx
            call simp(func,xb,xe,acc,ans,error,area,iflag)
            tn(i) = 0.5*ans/sqrt(0.031*pi*time)
         enddo
c
c     overwrite previous temperature profile
c
         do i=1,nx
            t(i) = tn(i)
         enddo
c
c     write out temperature profile before next step
c
         do i=1,nx
            write(10+n,*)x(i),t(i)
         enddo
```

```
c
      enddo

      stop
      end
c
      function func(xpr)
      implicit real*8(a-h,o-z)
      common/var1/x(400),t(400),tn(400)
      common/var2/dt,time
      common/intg/i,nx
      common/spl/s(400),ind(400)

      expno = -0.25*(x(i)-xpr)**2/(0.031*time)
      f     =  spline(nx,x,t,s,ind,xpr)
      func  =  f*exp(expno)

      return
      end
c
      subroutine pack(n,yc,h,t,s,m)
      implicit real*8(a-h,o-z)
      dimension s(m)
      wd=1.0/float(n-1)
      et=dexp(t)
      emt=1.0/et
      ych=yc/h
      bigb=dlog((1.0+(et-1.0)*ych)/(1.0+(emt-1.0)*ych))/(2.0*t)
      do 10 nn=2,n-1
         ybar=float(nn-1)*wd
         s(nn)=yc*(1.0+dsinh(t*(ybar-bigb))/dsinh(t*bigb))
 10   continue
      s(1)=0.0
      s(n)=h
      return
      end
c
      subroutine simp(fsimp,a,b,acc,ans,error,area,iflag)
c     ------------------------------------------------------------
c     SIMP integrate numerically the function fsimp between a and b
```

```
c     within the accuracy specified in acc. The integrated value is
c     return in ans.
c     ----------------------------------------------------------------

      implicit real*8(a-h,o-z)
      parameter(np=540)
      dimension fv(np),lorr(np),f1t(np),f2t(np),f3t(np),dat(np),
     $          arestt(np),estt(np),epst(np),psum(np)
      external fsimp
      u=9.0e-7
      fouru=4.0*u
      iflag=1
      eps=acc
      error=0.0
      lvl=1
      lorr(lvl)=1
      psum(lvl)=0.0
      alpha=a
      da=b-a
      area=0.0
      arest=0.0
      fv(1)=fsimp(alpha)
      fv(3)=fsimp(alpha+0.5*da)
      fv(5)=fsimp(alpha*da)
      kount=3
      wt=da/6.0
      est=wt*(fv(1)+4.0*fv(3)+fv(5))
 1    dx=da*0.5
      fv(2)=fsimp(alpha+0.5*dx)
      fv(4)=fsimp(alpha+1.5*dx)
      kount=kount+2
      wt=dx/6.0
      estl=wt*(fv(1)+4.0*fv(2)+fv(3))
      estr=wt*(fv(3)+4.0*fv(4)+fv(5))
      sum=estl+estr
      arestl=wt*(dabs(fv(1))+dabs(4.0*fv(2))+dabs(fv(3)))
      arestr=wt*(dabs(fv(3))+dabs(4.0*fv(4))+dabs(fv(5)))
      area=area+((arestr+arestl)-arest)
      diff=est-sum
      if(dabs(diff).le.eps*dabs(area)) go to 2
```

```
      y=fouru*dabs(alpha)
      if(dabs(dx).le.y) go to 5
      if(lvl.ge.30) go to 5
      if(kount.ge.2000) go to 6
      lvl=lvl+1
      lorr(lvl)=0
      f1t(lvl)=fv(3)
      f2t(lvl)=fv(4)
      f3t(lvl)=fv(5)
      da=dx
      dat(lvl)=dx
      arest=arestl
      arestt(lvl)=arestr
      est=estl
      estt(lvl)=estr
      eps=eps/1.4
      epst(lvl)=eps
      fv(5)=fv(3)
      fv(3)=fv(2)
      go to 1
2     error=error+diff/15.0
3     if(lorr(lvl).eq.0) go to 4
      sum=psum(lvl)+sum
      lvl=lvl-1
      if (lvl.gt.1) go to 3
      ans=sum
      return
4     psum(lvl)=sum
      lorr(lvl)=1
      alpha=alpha+da
      da=dat(lvl)
      fv(1)=f1t(lvl)
      fv(3)=f2t(lvl)
      fv(5)=f3t(lvl)
      arest=arestt(lvl)
      est=estt(lvl)
      eps=epst(lvl)
      go to 1
5     iflag=2
      go to 2
```

```
 6    iflag=3
      go to 2
      end
c
      subroutine spcoef(n,xn,fn,s,index)
      implicit real*8(a-h,o-z)
      dimension xn(n),fn(n),s(n),index(n),
     &          rho(400),tau(400)
      nm1=n-1
      do 1 i=1,n
         index(i)=i
 1    continue
      do 3 i=1,nm1
         ip1=i+1
         do 2 j=ip1,n
            ii=index(i)
            ij=index(j)
            if(xn(ii).le.xn(ij)) go to 2
            itemp=index(i)
            index(i)=index(j)
            index(j)=itemp
 2       continue
 3    continue
      nm2=n-2
      rho(2)=0.0
      tau(2)=0.0
      do 4 i=2,nm1
         iim1=index(i-1)
         ii=index(i)
         iip1=index(i+1)
         him1=xn(ii)-xn(iim1)
         hi=xn(iip1)-xn(ii)
         temp=(him1/hi)*(rho(i)+2.0)+2.0
         rho(i+1)=-1.0/temp
         d=6.0*((fn(iip1)-fn(ii))/hi-(fn(ii)-fn(iim1))/him1)/hi
         tau(i+1)=(d-him1*tau(i)/hi)/temp
 4    continue
      s(1)=0.0
      s(n)=0.0
      do 5 i=1,nm2
```

```
         ib=n-i
         s(ib)=rho(ib+1)*s(ib+1)+tau(ib+1)
 5    continue
      return
      end
c
      function spline(n,xn,fn,s,index,x)
      implicit real*8(a-h,o-z)
      dimension xn(n),fn(n),s(n),index(n)
      i1=index(1)
      if(x.ge.xn(i1)) go to 1
      i2=index(2)
      h1=xn(i2)-xn(i1)
      spline=fn(i1)+(x-xn(i1))*((fn(i2)-fn(i1))/h1-h1*s(2)/6.0)
      return
 1    in=index(n)
      if(x.le.xn(in)) go to 2
      inm1=index(n-1)
      hnm1=xn(in)-xn(inm1)
      spline=fn(in)+(x-xn(in))*((fn(in)-fn(inm1))/hnm1+hnm1*s(n-1)/6.0)
      return
 2    do 3 i=2,n
         ii=index(i)
         if(x.le.xn(ii)) go to 4
 3    continue
 4    l=i-1
      il=index(l)
      ilp1=index(l+1)
      a=xn(ilp1)-x
      b=x-xn(il)
      hl=xn(ilp1)-xn(il)
      spline=a*s(l)*(a**2/hl-hl)/6.0+b*s(l+1)*(b**2/hl-hl)/
     &       6.0+(a*fn(il)+b*fn(ilp1))/hl
      return
      end
c
```

APPENDIX B. TABLE FOR EXPERIMENTAL MEASUREMENT OF HOLES AND DISKS

Table B.1: Experimental Measurement of Disk by considering 20 to 50 Points across the circumference

Plate thickness mm	Size mm	20pts mm	30pts mm	40pts mm	50pts mm
3.20	50.80	50.540	50.549	50.546	-
3.20	76.20	-	75.961	75.953	75.970
3.20	101.60	101.312	101.385	101.378	-
6.40	50.8	50.494	50.514	50.515	50.462
6.40	76.2	75.989	75.980	75.975	76.007
6.40	101.6	-	101.264	101.314	101.323

Table B.2: Experimental Measurement of Hole by considering 20 to 50 Points across the circumference

Plate thickness mm	Size mm	20pts mm	30pts mm	40pts mm	50pts mm
3.20	50.80	50.941	50.969	50.959	-
3.20	76.20	76.447	76.376	-	76.420
3.20	101.60	101.757	101.746	101.748	101.757
6.40	50.8	50.954	50.973	50.977	50.981
6.40	76.2	76.427	76.410	76.450	76.432
6.40	101.6	101.734	101.799	101.808	101.736